PSF reconstruction for Keck AO
Phase 1 Final Report

Ralf Flicker (*rflicker@keck.hawaii.edu, rflicker@mac.com*)

W.M. Keck Observatory, 65-1120 Mamalahoa Hwy., Kamuela, HI 96743, USA

31 October 2008

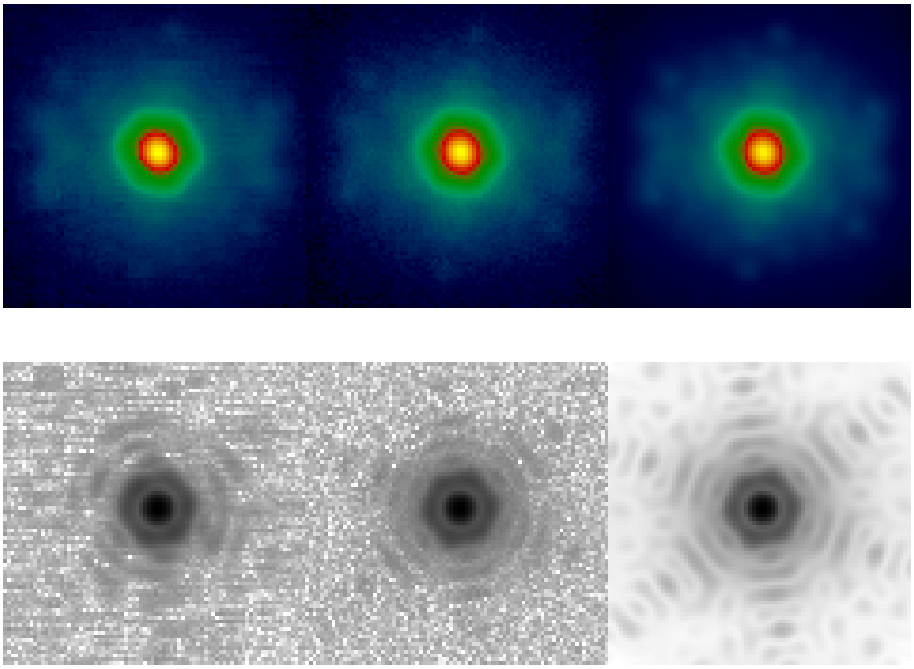

Sample BrG PSF reconstructions with the K2 AO system and the NIRC2 narrow-field camera (10 mas plate scale). Top: low-Strehl (25%) noise test on the artificial light source (fiber). Bottom: bright NGS high-Strehl (60%) on-sky test. The image on the left is the recorded NIRC2 image, and the on the right is the reconstructed PSF. The center image is also the reconstructed PSF, with simulated detector noise added to it for a more realistic comparison with the actual NIRC2 image.

Contents

Acknowledgments

This work has been supported by the National Science Foundation Science and Technology Center for Adaptive Optics, managed by the University of California at Santa Cruz under cooperative agreement No. AST - 9876783. The author wishes to thank the CfAO for their support, and the following coworkers for their contributions, insights and fruitful discussions: Chris Neyman, David LeMignant, Peter Wizinowich, Erik Johansson, Viswa Velur, Matthew Britton, Rich Dekany, Brent Ellerbroek, François Rigaut.

1 Introduction

This document collects and summarizes the work done to date within the framework of the CfAO funded project "PSF reconstruction at WMKO: Development, implementation and validation of PSF reconstruction techniques," initially funded for FY09. PSF reconstruction is planned to be an additional resource for astronomers observing with adaptive optics (AO). The point spread function (PSF) of AO observations can have a complex structure, making its estimation and modeling hard for the non-expert (and, it is fair to say, also for the expert). The recent availability of recorded real-time AO telemetry data such as wavefront sensor (WFS) centroids and sub-aperture intensities, by the capacity introduced by a new wavefront controller (WFC), makes realistic PSF estimation more feasible.

1.1 Project summary

This section is a summary of the goals, current status and future schedule of the multi-year collaborative proposal [1] to the CfAO "Development, implementation and validation of PSF reconstruction techniques." (This section was originally presented as the Y9 CfAO project annual report, April 2008, LeMignant & Flicker.) The project started in November 2007 at the W. M. Keck Observatory (WMKO) under the direction of D. Le Mignant (PI), with postdoctoral researcher R. Flicker employed for the principal algorithm development and implementation.

Project milestones

The proposal outlined three major phases of the project, described in roughly chronological order as:

1. Initial development phase; on-axis NGS only (8 months)
    a. Review previous research on PSF reconstruction and select candidate algorithms
    b. Develop K2 AO simulation tools for the purpose of producing simulated AO telemetry data
    c. Develop TRS (telemetry recorder/server) query and analysis tools
    d. Develop prototype PSF reconstruction algorithm containing the fundamental components (fitting, aliasing, noise and bandwidth errors); test on simulated data and apply to real on-axis NGS K2 AO data
2. On-sky validation and component development phase; off-axis NGS, LGS, optical aberrations (12 months)
    a. Develop and validate angular and focal anisoplanatism components for NGS and LGS
    b. Develop static and dynamic telescope aberration components (segment figures, vibrations, instrument optical distortions); strategy for measuring them
    c. Integrated product development, preliminary deployment to routine observing
3. Final product and future development phase (4 months)
    a. Integrated product and user interface development
    b. Initial studies into PSF reconstruction techniques for future multi-beacon tomographic AO systems (i.e. MCAO, MOAO, LTAO) and extremely-high-order AO systems (applicable to, e.g., NGAO)

Each phase entails a number of sub-tasks most of which are omitted here for brevity. Much of the PSF algorithm development is modular, consisting of several estimation algorithms that are researched and developed largely independently (e.g., noise estimation, seeing estimation, aliasing and anisoplanatism modeling etc – all described in more detail in the documentation available on the PSF reconstruction project TWiki [2]).

Current status and schedule

This section summarizes in words the progress on various tasks, leaving more detailed technical discussions to be found in the documentation on the PSF reconstruction TWiki page [2].

Phase 1 (75% complete)

The milestones of Phase 1, covering the period 2007–11–01 to 2008–07–01, are either accomplished or well under way (100% to 50% complete), with the project on schedule.

1a. (100% complete) Reviewing the literature, we resolved to base our algorithm development on the previously most commonly applied method, introduced by J.-P. Véran in [41] (henceforth the "Véran method"). One recent improvement [20] to the Véran method was adopted early on as the baseline algorithm for PSF reconstruction at WMKO, as it reduces the computational complexity without sacrificing realism, potentially allowing the algorithm to be scaled up to high-order AO systems with future development.

1b. (100% complete) In order to prototype the PSF reconstruction algorithm, and for future debugging and sanity-checking, it was deemed important to have a capable simulation tool that emulates the current AO system on the Keck 2 telescope as closely as possible. Such a numerical simulation tool was developed within the first half of Phase 1, and has been employed to generate streams of fake AO telemetry data on the same format as the actual TRS, greatly facilitating development of the PSF reconstruction algorithms.

1c. (50% complete) The new wavefront controller (former NGWFC) recently implemented on the K2 AO system [3] is crucial to the success of PSF reconstruction, as it allows several nights of full-frame-rate AO telemetry to be recorded for later post-processing. This complete recording and generous storage capacity offered by the TRS obviates the need for real-time data reduction, and allows the PSF reconstruction to be carried out at any later time with complete access to the raw data. A set of general TRS database query tools were available at the start of this PSF reconstruction project, but for the PSF reconstruction task a number of extensions and modifications were identified as necessary. There is currently an ongoing effort, lead by proposal participant Erik Johanson (WMKO), to develop additional software tools and add such functionality to the TRS in order to facilitate PSF reconstruction, as well as other applications.

1d. (50% complete) The first departure from the Véran method that we decided upon was to omit the pupil-averaging step, which approximates a non-stationary structure function by a stationary one in order to simplify computation. This approximation may lead to an underestimation of the optical transfer function (OTF), but we found that, in conjunction with the methodology in [20], the advance in affordable computing power has rendered the pupil-averaging approximation unnecessary. A second reason for avoiding pupil-averaging is that the structure function for focal anisoplanatism (cone-effect) with LGS is in itself non-stationary (Sect. 4.2), and could not be used within the Véran method without some form of additional approximation. By evaluating the OTF directly from the non-stationary structure function, we avoid applying any additional approximation to the focal anisoplanatism term.

The fitting and aliasing components have been modeled and implemented into the algorithm, as described in the documentation on the TWiki [2]. In brief, both are based on Fourier-domain modeling. The fitting component consists of a numerically generated Fourier domain mask that is applied to a model turbulence power spectral density function (PSD). The PSD mask takes into account the shape of the DM influence functions, producing a smoother and more realistic roll-off at the AO cut-off frequency than simple analytical models (e.g. [25]). The aliasing component is modeled by an analytical PSD model based on the formalism in [29], generalized here to closed-loop conditions (see Appendix 1 in [2]).

The noise/servo-lag component is the central object that is computed from real-time AO telemetry. The Véran method applies two approximations to this component that we too have used initially. In order to achieve a PSF reconstruction algorithm that is reliable also in high-noise conditions (faint guide star regime), however, we also consider more realistic representations of this component that include the temporal filtering (omitted in [41]). Considerable effort is devoted during the second half of Phase 1 to model this component and verify it against AO lab data. The details are outlined in [2]. One set of AO lab data was collected for initial model testing. Unfortunately the test needs to be repeated and new lab data collected, due to a failure to record all the necessary telemetry the first time.

On-sky data was also collected on bright NGS for testing the fitting and aliasing components, as well as providing data for validation of the seeing estimator (see Sect. 1.2). A reliable and accurate r_0 estimation is essential to PSF reconstruction, so testing and potentially making improvements to the algorithm currently in operation is a high-priority task that is being carried out presently.

Phase 2 (10% complete)

2a. (33% complete) As implied above, anisoplanatism modeling became pursued and largely accomplished within the time frame for Phase 1. The research was recently submitted to a peer-reviewed journal, and an upcoming engineering run with K2AO aims to collect NGS anisoplanatism data for on-sky validation, well ahead of schedule. The results produced include analytical formulas for angular and focal anisoplanatism structure functions, which take into account the finite outer scale of atmospheric turbulence. Although the outer scale is a poorly known quantity, it was found that, for a 10-meter telescope, outer scales on the order of ∼30 meters or less would have a significant impact on Strehl ratio and PSF shape.

Participants and collaborations

Ralf Flicker has been dedicated full-time to this project. Erik Johansson and David Le Mignant have provided support for the project at about 5-10% level. Other participants have been consulted for technical issues for modeling, analysis or data management. This includes Marcos van Dam (AO scientist at WMKO-left 12/07), Matthew Britton (AO scientist at COO), Jeff Mader (software engineer at WMKO) and Michael Fitzgerald (post-doctoral researcher at LLNL). All these individuals are already participants of the CfAO.

1.2 Technical summary

Algorithm methodology

In words rather than equations, the OTF is estimated in the following steps:

1. The residual error covariance matrix, consisting of noise, aliasing, turbulence and their cross-terms, is estimated by approximating the temporal dynamics and the cross-terms (section 3.4).
2. The estimated residual error covariance matrix is diagonalized, enabling the structure function to be computed as a sum over a reduced set (N_c terms instead of $\mathcal{O}(N_c^2)$) of orthogonal DM modes (section 2.2).
3. The OTF integral over controlled modes is evaluated from its autocorrelation definition, including the pupil function and the exponential of the the non-stationary structure function (section 2.3). This means that:
   - The "pupil-averaging" approximation is avoided (but the OTF calculation becomes more demanding)
   - There is no additional penalty for other non-stationary kernels, e.g., focal anisoplanatism (section 4.2)
4. Multiplicative OTF kernels of stationary structure functions can be calculated separately:
   - Fitting error (section 3.2)
   - Tip/tilt error (section 3.6)
   - Anisoplanatism in stationary approximations (section 4.1)

Assumptions and approximations

The OTF estimation of the controlled modes relies on the following fundamental assumptions:

A1 Uniform field amplitude (no scintillation)

A2 The point-wise residual phase error is statistically Gaussian (central-limit theorem)

A3 Controlled and uncontrolled modes are statistically uncorrelated

The covariance matrix estimation relies on the further assumptions, which are invoked as approximations:

A4 The deformable mirror (DM) shape is approximated by a linear superposition of independent influence functions

A5 Cross-terms between WFS aliasing and residual error are approximated by the aliasing term

A6 AO loop temporal dynamics are modeled in the "high-bandwidth" approximation

The terms that need to be modeled theoretically invoke the following standard assumptions:

A7 Fitting, aliasing and anisoplanatism error terms employ a von Karman turbulence model, with the outer scale as a free parameter

Technical challenges

The more challenging technical aspects of the project which are currently being worked on as part of Phase 1 include seeing estimation, noise modeling, and residual error covariance matrix modeling.

- Seeing estimation. The atmospheric seeing (or r_0) is one of the most important parameters to have a good estimate of. Even though we are employing the approximation that the long-exposure PSF can be represented by an average r_0 value (while we know that r_0 can vary strongly even on short time scales), the PSF is still very sensitive to this value. As part of the PSF reconstruction project we therefore deemed it necessary to validate the seeing estimation algorithms currently used with K2 AO (based on Schoeck et al. [32]). Data that was collected during two half-nights of observing (in January and April 2008) are being analyzed currently.

- Noise model. This is one of the critical components of the PSF reconstruction algorithm, and the realism of this component decides whether the algorithm can be applied in the high-noise regime of faint AO guide stars. Depending on how the calculation is pursued, we either estimate a noise covariance matrix in the WFS domain and a temporal noise transfer function, or we can try to estimate the temporally filtered noise covariance matrix in the DM domain in one step. Most previous PSF reconstruction projects have followed the first approach, which requires good knowledge of the noise in the WFS and other hard-to-measure quantities such as the centroid gain. No successful implementation of the latter approach has yet been demonstrated, but it is the goal of the current project to investigate this method and attempt to implement it. For the purpose of testing the noise modeling in an idealized setting, noisy AO telemetry data was collected from the AO bench operating on the internal (fiber) light source, with no atmospheric turbulence (hence no fitting or aliasing error) present. This data and the noise models are currently being tested.

- Covariance matrix model. This aspect of modeling covers how the components of noise, aliasing and residual turbulence error are combined into a single covariance matrix that is used in the final OTF calculation. Approximations can creep in at different stages here, as the quantities are either poorly known or their exact representations become too complicated to deal with numerically. Firstly, there are cross-terms between the AO telemetry and the noise and aliasing terms, and secondly there is the temporal filtering mentioned in relation to the noise model above. In following the approach suggested by Véran [41] both of these effects are approximated to a degree, but the goal of the project is to investigate the feasibility and performance of more realistic representations.

1.3 Future work

At the end of Phase 1, this project has succeeded in demonstrating the feasibility of PSF reconstruction for the WMKO K2 Shack-Hartmann AO system, but has not progressed to the point where it can be routinely applied. Some of the algorithm components require further development and calibration (e.g. the noise term and r_0 estimation, as mentioned above). It was also the ambition to improve on the temporal covariance matrix modeling (Sect. 3.4, method 2) in order to improve algorithm reliability on faint guide stars, but this aspect was not investigated yet. In addition to these details of Phase 1 that remain to be resolved, Phase 2 also presents a number of challenges and issues to be addressed:

- Noise model for LGS mode: the effects of spot elongation needs to be taken into account.

- Focal anisoplanatism in LGS mode. While a realistic structure function was developed (Sect. 4.2), its computation with spatial filtering (Sect. 4.5) becomes prohibitively expensive, and without the spatial filtering it will overestimate the anisoplanatism error by applying it also to the uncontrolled modes.

- Tilt anisoplanatism in LGS mode: while a simple component to calculate, the TRS data from the tip/tilt sensor needs to be calibrated to the FSM model used in the PSF reconstruction algorithm.

- For NGAO, there will also be some big issues to address:

  - Efficiency: simply scaling up the current algorithm will make numerical computations intractable, so probably a new kind of algorithm altogether will be required.
  - Tomographic wavefront reconstruction or model-based tomography error kernel.

– Tomographic null-mode kernel: some modeling work has already been done on this (Sect. 6), but the complexity of the problem depends on the modal basis employed for the null-mode system. In the case of only global and differential tilt modes, the solutions are straightforward (Gaussian kernels with field-varying parameters) and have already been worked out (e.g. Ref. [13, 14]), but the more general case of an arbitrary null-mode basis has not been addressed.

2 OTF calculation

We first outline the principles of the commonly employed U_{ij} method, establish the splitting of wavefronts into controlled and uncontrolled modes (1), and then introduce more recent developments (the V_{ii} method) that lead to the final expression (42) for the OTF.

2.1 The U_{ij} algorithm

This methodology was first developed and implemented by Véran [41, 42] for curvature-based AO systems (PUEO), and has also become the most commonly applied method for Shack-Hartmann-based PSF reconstruction schemes to date. The method divides the phase ϕ into two complementary and orthogonal components, the vector space $\phi_\parallel$ spanned by the deformable mirror modes (the "parallel" phase of controlled modes) and its orthogonal complement $\phi_\perp$ (the "orthogonal" phase of uncontrolled modes). Due to deviations from the ideal, the actually controlled modes will in reality not be exactly orthogonal to the theoretically modeled orthogonal phase, but as a mathematical model it is a sufficiently realistic approximation. By this separation into $\phi_\parallel$ and $\phi_\perp$ it becomes possible to apply different estimation techniques to the two domains: the residual error on the controlled modes are estimated from AO loop data, and the error on the uncontrolled modes are estimated by statistical models of atmospheric turbulence.

Residual phase

With the division of spatial frequency regions into high-order ($\phi_\perp$) and low-order ($\phi_\parallel$) components, we describe the two-dimensional phase retardation of a time-dependent turbulence-aberrated wavefront by

$$\phi(\mathbf{x},t) = \phi_\parallel(\mathbf{x},t) + \phi_\perp(\mathbf{x},t). \tag{1}$$

The phase correction φ introduced by the DM of the AO system can be modeled to a good approximation (see Sect. 3.3) as a linear sum of N_c actuator influence functions $h_i(\mathbf{x})$ according to

$$\varphi(\mathbf{x},t) = \sum_{i=1}^{N_c} c_i(t) h_i(\mathbf{x}), \tag{2}$$

where $c_i(t)$ are modal coefficients proportional to the actuator voltages. The parallel phase $\phi_\parallel$ is by definition described in the same modal basis as the DM, so we can write

$$\phi_\parallel(\mathbf{x},t) = \sum_{i=1}^{N_c} a_i(t) h_i(\mathbf{x}). \tag{3}$$

The PSF after AO compensation is governed by the residual phase $\epsilon(\mathbf{x},t)$ according to

$$\begin{aligned} \epsilon(\mathbf{x},t) &= \phi(\mathbf{x},t) - \varphi(\mathbf{x},t) && (4)\\ &= \phi_\perp(\mathbf{x},t) + \sum_{i=1}^{N_c} [a_i(t) - c_i(t)] h_i(\mathbf{x}) && (5)\\ &= \phi_\perp(\mathbf{x},t) + \epsilon_\parallel(\mathbf{x},t), && (6) \end{aligned}$$

where we defined $\epsilon_i(t) = a_i(t) - c_i(t)$ as the modal coefficient of the residual parallel phase $\epsilon_\parallel(\mathbf{x},t)$, and

$$\epsilon_\parallel(\mathbf{x},t) = \sum_{i=1}^{N_c} \epsilon_i(t) h_i(\mathbf{x}). \tag{7}$$

Structure function

The spatial phase structure function D_ϕ is defined as

$$D_\phi(\mathbf{x},\boldsymbol{\rho}) = \left\langle |\phi(\mathbf{x},t) - \phi(\mathbf{x}+\boldsymbol{\rho},t)|^2 \right\rangle, \tag{8}$$

where angular brackets denote ensemble average. Expanding the square and rearranging terms allows us to relate the structure function to the correlation function $C_\phi(\boldsymbol{\rho}) = \langle \phi(\mathbf{x},t)\phi(\mathbf{x}+\boldsymbol{\rho},t)\rangle$ assuming homogeneity

$$D_\phi(\boldsymbol{\rho}) = 2\left[C_\phi(0) - C_\phi(\boldsymbol{\rho})\right], \tag{9}$$

which will be eminently useful. If we assume (A3) that $\epsilon_\parallel$ and $\phi_\perp$ are statistically uncorrelated, then the structure function D_ϵ of the residual phase error is

$$D_\epsilon(\mathbf{x},\boldsymbol{\rho}) = D_{\phi_\perp}(\mathbf{x},\boldsymbol{\rho}) + D_{\epsilon_\parallel}(\mathbf{x},\boldsymbol{\rho}), \tag{10}$$

where $D_{\phi_\perp}$ is the structure function of everything that the AO system does not attenuate (i.e. the fitting error), and is estimated separately (see Sect. 3.2). With the definition (7) we have that

$$D_{\epsilon_\parallel}(\mathbf{x},\boldsymbol{\rho}) = \left\langle \left| \sum_{i=1}^{N_c} \epsilon_i(t)[h_i(\mathbf{x}) - h_i(\mathbf{x}+\boldsymbol{\rho})] \right|^2 \right\rangle \tag{11}$$

$$= \sum_{i=1}^{N_c}\sum_{j=1}^{N_c} \langle \epsilon_i(t)\epsilon_j(t)\rangle \left[h_i(\mathbf{x}) - h_i(\mathbf{x}+\boldsymbol{\rho})\right]\left[h_j(\mathbf{x}) - h_j(\mathbf{x}+\boldsymbol{\rho})\right]. \tag{12}$$

One may define an aperture-averaged structure function $\bar{D}(\boldsymbol{\rho})$ according to

$$\bar{D}_\phi(\boldsymbol{\rho}) = \frac{\int d\mathbf{x}\, D_\phi(\mathbf{x},\boldsymbol{\rho}) P(\mathbf{x}) P(\mathbf{x}+\boldsymbol{\rho})}{\int d\mathbf{x}\, P(\mathbf{x}) P(\mathbf{x}+\boldsymbol{\rho})}, \tag{13}$$

where $P(\mathbf{x})$ defines the aperture transmission function. Since the autocorrelation in the denominator is band-limited, the fraction must only be computed within the support of $\int d\mathbf{x}\, P(\mathbf{x})P(\mathbf{x}+\boldsymbol{\rho})$. The homogenized structure function $\bar{D}_{\epsilon_\parallel}$ can be written more simply as

$$\bar{D}_{\epsilon_\parallel}(\boldsymbol{\rho}) = \sum_{i=1}^{N_c}\sum_{j=1}^{N_c} \langle \epsilon_i(t)\epsilon_j(t)\rangle\, U_{ij}(\boldsymbol{\rho}), \tag{14}$$

where the U_{ij} functions are given by

$$U_{ij}(\boldsymbol{\rho}) = \frac{\int d\mathbf{x}\, \left[h_i(\mathbf{x}) - h_i(\mathbf{x}+\boldsymbol{\rho})\right]\left[h_j(\mathbf{x}) - h_j(\mathbf{x}+\boldsymbol{\rho})\right] P(\mathbf{x}) P(\mathbf{x}+\boldsymbol{\rho})}{\int d\mathbf{x}\, P(\mathbf{x}) P(\mathbf{x}+\boldsymbol{\rho})}. \tag{15}$$

The static U_{ij} functions can be computed for a given set of mirror modes $h_i(\mathbf{x})$, while the covariance matrix $\langle \epsilon_i(t)\epsilon_j(t)\rangle$ is computed from the AO telemetry stream of DM actuator commands and WFS measurements during the particular observation (see Sect. 3.4).

Optical transfer function

Let $K = K(\boldsymbol{\alpha},\boldsymbol{\beta})$ be the anisoplanatic PSF as a function of image and object space angular coordinates $(\boldsymbol{\alpha},\boldsymbol{\beta})$, resulting from the anisotropic complex field $\psi = \psi(\mathbf{x},\mathbf{y})$ in the image and object space spatial coordinates $(\mathbf{x},\mathbf{y})$. For incoherent quasi-monochromatic sources it can be shown [5] that the instantaneous PSF in the far-field approximation is given by $K(\boldsymbol{\alpha},\boldsymbol{\beta}) = |\mathcal{F}[\psi(\mathbf{x},\mathbf{y})]|^2$, where $\mathcal{F}$ denotes the Fourier transform. Since the OTF is $B = \mathcal{F}(K)$, it can be shown by the Wiener-Khinchin theorem that the long-exposure OTF is

$$\langle B(\mathbf{u},\mathbf{v})\rangle = \int d\mathbf{w}\, \langle \psi(\mathbf{w},\mathbf{v})\psi^*(\mathbf{w}+\mathbf{u},\mathbf{v})\rangle, \tag{16}$$

where $(\mathbf{u},\mathbf{v},\mathbf{w})$ are angular frequency coordinates of the OTF domain, and the superscript asterisk $(^*)$ indicates complex conjugate. Assuming the field amplitude to be uniform (A1) (and hence also isoplanatic), the complex field may be described as

$$\psi(\mathbf{x},\mathbf{y}) = P(\mathbf{x}) \exp[i\phi(\mathbf{x},\mathbf{y})], \tag{17}$$

where P is a real-valued binary aperture transmission function and ϕ is the optical phase retardation. Combining equations (16) and (17) gives

$$\langle B(\mathbf{u},\mathbf{v})\rangle = \int d\mathbf{w}\, P(\mathbf{w})P(\mathbf{w}+\mathbf{u}) \left\langle e^{i\phi(\mathbf{w},\mathbf{v})} e^{-i\phi(\mathbf{w}+\mathbf{u},\mathbf{v})} \right\rangle. \tag{18}$$

Assuming the phase ϕ to be a zero-mean Gaussian random variable (A2) leads to $\langle \exp(i\phi)\rangle = \exp(-\frac{1}{2}\langle\phi^2\rangle)$, and the OTF simplifies to

$$\begin{aligned} \langle B(\mathbf{u},\mathbf{v})\rangle &= \int d\mathbf{w}\, P(\mathbf{w})P(\mathbf{w}+\mathbf{u}) \exp\left[-\frac{1}{2}\langle|\phi(\mathbf{w},\mathbf{v}) - \phi(\mathbf{w}+\mathbf{u},\mathbf{v})|^2\rangle\right] &(19)\\ &= \int d\mathbf{w}\, P(\mathbf{w})P(\mathbf{w}+\mathbf{u}) \exp\left[-\frac{1}{2} D_\phi(\mathbf{w},\mathbf{u},\mathbf{v})\right] &(20)\end{aligned}$$

by the definition of the structure function. If the structure function was homogeneous across the aperture plane, this would mean that $D_\phi(\mathbf{w},\mathbf{u},\mathbf{v}) = D_\phi(\mathbf{u},\mathbf{v})$, and the OTF expression simplifies further

$$\begin{aligned} \langle B(\mathbf{u},\mathbf{v})\rangle &= \underbrace{\exp\left[-\frac{1}{2} D_\phi(\mathbf{u},\mathbf{v})\right]}_{B_\phi} \underbrace{\int d\mathbf{w}\, P(\mathbf{w})P(\mathbf{w}+\mathbf{u})}_{B_P} &(21)\\ &= B_\phi(\mathbf{u},\mathbf{v}) \times B_P(\mathbf{u}), &(22)\end{aligned}$$

where B_ϕ is recognized as the long-exposure optical transfer function of the turbulent phase ϕ, and B_P is the static OTF of the telescope. To arrive at this result for the purpose of PSF reconstruction, Véran [41] invokes the approximation that $D_{\epsilon_\parallel} \approx \bar{D}_{\epsilon_\parallel}$, which allows the residual AO OTF to be approximated by equation (21) since $D_{\phi_\perp} = D_{\phi_\perp}(\boldsymbol{\rho})$ is explicitly homogeneous. In the case of an isoplanatic PSF or when evaluated along a single field angle, the result thus can be written

$$\begin{aligned} \langle B(\boldsymbol{\rho}/\lambda)\rangle &\approx B_{\phi_\perp}(\boldsymbol{\rho}/\lambda) \times B_{\epsilon_\parallel}(\boldsymbol{\rho}/\lambda) \times B_P(\boldsymbol{\rho}/\lambda) &(23)\\ &= \exp\left\{-\frac{1}{2} D_{\phi_\perp}(\boldsymbol{\rho}/\lambda)\right\} \times \exp\left\{-\frac{1}{2}\bar{D}_{\epsilon_\parallel}(\boldsymbol{\rho}/\lambda)\right\} \times (P \star P)(\boldsymbol{\rho}/\lambda), &(24)\end{aligned}$$

where $\star$ denotes convolution or autocorrelation.

2.2 The V_{ii} algorithm

A modification to the U_{ij} algorithm was recently developed by Gendron et al. [20]. A practical problem with the U_{ij} algorithm is that the computation of $\mathcal{O}(N_c^2)$ U_{ij} functions becomes very expensive for high-order AO systems. The V_{ii} method reduces the computational load to $\mathcal{O}(N_c)$ functions by diagonalizing the $\langle\epsilon\epsilon^T\rangle$ covariance matrix. The eigenvalue decomposition of the square symmetric matrix $\langle\epsilon\epsilon^T\rangle$ can be written

$$\langle\epsilon\epsilon^T\rangle = S\Lambda S^T, \tag{25}$$

where S is a square orthogonal matrix and $\Lambda = \mathrm{diag}(\{\lambda_i\}_{i=1}^{N_c})$ is the diagonal matrix of eigenvalues. Rewriting this as

$$\Lambda = S^T\langle\epsilon\epsilon^T\rangle S = \langle(S^T\epsilon)(S^T\epsilon)^T\rangle = \langle\eta\eta^T\rangle \tag{26}$$

results in a diagonal covariance matrix of the transformed vector $\eta = S^T\epsilon$. Conversely, substituting $\epsilon = S\eta$ into (14) and rearranging allows the structure function to be written

$$\begin{aligned} \bar{D}_{\epsilon_\parallel}(\boldsymbol{\rho}) &= \sum_{i=1}^{N_c}\sum_{j=1}^{N_c} \langle(S\eta)_i(S\eta)_j\rangle\, U_{ij}(\boldsymbol{\rho}) &(27)\\ &= \sum_{i=1}^{N_c}\sum_{j=1}^{N_c} U_{ij}(\boldsymbol{\rho}) \left(\sum_{k=1}^{N_c}\sum_{l=1}^{N_c} S_{ik}S_{jl}\langle\eta_k\eta_l\rangle\right) &(28)\end{aligned}$$

$$= \sum_{k=1}^{N_c} \langle \eta_k \eta_k \rangle \sum_{i=1}^{N_c} \sum_{j=1}^{N_c} S_{ik} S_{jk} U_{ij}(\boldsymbol{\rho}) \tag{29}$$

$$= \sum_{k=1}^{N_c} \langle \eta_k \eta_k \rangle V_k(\boldsymbol{\rho}), \tag{30}$$

where

$$V_k(\boldsymbol{\rho}) = \frac{\int d\mathbf{x} \left(\sum_{i=1}^{N_c} S_{ik} \left[h_i(\mathbf{x}) - h_i(\mathbf{x}+\boldsymbol{\rho}) \right] \right) \left(\sum_{j=1}^{N_c} S_{jk} \left[h_j(\mathbf{x}) - h_j(\mathbf{x}+\boldsymbol{\rho}) \right] \right) P(\mathbf{x}) P(\mathbf{x}+\boldsymbol{\rho})}{\int d\mathbf{x}\, P(\mathbf{x}) P(\mathbf{x}+\boldsymbol{\rho})} \tag{31}$$

$$= \frac{\int d\mathbf{x} \left| h'_k(\mathbf{x}) - h'_k(\mathbf{x}+\boldsymbol{\rho}) \right|^2 P(\mathbf{x}) P(\mathbf{x}+\boldsymbol{\rho})}{\int d\mathbf{x}\, P(\mathbf{x}) P(\mathbf{x}+\boldsymbol{\rho})}, \quad \text{and :} \quad h'_k(\mathbf{x}) = \sum_{i=1}^{N_c} S_{ik} h_i(\mathbf{x}), \tag{32}$$

or in vector notation $h' = S^T h$ is the transformed modal basis within which the covariance matrix $\langle \eta \eta^T \rangle$ is diagonal. This requires the computation of only N_c functions $V_k(\boldsymbol{\rho})$ (or V_{ii} in the notation of Gendron et al.). To practically compute the V_k functions we rewrite the numerator in terms of convolutions and use the Fourier transform to evaluate them:

$$V_k(\boldsymbol{\rho}) \times (P \star P) = \int d\mathbf{x} \left| h'_k(\mathbf{x}) - h'_k(\mathbf{x}+\boldsymbol{\rho}) \right|^2 P(\mathbf{x}) P(\mathbf{x}+\boldsymbol{\rho}) \tag{33}$$

$$= \int d\mathbf{x}\, h'^2_k(\mathbf{x}) P(\mathbf{x}) P(\mathbf{x}+\boldsymbol{\rho}) + \int d\mathbf{x}\, h'^2_k(\mathbf{x}+\boldsymbol{\rho}) P(\mathbf{x}+\boldsymbol{\rho}) P(\mathbf{x}) \tag{34}$$

$$- 2 \int d\mathbf{x}\, h'_k(\mathbf{x}) P(\mathbf{x}) h'_k(\mathbf{x}+\boldsymbol{\rho}) P(\mathbf{x}+\boldsymbol{\rho}) \tag{35}$$

$$= 2 \left[(h'^2_k P) \star P - (h'_k P) \star (h'_k P) \right] \tag{36}$$

$$= 2 \left\{ \mathcal{F}^{-1} \left[\mathcal{F}(h'^2_k P) \widetilde{P}^* - |\mathcal{F}(h'_k P)|^2 \right] \right\} \tag{37}$$

where widetilde $\widetilde{P}$ is shorthand for the Fourier transform, and the denominator is simply $P \star P = \mathcal{F}^{-1}(|\widetilde{P}|^2)$.

2.3 Non-stationary calculation

Although it might have seemed computationally implausible at one time, the diagonalization introduced in 2.2 together with Moore's Law may render the stationarity approximation unnecessary. As we shall see later on, the focal anisoplanatism structure function will in any case force us to calculate a non-stationary terms, so we might as well get some practice starting right here. Recalling the original structure function expression and applying the diagonalization of the covariance matrix, we obtain

$$D_{\epsilon_\parallel}(\mathbf{x}, \boldsymbol{\rho}) = \sum_{i=1}^{N_c} \sum_{j=1}^{N_c} \langle \epsilon_i(t) \epsilon_j(t) \rangle \left[h_i(\mathbf{x}) - h_i(\mathbf{x}+\boldsymbol{\rho}) \right] \left[h_j(\mathbf{x}) - h_j(\mathbf{x}+\boldsymbol{\rho}) \right] \tag{38}$$

$$= \sum_{k=1}^{N_c} \langle \eta_k \eta_k \rangle H'_k(\mathbf{x}, \boldsymbol{\rho}), \tag{39}$$

where

$$H'_k(\mathbf{x}, \boldsymbol{\rho}) = \left| \sum_{i=1}^{N_c} S_{ik} \left[h_i(\mathbf{x}) - h_i(\mathbf{x}+\boldsymbol{\rho}) \right] \right|^2 \tag{40}$$

$$= \left| h'_k(\mathbf{x}) - h'_k(\mathbf{x}+\boldsymbol{\rho}) \right|^2, \quad \text{and :} \quad h'_k(\mathbf{x}) = \sum_{i=1}^{N_c} S_{ik} h_i(\mathbf{x}). \tag{41}$$

And the OTF is computed explicitly as

$$\langle B(\boldsymbol{\rho}/\lambda) \rangle = \int d\mathbf{x}\, P(\mathbf{x}) P(\mathbf{x}+\boldsymbol{\rho}) \exp \left\{ -0.5 \sum_{k=1}^{N_c} \lambda_k \left| h'_k(\mathbf{x}) - h'_k(\mathbf{x}+\boldsymbol{\rho}) \right|^2 \right\} \tag{42}$$

2.4 From PSD to OTF

Very useful in the U_{ij} methodology is the Wiener-Khinchin theorem, which states that the autocorrelation C_ϕ of a stochastic variable ϕ is equal to the Fourier transform of its power spectrum Φ_ϕ, i.e.

$$\mathcal{F}\left[\Phi(\mathbf{f})\right](\boldsymbol{\rho}) = \int d\mathbf{x}\, \langle \phi(\mathbf{x})\, \phi(\mathbf{x}+\boldsymbol{\rho})\rangle \;=\; C_\phi(\boldsymbol{\rho}), \tag{43}$$

provided that the Fourier transform exists. The last equality also holds when the statistics of ϕ is spatially stationary and has zero mean. While perfect in theory, there are some practical problems with applying the Wiener-Khinchin theorem to a turbulence PSD, in that the correlation function one is trying to obtain is not guaranteed to be band-limited within the computational range, i.e., the numerically computed FFT might not be able to reproduce the exact Fourier transform. We can see that this is the case for a pure Kolmogorov PSD, where simply applying the FFT to a $f^{-11/3}$ power law will roll off the transform at the edges of the computational grid, while in theory the structure function should be exactly proportional to a 5/3-power law. The consequence of using the FFT is a correlation function that underestimates the total variance, and also has a somewhat wrong shape at large separations. For a von Kármán PSD the situation improves somewhat, and gets better the smaller L_0 is, since this predicts a C_ϕ that is limited and approaches an asymptotic value at large separations, so the function naturally approximates a band-limited function eventually.

It is possible to apply an ad hoc correction term to the PSD in order to improve the accuracy of turbulence correlation functions calculated by FFT (see section 3.1 of the older draft of this document, 15 April 2008). With an outer scale $L_0 < 30$ meters however the error is small, and we may safely use the FFT method directly without committing a significant error. For larger outer scales, a L_0-dependent normalization factor of order unity can be applied:

$$\alpha(L_0) = a_0 - a_1 \exp(-a_2 L_0), \tag{44}$$

such that $\Phi(f) \mapsto \alpha(L_0) \times \Phi(f)$, and the parameters are $a = [1.28925, 0.218983, 0.00326031]$. Anyway. From the definition of the structure function and correlation function we can obtain the former from the latter as

$$D_\phi(\boldsymbol{\rho}) = 2[C_\phi(0) - C_\phi(\boldsymbol{\rho})]. \tag{45}$$

This provides a path for PSD domain modeling of AO terms to the structure function. If the terms are stationary, their OTFs can be computed independently from the AO OTF (42) as indicated already in (24), simply as

$$\langle B_\phi(\boldsymbol{\rho}/\lambda)\rangle = \exp\left\{-\frac{1}{2} D_\phi(\boldsymbol{\rho}/\lambda)\right\}. \tag{46}$$

For instance the fitting error and the tip/tilt error OTFs (and in the isoplanatic approximation also the anisoplanatism error) will be computed this way, and multiplied onto the controlled modes residual wavefront error OTF (42).

3 Component modeling

The different algorithm components that need to be modeled or estimated include:

- Residual wavefront error covariance matrix
- DM fitting error PSD
- WFS noise covariance
- WFS aliasing covariance
- Tilt error structure function
- NGS anisoplanatism (stationary approximation)
- LGS anisoplanatism (non-stationary)
- Tilt anisoplanatism (in LGS mode)
- Static aberrations

3.1 Turbulence model

Until better data comes in or until we are otherwise prompted to consider more sophisticated models, we will adopt the von Kármán turbulence model with a spatial power spectrum according to

$$\Phi(f) = \frac{0.023}{r_0^{5/3}}(f^2 + f_0^2)^{-11/6}, \tag{47}$$

where $f = |\mathbf{f}|$ and $f_0 = 1/L_0$ defines the outer scale L_0 in this model. The corresponding structure function can be written [9, 34]

$$D_\phi(\rho) = a_1 \left[a_2 - (\rho f_1)^{5/6} K_{5/6}(\rho f_1)\right] \left(\frac{L_0}{r_0}\right)^{5/3} \tag{48}$$

where $a1 \approx 0.185$, $a2 = 1.00563$ and $K_{5/6}$ is a modified Bessel function of the second kind (by some authors referred to as a modified Bessel function of the third kind, or the McDonald function). Note that here, $f_1 = 2\pi/L_0$ defines the outer scale differently than does f_0 (different authors have traditionally used such conflicting conventions, we'll just have to live with the confusion). Since the structure function can be expressed in terms of the correlation function, $D_\phi(\rho) = 2[C_\phi(0) - C_\phi(\rho)]$, we can find a useful expression for the correlation function as well:

$$C_\phi(\rho) = \frac{a_1}{2}(\rho f_1)^{5/6} K_{5/6}(\rho f_1) \left(\frac{L_0}{r_0}\right)^{5/3}. \tag{49}$$

In the instances when theoretical modeling of the turbulence vertical profile needs to be invoked, we will assume the Taylor hypothesis of frozen flow, and employ discrete turbulence profiles restricted to a small number of thin layers. This means that we model the structure constant as

$$C_n^2(z) = \sum_{l=1}^{N_l} c_l \delta(z - z_l), \tag{50}$$

where z_l are the layer altitudes and $c_l = f_l \mu_0$ are turbulence strengths, defined in terms of the turbulence moment $\mu_0 = 0.06\lambda^2 r_0^{-5/3}$ and the fractional weights $\sum_l f_l = 1$. Together with a wind profile v_l, the three parameters $\{f_l, z_l, v_l\}_{l=1}^{N_l}$ define a turbulence profile. Unless otherwise stated, the RD-MKR profile (see KAON 503) will be used for testing and generating example plots.

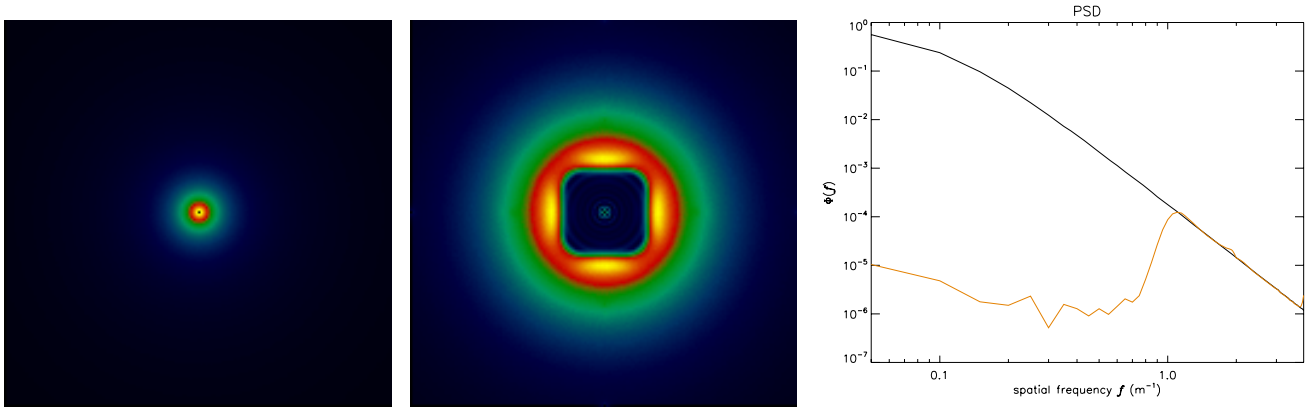

Figure 1: PSDs averaged in the Monte Carlo simulation. Left: open loop input turbulence PSD Φ. Center: fitting error PSD $\Phi_\perp$. Right: cut along the x-axis comparing the pure turbulence (black curve) with the fitting error PSD (orange curve).

3.2 Fitting error

The AO fitting error comes from the part of the turbulence that is not attenuated by the AO system, i.e. it represents the uncontrolled modes (the orthogonal phase $\phi_\perp$). Since it is the complement of the space spanned by the mirror modes, we can compute the fitting error by assuming perfect correction by the AO system. Although several theoretical approaches were investigated, we ultimately decided upon one of the simplest of all methods: to apply a spatial filter function $\mathcal{H}(\mathbf{f})$ to the turbulence PSD and using the Wiener-Khinchin method (section 2.4) for obtaining the OTF. Under assumption A3 we can split the spatial PSD Φ of phase ϕ into $\Phi = \Phi_\parallel + \Phi_\perp$, or

$$\Phi_\perp(\mathbf{f}) = \Phi(\mathbf{f}) - \Phi_\parallel(\mathbf{f}) = \mathcal{H}(\mathbf{f})\Phi(\mathbf{f}), \tag{51}$$

where the last step is just the definition of $\mathcal{H}$. This gives

$$\mathcal{H}(\mathbf{f}) = 1 - \frac{\Phi_\parallel(\mathbf{f})}{\Phi(\mathbf{f})} = \frac{\Phi_\perp(\mathbf{f})}{\Phi(\mathbf{f})}. \tag{52}$$

Now we can either try to calculate $\mathcal{H}$ analytically (hard), measure it from a simulation (easy but time consuming), or posit its shape a priori (even easier, but a less realistic approximation). The last method has been used by e.g. Véran and Jolissaint, by assuming the filter function to be a $\{0,1\}$-valued binary mask $\mathcal{A}$. This ignores the actual shape of the influence functions and approximates the effect of the geometrical layout of actuators on the DM, but makes analytical calculations easy. The fitting error structure function is then uniquely defined by the spatial cut-off frequency $f_c = 1/2d$ given by the actuator separation d. Véran derived the formula

$$D_{\phi_\perp}(\boldsymbol{\rho}) = \int_{\mathcal{A}} d\mathbf{f}\,[1 - \cos(2\pi\mathbf{f}\cdot\boldsymbol{\rho})]\Phi(\mathbf{f}) \tag{53}$$

for a square integration region where $\mathcal{A} = 1$ for $|f_x|, |f_y| > f_c$ and zero otherwise, while Jolissaint used the formula

$$D_{\phi_\perp}(\boldsymbol{\rho}) = 4\pi \int_{\mathcal{A}} d\mathbf{f}\,[1 - J_0(f\rho)] f\Phi(f) \tag{54}$$

for a circular region, $\mathcal{A} = 1$ for $f > f_c$ and 0 otherwise. Using the numerical evaluation of the PSD with a circular PSD mask and the Wiener-Khinchin theorem, I obtain a fitting error phase variance coefficient $a_F = 0.29$, while Jolissaint obtains a numerical value of 0.274, and Hardy [23] cites a coefficient of $a_F = 0.28$.

These analytical calculations give reasonable numbers, but they overemphasize the sharpness of the high-pass filter which in reality is a smooth function, as seen in figures 1 and 2. Moreover, it violates the separation of the wavefront into orthogonal sets of controlled an uncontrolled modes, which we defined by the DM influence functions (section 2.1). For these reasons we opted to estimate a slightly more realistic filter function from numerical simulations.

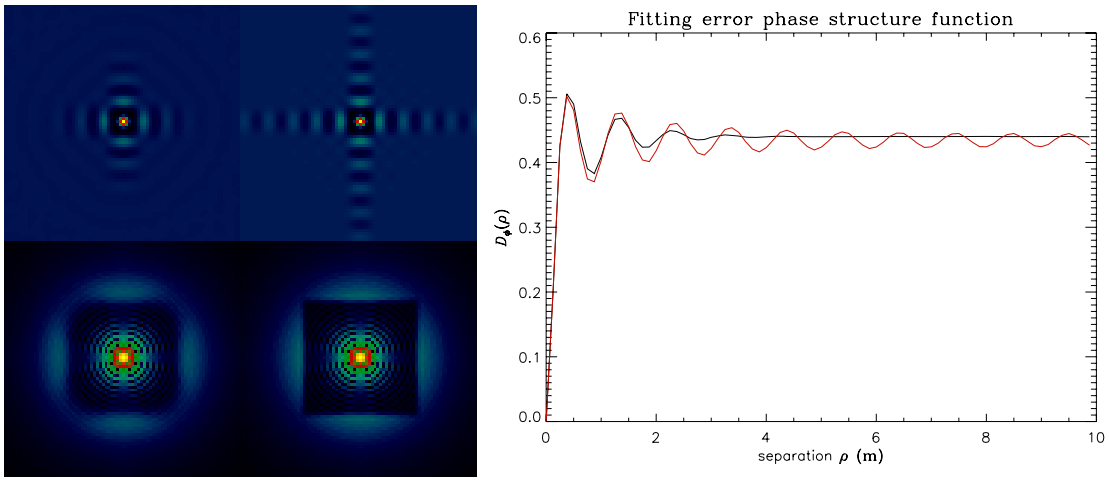

Figure 2: Fitting error OTFs, PSFs and structure functions, comparing the Monte Carlo simulation and the analytical calculation (53). Right: structure functions for the Monte Carlo (black curve) and analytical (red curve) method. Top left: OTFs by the Monte Carlo simulation (left) and the analytical approximation (right). Bottom left: PSFs (including the telescope kernel) from the Monte Carlo simulation (left) and in the analytical approximation (right).

Monte Carlo simulation

The filter function $\mathcal{H}(\mathbf{f})$ was obtained numerically by computing both Φ and $\Phi_\perp$ explicitly in a numerical Monte Carlo simulation of the K2 AO system, and taking the ratio of the two as in (52). $\mathcal{H}(\mathbf{f})$ will in practice not depend on any of the turbulence parameters r_0, L_0 or C_n^2 of the von Karman turbulence model, but only on the shape and arrangement of the influence functions h, and so we only need to pre-compute one filter function $\mathcal{H}$ for each plate scale and PSF reconstruction grid scale that we want to use. For K2 AO this means 4-5 separate filter functions which only need to be computed once.

To avoid edge-effects in the simulation I used periodic random phase screens generated by the FFT method and performed the fitting of the influence functions using an extended actuator grid, covering the entire phase screen. Using a relatively small computational grid this still required 1600 actuators, the central 325 of which belonged to a $D = 10$ m telescope pupil, and the rest only provide boundary conditions (i.e. covering the entire screen with actuators eliminates boundaries altogether). The influence functions used were of the YAO type (section 3.3) with 20% cross-coupling.

The simulation ran for 50000 iterations over 5000 independently generated screens, where each screen was looped over for 10 frames while shifting the screen a few pixels. The PSDs are shown in Fig. 1, where the total input turbulence phase variance was $\sigma_\phi^2 = 10.3$ rad^2, and the residual fitting error phase variance was $\sigma_{\phi_\perp}^2 = 0.224$ rad^2. Since $d/r_0 = 1$ this implies a coefficient $a_F = 0.224$ which appears to be underestimating the fitting error if the correct coefficient should be $a_F = 0.28$ (though we might as well question this number instead). We may expect that this simulation would underestimates the fitting error slightly, since we used a relatively coarse sampling of only 4 pixels per actuator pitch (which cuts off some input power from the PSD). Fig. 2 shows fitting error OTFs, PSFs and structure functions, comparing the Monte Carlo simulation with method 3 of computing the fitting error, i.e. a binary mask on the turbulence PSD. It is seen that using a sharp mask on Φ is going to overemphasize the ringing in the structure function and the OTF, and produce a too sharp inner working region of the PSF. The effect on the Strehl of the FWHM is negligible, but the detailed structure of the PSF halo is clearly affected by the exact shape of the PSD mask.

3.3 DM model

The model of DM influence functions $h_i(\mathbf{x})$ is relevant in several places in the PSF reconstruction algorithm. They define the basis of controlled modes (3) for the residual error structure function (12), and thus determine how WFS signals (including noise, aliasing and turbulence) are propagated into wavefront errors; they define the filter function for the fitting error, and in some anisoplanatism models define the anisoplanatism error propagated onto controlled

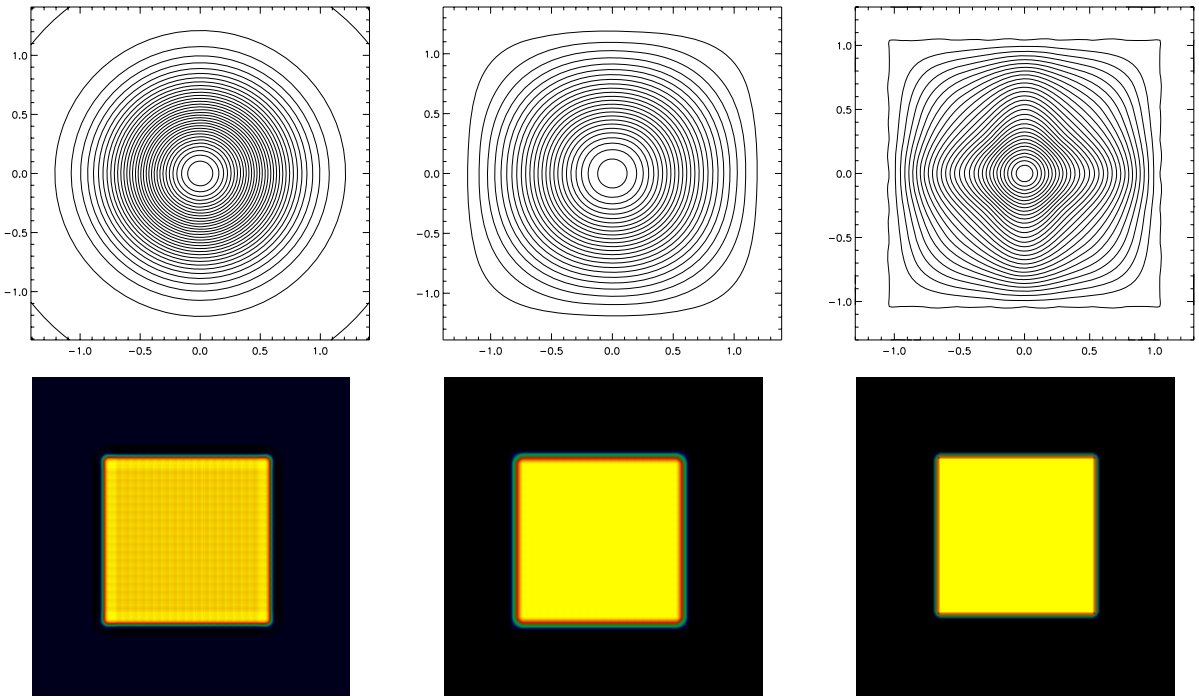

Figure 3: Influence function models, double-Gaussian Keck model (left), the parameterized YAO model (middle), and a bilinear spline model (right), showing contour plots of a single influence function (top row) and the corresponding piston mode produced by a square array of actuators (bottom row). The bilinear spline has no actuator cross-coupling, and produces a perfect piston mode; the double-Gaussian has a lot of cross-coupling and makes a pretty bad piston; the YAO model lies somewhere in between, with a modest amount of cross-coupling and a reasonably flat piston mode.

modes. M. van Dam in [40] finds that a combination of two Gaussian functions can be used to approximate the Xinetics PZT DM in use at the Keck Observatory AO system. This model does not reproduce a piston mode very well, and it does not model the effect of neighboring actuators in square grid layout, which causes the individual influence function do deviate from circular symmetry and attain an x/y symmetric shape instead. Recently a modified Gaussian influence function was presented (Huang et al., "Modified Gaussian influence function of deformable mirror actuators", Optics Express 16, 2008), which offers a lot of improvement over the double-Gaussian model. This model has not yet been implemented or tested within the K2 AO simulation tool, and it is not clear that it would bring any significant improvement over the YAO model.

We have opted for a different influence function model (taken from the YAO simulation package) that may improve somewhat upon the drawbacks of the double-Gaussian. The influence function is given by the following parameterized model:

$$h(x,y) = \begin{cases} g(x)g(y), & |x|,|y| \le p_4 \\ 0, & \text{elsewhere} \end{cases} \tag{55}$$

where

$$g(x) = 1 - |x|^{p_1} + p_3|x|^{p_2}\ln|x|, \tag{56}$$

where the parameters p_1, p_2, p_3 and p_4 are in turn parameterized functions of the coupling constant β. The coupling constant is the only free parameter of this influence function model, and is typically given a value around ~ 0.2. This model has the salient features that it produces a fairly flat and realistic piston mode, and it also progresses from a mostly radial symmetry in the center to an x/y symmetry at the edges, which is a realistic feature that results from having a rectangular layout of actuators on the DM. The parameters of the model are given by:

$$a = [0, 4.49469, 7.25509, -32.1948, 17.9493] \tag{57}$$

$$b = [0, 2.49456, -0.65952, 8.78886, -6.23701] \tag{58}$$

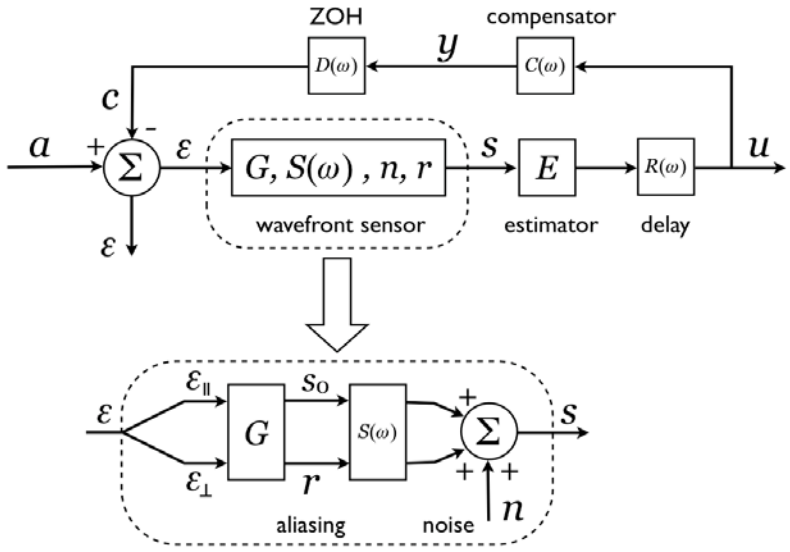

Figure 4: Schematic of AO temporal control loop (top) and a blowup of the WFS model (bottom). E and G are spatial matrix mappings, independent of time, while S, R, C and D are temporal filters, generally matrix-valued but assumed in this analysis to be scalar filters

$$
\begin{aligned}
c &= [0, 1.16136, 2.97422, -13.2381, 20.4395] && (59)\\
p_1 &= a_0 + a_1\beta + a_2\beta^2 + a_3\beta^3 && (60)\\
p_2 &= b_0 + b_1\beta + b_2\beta^2 + b_3\beta^3 && (61)\\
p_4 &= c_0 + c_1\beta + c_2\beta^2 + c_3\beta^3 && (62)\\
p_3 &= \frac{(p_4^{p_2}\beta - 1 + p_4^{-p_1})}{-\log p_4} && (63)
\end{aligned}
$$

where the a, b and c parameters were obtained (not by me) from a fitting procedure. This influence function is shown in the middle panels of Fig. 3, where I also include a simple bilinear influence function (rightmost panels of Fig. 3).

3.4 Covariance matrix $\langle \boldsymbol{\epsilon}\boldsymbol{\epsilon}^T \rangle$

Exact temporal modeling of the residual mode covariance matrix $\langle \boldsymbol{\epsilon}\boldsymbol{\epsilon}^T \rangle$ turns out to be problematic, and most PSF reconstruction implementations so far have applied varying levels of approximation to this aspect of the system modeling. Referring to the generic AO block diagram in Fig. 4, we can examine the loop dynamics in terms of the phase modal coefficients $\mathbf{a}$ (input turbulence), $\mathbf{c}$ (DM mode) and $\boldsymbol{\epsilon}$ (residual error). The other variables are: $\mathbf{s}_0$ is an ideal noise-free and aliasing-free WFS measurement; $\mathbf{n}$ is the noise and $\mathbf{r}$ is the aliasing, and $\mathbf{s}$ is the actual WFS measurement, assuming the components add linearly; the $\mathbf{u}$ and $\mathbf{y}$ are internal variables used in defining the compensator. The $\mathbf{s}$ and $\mathbf{c}$ vectors are the only ones which we have access to from AO telemetry data, and which we must employ in order to estimate $\langle \boldsymbol{\epsilon}\boldsymbol{\epsilon}^T \rangle$.

A subtlety to be aware of is that the low- and high-spatial-frequency modal sets $\phi_{\|}$ and $\phi_{\perp}$ were defined by the DM modal basis $h_i(\mathbf{x})$, and strictly speaking this need not be equivalent to the subsets of ϕ that are aliasing-free and produce aliasing in the WFS, respectively. Hence, the aliasing $\mathbf{r}$ can not be said to have come solely from $\phi_{\perp}$, since the DM influence functions themselves may produce a (very small) amount of aliasing. In practice, however, in a Fried-geometry Shack-Hartmann AO system, the modal basis of the DM influence functions and the basis that is aliasing-free are very close to each other, and to a first-order approximation we can say that aliasing only arises from $\phi_{\perp}$ (and hence $\epsilon_{\perp}$).

To remind ourselves of the context, we are trying to calculate $\langle \boldsymbol{\epsilon}\boldsymbol{\epsilon}^T \rangle$ because it arises in the residual wavefront

error structure function (38) that we defined in Sect. 2.3:

$$D_{\epsilon_\parallel}(\mathbf{x},\boldsymbol{\rho}) = \sum_{i=1}^{N_c}\sum_{j=1}^{N_c} \langle \epsilon_i(t)\epsilon_j(t)\rangle \, [h_i(\mathbf{x}) - h_i(\mathbf{x}+\boldsymbol{\rho})][h_j(\mathbf{x}) - h_j(\mathbf{x}+\boldsymbol{\rho})] \tag{64}$$

Since we can not access directly the vector $\boldsymbol{\epsilon}$, we need to express the covariance matrix $\langle \epsilon\epsilon^T\rangle$ in other variables which can be obtained from AO telemetry data, such as $\mathbf{u}$ (via $\mathbf{s}$). Examining the block diagrams in Fig. 4 of the closed-loop AO system and the WFS model, we can write down the following relationships in the temporal frequency domain (where tilde denotes the temporal Fourier transform):

$$\widetilde{\boldsymbol{\epsilon}} = \widetilde{\mathbf{a}} - \widetilde{\mathbf{c}} \tag{65}$$
$$\widetilde{\mathbf{c}} = D(\omega)C(\omega)\widetilde{\mathbf{u}} \tag{66}$$
$$\widetilde{\mathbf{u}} = R(\omega)E\widetilde{\mathbf{s}} \tag{67}$$
$$\widetilde{\mathbf{s}} = S(\omega)(\widetilde{\mathbf{s}}_0 + \widetilde{\mathbf{r}}) + \widetilde{\mathbf{n}} \tag{68}$$
$$\widetilde{\mathbf{s}}_0 = G\widetilde{\boldsymbol{\epsilon}}_\parallel \tag{69}$$

where all the vectors are represented in Fourier domain as functions of the temporal frequency ω, and we omitted the frequency argument for simplicity. Examples of the temporal filters are given in e.g. [21].

Classical analysis

A classical result useful for AO analysis and simulation, but not so much for PSF reconstruction, is obtained by combining and rearranging terms into the following closed-loop relation:

$$[I + DCRESG]\widetilde{\boldsymbol{\epsilon}} = \widetilde{\mathbf{a}} - DCRE\widetilde{\mathbf{n}} - DCRES\widetilde{\mathbf{r}}, \tag{70}$$

where G is the DM-to-WFS interaction matrix and E is the WFS-to-DM wavefront reconstruction matrix. In the general case, the expression $I + DCRESG$ is matrix valued, and a matrix inverse must be computed for every value of ω in order to solve for $\boldsymbol{\epsilon}$. This appears to be impractical, and a common approach to approximate the solution is to make the following additional assumptions: 1) the transfer functions D, C, R and S are all scalar-valued, and 2) $EG \approx I$. Condition #1 can be met if there is no mix-and-match of different WFS types and DM controllers that have different sets of parameters (no modal control). Condition #2 must generally be treated as an approximation, in particular for the standard MAP or SVD estimator this requirement is known to be violated. But accepting it as an approximation, we can separate the temporal from the spatial operators in (70) and solve for $\boldsymbol{\epsilon}$ simply by scalar division. The result is:

$$\widetilde{\boldsymbol{\epsilon}}(\omega) = \mathcal{H}_\epsilon(\omega)\widetilde{\mathbf{a}}(\omega) - \mathcal{H}_n(\omega)\widetilde{\mathbf{m}}(\omega) - \mathcal{H}_\epsilon(\omega)\widetilde{\mathbf{v}}(\omega), \tag{71}$$

where $\mathcal{H}_\epsilon = 1/(1+\mathcal{H})$ is the error transfer function, $\mathcal{H}_n = DCR/(1+\mathcal{H})$ is the noise transfer function and $\mathcal{H} = DCRS$ is the open loop transfer function. We also introduced the actuator command vectors $\mathbf{m} = E\mathbf{n}$ and $\mathbf{v} = E\mathbf{r}$ for the noise and aliasing error signals propagated onto DM commands. When integrated over the real line, Parseval's theorem allows us to equate $\langle \epsilon_i\epsilon_j\rangle = \langle \widetilde{\epsilon}_i\widetilde{\epsilon}_j^*\rangle$, where superscript asterisk * denotes the complex conjugate. We may invoke this equality here since we know the PSDs must be band-limited, and there is no power in the zero-frequency component (we remove the DC term). The covariance matrix elements are then

$$\langle \epsilon_i\epsilon_j\rangle = \int d\omega \, \langle \widetilde{\epsilon}_i(\omega)\widetilde{\epsilon}_j^*(\omega)\rangle \tag{72}$$
$$= \int d\omega \, |\mathcal{H}_\epsilon|^2 \, \langle \widetilde{a}_i(\omega)\widetilde{a}_j^*(\omega)\rangle + \int d\omega \, |\mathcal{H}_n|^2 \, \langle \widetilde{m}_i(\omega)\widetilde{m}_j^*(\omega)\rangle + \int d\omega \, |\mathcal{H}_\epsilon|^2 \, \langle \widetilde{v}_i(\omega)\widetilde{v}_j^*(\omega)\rangle, \tag{73}$$

where it was assumed that $\mathbf{a}$, $\mathbf{m}$ and $\mathbf{v}$ are all statistically uncorrelated (which they are). This is a nice expression for theoretical modeling, but not very useful for PSF reconstruction since it contains the open loop turbulence vector $\mathbf{a}$ which is unknown. The covariance matrix needs to be reformulated in terms of $\mathbf{u}$.

Method 1

For PSF reconstruction, we can explore the direct relation between $\boldsymbol{\epsilon}$ and $\mathbf{u}$ that is given by equations (67)-(69), which reads

$$\widetilde{\mathbf{u}} = RE\left[S(G\widetilde{\boldsymbol{\epsilon}} + \widetilde{\mathbf{r}}) + \widetilde{\mathbf{n}}\right] \tag{74}$$

Without (much) loss of generality we may again assume that the temporal filters are scalar-valued, which gives

$$EG\widetilde{\boldsymbol{\epsilon}} = \frac{1}{RS}\widetilde{\mathbf{u}} - \frac{1}{S}\widetilde{\mathbf{m}} - \widetilde{\mathbf{v}}. \tag{75}$$

This expression can be used to evaluate the covariance matrix $\langle \boldsymbol{\epsilon}\boldsymbol{\epsilon}^T \rangle$ at varying levels of approximation. At the most drastic level of approximation we ignore the temporal filtering altogether (e.g. assume that the transfer functions are equal to one), and also invoke as before the approximation $EG \approx I$, which gives the simplest possible form:

$$\boldsymbol{\epsilon} = \mathbf{u} - \mathbf{m} - \mathbf{v}. \tag{76}$$

In evaluating the covariance matrix one will obtain cross-terms, and it may be a matter of taste or prudence how to arrange the expression before computing the covariance, which determines whether you will have cross-terms with $\boldsymbol{\epsilon}$ or with $\mathbf{u}$. The traditional choice has been to compute the cross-terms in terms of $\boldsymbol{\epsilon}$, and following this pattern we obtain

$$\langle \boldsymbol{\epsilon}\boldsymbol{\epsilon}^T \rangle = \langle \mathbf{u}\mathbf{u}^T \rangle - \langle \mathbf{m}\mathbf{m}^T \rangle - \langle \mathbf{v}\mathbf{v}^T \rangle - 2\langle \boldsymbol{\epsilon}\mathbf{m}^T \rangle - 2\langle \boldsymbol{\epsilon}\mathbf{v}^T \rangle. \tag{77}$$

Véran [41] argues that the aliasing terms can be approximated as $-\langle \mathbf{v}\mathbf{v}^T \rangle - 2\langle \boldsymbol{\epsilon}\mathbf{v}^T \rangle \approx \langle \mathbf{v}\mathbf{v}^T \rangle$, and assuming the noise to be uncorrelated with ϵ gives the solution:

$$\langle \boldsymbol{\epsilon}\boldsymbol{\epsilon}^T \rangle = \langle \mathbf{u}\mathbf{u}^T \rangle - \langle \mathbf{m}\mathbf{m}^T \rangle + \langle \mathbf{v}\mathbf{v}^T \rangle. \tag{78}$$

Method 2

Keeping the modeling of the aliasing cross-terms as in Method 1, but going back to include the previously omitted temporal filters, gives the somewhat more complicated expression

$$\langle \epsilon_i \epsilon_j \rangle = \langle v_i v_j \rangle - \langle m_i m_j \rangle \int d\omega \ \mathrm{sinc}^{-2}(\omega T) + \int d\omega \ \langle \widetilde{u}_i(\omega) \widetilde{u}_j^*(\omega) \rangle \, \mathrm{sinc}^{-2}(\omega T), \tag{79}$$

where it was assumed that R is a pure delay τ, i.e. $R(\omega) = \exp(-2\pi i \tau)$ and $S(\omega) = \mathrm{sinc}(\omega T)\exp(-i\pi\omega T)$, so that taking the modulus squared eliminates the complex exponentials. (see Sect. 3.5 for an evaluation of the cross-term). It was also assumed that the temporal noise PSD is constant (i.e. white noise – see Sect. 3.7), and the covariance term could be was extracted from the integral. While this expression invokes different (fewer) approximations, it is instead rather more demanding to compute since we now need cross-PSDs for all the time series of $\mathbf{u}$. This might not be so onerous as it sounds though. With 349 actuators we then "only" have a total of 61075 PSDs $\langle \widetilde{u}_i(\omega) \widetilde{u}_j^*(\omega) \rangle$ to compute. This is probably quite manageable, since they are computed by 1-dimensional Fourier transforms, they can be computed off-line, and we probably don't need very high resolution either (to be verified), since we don't expect a lot of power at the lowest temporal frequencies. A real-time calculation it is not, however.

Method 3

This is variation that can be applied equivalently to either Method #1 or Method #2, since it involves only a different treatment of the spatial operators. The analysis will derived here for Method #1. Up until now we have not cared about the actual form of the reconstructor E, but we made the statement that $EG \approx I$ as invoked in both Method #1 and #2 might be a pretty bad approximation. Assuming a specific form for E we can develop expression (75) further. Currently in use at the Keck AO system is a MAP estimator of the form

$$E_{\mathrm{MAP}} = (G^T C_n^{-1} G + C_c^{-1})^{-1} G^T C_n^{-1}, \tag{80}$$

where $C_n = \langle \mathbf{n}\mathbf{n}^T \rangle$ is the noise covariance matrix and $C_c = H^+ \langle \boldsymbol{\phi}_\parallel \boldsymbol{\phi}_\parallel^T \rangle (H^+)^T$ is the open loop phase covariance matrix mapped onto actuators. Instead of invoking $EG \approx I$ in (75) we expand the expression, defining for brevity the matrix $A = G^T C_n^{-1} G$

$$A\boldsymbol{\epsilon} = (A + C_c^{-1})\mathbf{u} - G^T C_n^{-1}(\mathbf{n} + \mathbf{r}). \tag{81}$$

Assuming that the inverse A^{-1} exists (A is usually singular, and the inverse can be approximated by SVD), we have the new expression for the residual mode covariance matrix:

$$\boldsymbol{\epsilon} = (I + A^{-1}C_c^{-1})\mathbf{u} - E_{\mathrm{GM}}(\mathbf{n} + \mathbf{r}), \tag{82}$$

where $E_{\mathrm{GM}} = A^{-1}G^T C_n^{-1} = (G^T C_n^{-1} G)^{-1} G^T C_n^{-1}$ is the Gauss-Markov estimator. This is only subtly different from (75) in Method #2, as the approximation now takes place in a different location: instead of invoking $EG \approx I$ we have to approximate A^{-1} by filtering its singular modes in the inversion. I have no idea if this is a better or a poorer representation, but it would be a simple thing to compare it to Method #1, and all those cross-PSDs are going to be computed anyway we can also do the comparison with Method #2.

3.5 Spatial aliasing

WFS aliasing covariance matrices are rather difficult to calculate analytically, to say nothing of its cross terms with other effects. The approach adopted here is to model the aliasing PSD in spatial Fourier domain, obtain the correlation function by Fourier transform and then propagate the error onto the controlled modes by the inverse of the influence function matrix. The expression for the WFS aliasing covariance matrix (as was shown in Sect. 3.4) propagated onto DM actuators is:

$$\langle v_i v_j \rangle = \int d\omega\, T(\omega) E \langle r_i(\omega) r_j^*(\omega) \rangle E^T, \tag{83}$$

where $T(\omega)$ is a temporal filter function. Modeling the cross-PSDs $\langle r_i(\omega) r_j^*(\omega) \rangle$ appear to be not very straightforward (I have no idea how to do it), and a different strategy for approximating $\langle \mathbf{v}\mathbf{v}^T \rangle$ will be explored in this section.

There are well-developed spatial Fourier domain models that predict the phase-error PSD resulting from WFS aliasing. The method I propose here is to use such a PSD-based aliasing model, then by the Wiener-Khinchin theorem one can obtain the corresponding phase correlation function. This correlation function can then be transformed into $\langle \mathbf{v}\mathbf{v}^T \rangle$ via the inverse of the actuator cross-coupling matrix, which can be generated numerically for a given DM actuator pattern and DM influence function. The derivation of the PSD is given in Sect. 5 of the appendix ("Analytical evaluations of closed-loop adaptive optics spatial power spectral densities"). The formula (assuming a leaky integrator) is given by

$$\Phi_{alias}(\mathbf{f}) = \frac{0.00575}{\mathrm{sinc}^2(\mathbf{f}d)} \times \sum_{\mathbf{m}\neq(0,0)} \frac{(\mathbf{f}^{-1}\cdot\mathbf{f}_m)^2\,\mathrm{sinc}^2(d\mathbf{f}_m)}{(|\mathbf{f}_m|^2 + f_0^2)^{11/6}} \sum_{l=1}^{N_l} r_{0l}^{-5/3} \mathrm{sinc}^2(\mathbf{f}_m \cdot \mathbf{v}_l t_i) B_l(\mathbf{f}_m) \tag{84}$$

where $\mathbf{f}_m = (f_x - m/d, f_y = n/d)$ and d is the sub-aperture size. The function $B_l(\mathbf{f}_m)$ is the closed-loop attenuation factor, which in open loop is 1, and which for a leaky integrator has the form

$$B_l(\mathbf{f}_m) = \frac{g^2}{1 - 2a\cos b_l + a^2}, \tag{85}$$

where $a = \xi - g$, with ξ being the leak factor and g the loop gain, and $b_l = 2\pi \mathbf{f}_m \cdot \mathbf{v}_l t_i$, where t_i is the WFS integration time and $\mathbf{v}_l$ is the wind profile. This assumes the Taylor hypothesis and a layered turbulence model $\{r_{0l}, v_l\}$, as defined in Sect. 3.1. It may be possible to also derive a B_l for a double-pole controller, but I have not attempted this yet.

The phase variance due to aliasing has been quoted by various authors as $\sigma^2_{alias} \approx 0.3\sigma^2_{fitting}$ for a Shack-Hartmann WFS. What the closed loop analysis here shows is that this is at best roughly true, and there can be significant deviations from this rule-of-thumb in certain regions of parameter space (see Fig. 5). It is understood that the aliasing error is, broadly speaking, anti-correlated with the servo-lag error. At lower frame rates or higher wind speeds, the orthogonal phase $\phi_\perp$ that results in aliasing will be partially averaged out while the WFS is integrating photons, and hence the aliasing error will decrease (at the expense of an increased bandwidth error). This behavior is captured realistically by the PSD model (84), as illustrated in Fig. 5. So the first virtue of using this PSD model is to obtain a more realistic estimate of the total aliasing variance to insert into the PSF reconstruction algorithm, which accounts for the closed-loop temporal filtering.

Next we can obtain the aliasing correlation function $C_{alias}(\boldsymbol{\rho})$ by Fourier transform of $\Phi_{alias}(\mathbf{f})$. Upon reformatting a little, C_{alias} becomes the phase covariance matrix defined at the actuator positions $C_{alias} = \langle \boldsymbol{\varphi}_\mathbf{v} \boldsymbol{\varphi}_\mathbf{v}^T \rangle$, where

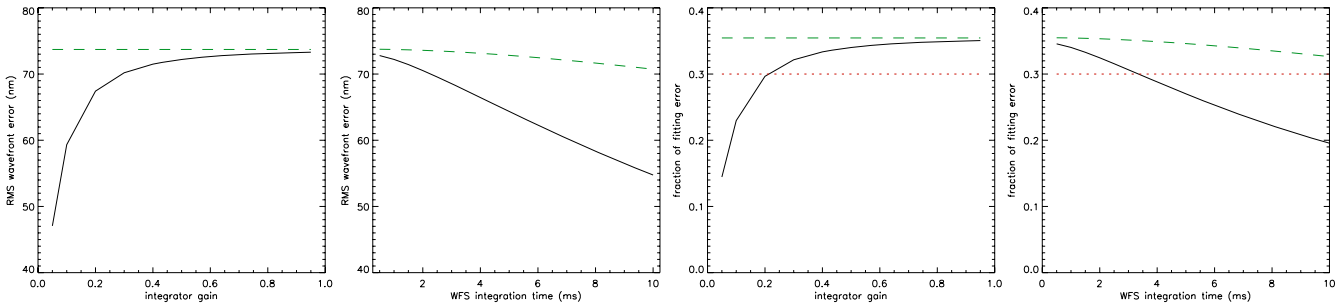

Figure 5: Aliasing wavefront error computed from analytical PSDs, as a function of WFS integration time t_i and loop gain g (solid curves are the closed-loop calculation; dashed curves are open loop).

$\boldsymbol{\varphi}_{\mathbf{v}} = H\mathbf{v}$ (now $\mathbf{v}$ is the aliasing command vector, not the wind velocity), and H is the DM influence function matrix. Conversely, $\mathbf{v} = H^{+}\boldsymbol{\varphi}_{\mathbf{v}}$, and we finally obtain the aliasing covariance matrix as

$$\langle \mathbf{v}\mathbf{v}^T \rangle = H^{+} \langle \boldsymbol{\varphi}_{\mathbf{v}} \boldsymbol{\varphi}_{\mathbf{v}}^T \rangle (H^{+})^T. \tag{86}$$

The virtue of doing it this way, rather than just taking the aliasing PSD Φ_{alias} and computing the OTF directly by the sequence established in Sect. 2.1, is that error now gets propagated onto the mirror modes properly. In a direct calculation of the OTF from the PSD we would not be observing the definition of the parallel phase $\varphi_{\parallel}$, as the modal basis of the DM modes. All the same, this $\langle \mathbf{v}\mathbf{v}^T \rangle$ is a model-based approximation to the real aliasing contribution, since we basically tossed out the originally derived expression in (83) and put in place a whole new estimation of the term.

3.6 Tilt structure function

The tip/tilt (TT) structure function is stationary and can be taken outside of the OTF integral, even in the non-stationary computation of the rest of the OTF. The structure function is given by the quadratic form

$$D_{tt}(\boldsymbol{\rho}) = \frac{4}{R^2} \left[\Gamma_{11}^2 \rho_x^2 + \Gamma_{22}^2 \rho_y^2 + 2\Gamma_{12} \rho_y \rho_x \right], \tag{87}$$

where the gamma coefficients are elements of the covariance matrix

$$\Gamma = \begin{bmatrix} \langle c_2^2 \rangle & \langle c_2 c_3 \rangle \\ \langle c_3 c_2 \rangle & \langle c_3^2 \rangle \end{bmatrix}, \tag{88}$$

and $c_{1,2}$ are the estimated residual tip/tilt coefficients in the phase error expansion $\varphi_{tt}(\mathbf{x}, t) = c_2(t)Z_2(\mathbf{x}) + c_3(t)Z_3(\mathbf{x})$, where the Zernike modes are defined as $Z_2(\mathbf{x}) = 2x$ and $Z_3(\mathbf{x}) = 2y$. Since D_{tt} is independent of $\mathbf{x}$ it can be taken outside of the OTF integral, under the assumption that ϵ and $c_{2,3}$ are orthogonal, i.e. TT has been perfectly filtered from the DM commands. This may not be completely true, and an alternative approach could include TT in the non-stationary calculation by appending TT to the DM set $h(\mathbf{x})$ and ϵ. In the separable case, the quadratic form of D_{tt} makes the TT OTF into a Gaussian function, with the width and orientation specified by the covariance matrix Γ:

$$\langle B_{tt}(\boldsymbol{\rho}/\lambda) \rangle = \exp\left\{ -\frac{1}{2} D_{tt}(\boldsymbol{\rho}) \right\} \tag{89}$$

3.7 Noise covariance matrix

The principal noise estimation techniques employed are:

1. Modeling from first principles, detector physics and photon statistics (e.g. Véran et al. 1997 [41], Jolissaint et al. 2004 [25])

2. Curl calculations (e.g. Tyler 2000 [37] and tOSC reports no. TR-816 and TR-881; also Hardy 1998 [23])

3. Temporal autocorrelation of control loop variables (e.g. Gendron & Léna 1995 [22], Egner 2004 [??])

The first two methods both suffer from the problematic of accounting for deviations from the ideal, for instance partially illuminated sub-apertures (at Keck this is a function of time, since the WFS rotates with respect to the telescope pupil) or spot aberrations. With the physical modeling it is probably impossible to know and model these imperfections accurately. The curl methods can only estimate an average noise level, and again one must be careful to exclude sub-apertures that may be corrupted by external effects that produce a non-zero curl not related to either the noise or the aliasing. The curl method is probably not useful for us in this application.

The average sub-aperture intensity levels are reported by TRS, so could be used as input in method 1. But there is the additional problem of estimating the spot size with undersampled sub-apertures, since a given pixel-noise level will translate into varying centroid noise levels depending on the spot size and the centroid gain setting. This complicates calculations from first principles considerably by introducing another poorly known quantity. There are proposed methods for estimating the spot size (e.g. TT dithering or slope discrepancy [38]), but their accuracy and viability are somewhat disputed, and may work even worse with LGS.

The autocorrelation method has the virtue that it (if it worked) would characterize each sub-aperture from the telemetry data itself without any a priori assumptions, so that particular effects causing the noise level to deviate from the norm are taken into consideration. It becomes less straightforward in closed loop where the turbulence correlation is much smaller, and to make the method work a somewhat ad hoc term is applied (Hamilton 1994). It may be considered whether the method could instead be applied directly to the actuator commands rather than sub-aperture slopes. While this requires a lot more computation (the matrix is no longer diagonal), we would get the propagated noise on actuators directly and also avoid the problem of needing to estimate spot sizes, and also avoid the closed-loop complication. This would be ideal, but unfortunately it has so far proven to be difficult to get good results from this method.

Physical modeling

Using standard formulas for Shack-Hartmann centroid noise variances from e.g. Hardy 1998 [23], or the more specific derivations by e.g. Jolissaint et al. 2004 [25]), we use a formula for the centroid standard deviation like

$$\sigma_2 = \frac{8}{\pi}\frac{\theta}{SNR}, \tag{90}$$

$$SNR = \frac{n_{phot}}{\sqrt{n_{phot} + N_{pix}(n_{bg} + e^2)}}, \tag{91}$$

where n_{phot} is the sub-aperture photoelectrons count given by TRS, θ is the estimated spot size, n_{bg} is the estimated number of background photoelectrons per detector pixel, N_{pix} is the number of detector pixels per sub-aperture and e is the RMS of a Gaussian electronic read-out noise. The noise RMS σ_2 multiplied by the centroid gain forms the RMS noise vector $\langle \mathbf{n} \rangle$, and we can construct the noise covariance matrix $\langle \mathbf{n}\mathbf{n}^T \rangle$ by populating the diagonal with σ_2^2, that is $\langle n_i n_j \rangle = \delta_{ij}\sigma_2^2(i)$, for sub-aperture i. The propagated noise covariance is obtained by multiplying with the reconstruction matrix E: $\langle \mathbf{m}\mathbf{m}^T \rangle = E\langle \mathbf{n}\mathbf{n}^T \rangle E^T$.

Curl calculation

(we will not do it this way, but I wrote this down anyway while I was thinking about it)
Vector algebra shows that $\nabla \times \nabla\phi = 0$ (curl grad $\phi = 0$) in a simply connected domain ϕ, which we can exploit as a constraint on the slope measurement $\mathbf{s} = \nabla\phi$. In matrix notation, the curl $\mathbf{q}$ can be computed on a slope vector $\mathbf{s}$ by a linear operator Q

$$\mathbf{q} = Q\mathbf{s}, \tag{92}$$

where the curl matrix Q has the dimensions $N_r \times N_m$, the number of curls N_r times the number of measurements N_m. When implemented in practice, one should also exclude sub-apertures with partial illumination or otherwise affected to produce a non-zero curl that does not originate from the aliased wavefront measurement or detector noise. *(Question: does the segmented primary mirror or the segment aberrations prevent a curl-based noise estimation from being carried out?)* The WFS slope vector can be written $\mathbf{s} = \mathbf{s}_0 + \mathbf{r} + \mathbf{n}$, where $\mathbf{s}_0$ is the aliasing-free turbulence measurement, $\mathbf{r}$ is the aliasing vector, and $\mathbf{n}$ is the noise. Since $Q\mathbf{s}_0 = 0$ and $\langle r_i n_j \rangle = 0 \; \forall \; \{i, j\}$ we have that

$$\mathbf{q} = Q\mathbf{r} + Q\mathbf{n} \tag{93}$$

and

$$\sigma_q^2 = \langle \mathbf{q}^T \mathbf{q} \rangle = \langle \mathbf{r}^T Q^T Q \mathbf{r} \rangle + \langle \mathbf{n}^T Q^T Q \mathbf{n} \rangle \quad (94)$$

$$= \langle \mathbf{r}^T Q^T Q \mathbf{r} \rangle + \mathrm{Tr}(Q^T Q)\sigma_n^2, \quad (95)$$

where σ_n^2 is the noise variance in a single sub-aperture, and we assumed that the noise is uncorrelated between sub-apertures, i.e. the covariance matrix $\langle \mathbf{n}\mathbf{n}^T \rangle = \sigma_n^2 I$ is proportional to the identity matrix. The aliasing may be correlated across the WFS however. There may be different ways of using this information. If we had a model for the aliasing curl variance $\sigma_{q_r}^2 = \langle \mathbf{r}^T Q^T Q \mathbf{r} \rangle$, we could measure the total curl variance σ_q^2 and solve for the noise variance:

$$\sigma_n^2 = \frac{\sigma_q^2 - \sigma_{q_r}^2}{\mathrm{Tr}(Q^T Q)}. \quad (96)$$

Autocorrelation

We investigate whether this can be done on the actuators, to get the propagated noise directly. The actuator cross-correlation as a function of time l is

$$V_{xy}(l) = N^{-1} \sum_{i=l}^{N} (x_i - \langle x \rangle)(y_{i-l} - \langle y \rangle) \quad (97)$$

$$= \langle (x_i - \langle x \rangle)(y_{i-l} - \langle y \rangle) \rangle \,. \quad (98)$$

If the loop frame rate is much faster than the turbulence decorrelation time, then the noise level can be approximated by

$$V_{xy}(0) - V_{xy}(1) = \langle (x_0 - \langle x \rangle)(y_0 - \langle y \rangle) \rangle - \langle (x_1 - \langle x \rangle)(y_0 - \langle y \rangle) \rangle \quad (99)$$

$$= \langle (x_0 - x_1)(y_0 - \langle y \rangle) \rangle \quad (100)$$

$$= \langle (x_0 - x_1) y_0 \rangle \,, \quad (101)$$

where it was assumed that $\langle x_0 \rangle = \langle x_1 \rangle$ by ergodicity. The result 101 is straightforward to compute from TRS data by shifting the telemetry stream one time step, taking the difference and matrix multiplying with itself to give the actuator noise covariance matrix. This is similar to a high-bandwidth approximation, but we avoid the problem of estimating centroid gains. At lower bandwidths or shorter turbulence coherence times, one needs to calculate the cross-correlation at a few more time steps, i.e. $V_{xy}(2), V_{xy}(3)$ etc in order to extrapolate by curve fitting the noise-free correlation at the origin $V'_{xy}(0)$. The noise level is then estimated from $V_{xy}(0) - V'_{xy}(0)$, but the remaining problem not solved here is how to account for temporally filtered noise whose correlation function is not a delta function.

3.8 Other components

r_0 and L_0 estimation

Method implemented [32, 39], undergoing validation and testing. Algorithm for r_0 needs tuning – loop dynamics not taken out of the estimation (this problem almost exactly the same as the PSF reconstruction problem itself, and suffers from the same approximations and limitations). Will try to data mine interferometer fringe tracker data for L_0 and correlate with MASS/DIMM measurements and model fitting to get more insights. (code for this)

Static aberrations

Known static aberrations may be included in the OTF calculation by adding a fixed component γ to the phase ϕ. This increases the computational load somewhat by making the OTF integrand complex valued, but should not be an issue. Since γ is not a stochastic variable, it can be taken outside of the ensemble average, and the OTF computed with the modified pupil function $P(\mathbf{x}) \to P(\mathbf{x}) \exp[i\gamma(\mathbf{x})]$. These aberrations could include all types of common-path errors, provided they can be measured or estimated somehow, such as for instance uncorrected segment aberrations. It is less clear to me how one would try to include non-common path aberrations, such as distortions in the NIRC2 camera. After image sharpening, there will still be higher-order non-common path aberrations, and moreover these

will vary across the field of view. If the aberrations do not vary over time, it might be possible to map them out across the focal plane as a set of Zernike coefficients, by doing the image sharpening at multiple locations in the focal plane. This might allow one to calculate the distortion that should be included in the PSF reconstruction when doing it for a field position other than the currently calibrated one, as for instance would be the case for anisoplanatic PSF reconstruction. But even in this case, we can only hope to catch the low-frequency modes that can represented by the DM, and we have no way of measuring aberrations on higher spatial frequencies that go into the PSF.

Spot size estimation

Maybe like van Dam 2005 [38] (needs to be developed, validated). Doesn't work with LGS. More on slope discrepancy: [37]. Alternatively tip/tilt dithering.

4 Anisoplanatism

This section was originally "Outer scale effects on anisoplanatism in adaptive optics," R. Flicker, August 21, 2008.

Abstract

The structure functions for angular and focal anisoplanatism in an astronomical adaptive optics system are derived for the case of a finite outer scale in a von Karman type turbulence model. The results derived are applicable to the problem of point spread function (PSF) reconstruction and anisoplanatism PSF modeling. The analytical von Karman model is compared with numerical simulations and with an analytical Kolmogorov anisoplanatism model. It is found that for 10-meter class telescopes, an outer scale smaller than 30 meters can have a non-negligible impact on the anisoplanatism PSF estimation, and under these conditions the von Karman structure function model should be preferred.

Introduction

Astronomical adaptive optics (AO) compensates for turbulence-induced wave-front aberrations in the direction of a reference light source, most commonly a natural guide star (NGS). Angular anisoplanatism in a conventional NGS AO system manifests at angular positions on the sky $\boldsymbol{\theta} = (\theta_x, \theta_y)$ that are different from the position of the NGS, which we may take to define the zero position $\boldsymbol{\theta} = 0$ in the following. Wave-fronts propagating at an angle $\boldsymbol{\theta} \neq 0$ through the atmosphere will acquire aberrations from turbulence that are different from those measured and corrected by the AO system, which gives rise to the field-dependent wave-front error in the telescope pupil plane that is called anisoplanatism. This paper is cumulative with previous investigations into the properties of anisoplanatism by deriving two new results, relating to the effects of a finite turbulence outer scale. Most adaptive optics analysis in astronomy relies on variants of the Kolmogorov turbulence model, which has been experimentally verified by numerous observations, including [27, 7], but there is still much uncertainty regarding the nature of the power spectrum at lower spatial frequencies, and the validity of the von Karman outer scale model. To date there has been no routine outer scale monitoring implemented at astronomical observatories, which makes the outer scale a poorly known quantity. For the purpose of this paper, however, a simplistic model will adopted wherein the outer scale is independent of altitude and zenith angle. Both of these constraints can be relaxed and a more detailed model included in the analysis, should more information on the outer scale become available.

The current investigation is primarily motivated by a problem in point spread function (PSF) reconstruction, where explicit knowledge of the structure function and a viable way to compute the optical transfer function (OTF) is required. Pertinent reasons for astronomers for wanting to know the PSF include the potential for more accurate photometry and astrometry, and improved deconvolution reliability when the PSF is better known, see e.g. [11, 10, 26, 16, 33, 4]. Anisoplanatism in adaptive optics has been analyzed assuming Kolmogorov turbulence statistics in many previous instances, including comprehensive studies by, e.g., Fried [18], Fried & Belsher [19], Sasiela [31] and Tyler [36]. These studies are chiefly concerned with calculating phase variances and Strehl ratios directly, in general not yielding intermediate results that are suitable for the problem of PSF reconstruction. In the Kolmogorov turbulence model with an infinite outer scale, the angular anisoplanatism structure function was derived by Britton [6] (see also Sect. 4.1). Of interest to the topic of PSF reconstruction is to know within which parameter space of outer scale and telescope size the Kolmogorov model remains a good approximation, and beyond which a von Karman model that incorporates a finite outer scale ought to be applied instead.

4.1 Angular anisoplanatism

Denote the optical phase of the wave-fronts integrated along the line of sight of the AO reference beam "a" and the observing direction "b" by $\phi_a(\mathbf{r}, t)$ and $\phi_b(\mathbf{r}, t)$, where $\mathbf{r} = (x, y)$ is a spatial coordinate in the telescope pupil plane and ϕ_b is inclined by an angle $\boldsymbol{\theta}$ to ϕ_a. The instantaneous anisoplanatism phase error ϕ_Δ is

$$\phi_\Delta(\mathbf{r}, t) = \phi_a(\mathbf{r}, t) - \phi_b(\mathbf{r}, t), \tag{102}$$

and the anisoplanatism structure function is given by

$$D_\Delta(\mathbf{r}_1, \mathbf{r}_2, \boldsymbol{\theta}) \quad = \quad \langle |\phi_\Delta(\mathbf{r}_1, t) - \phi_\Delta(\mathbf{r}_2, t)|^2 \rangle \tag{103}$$

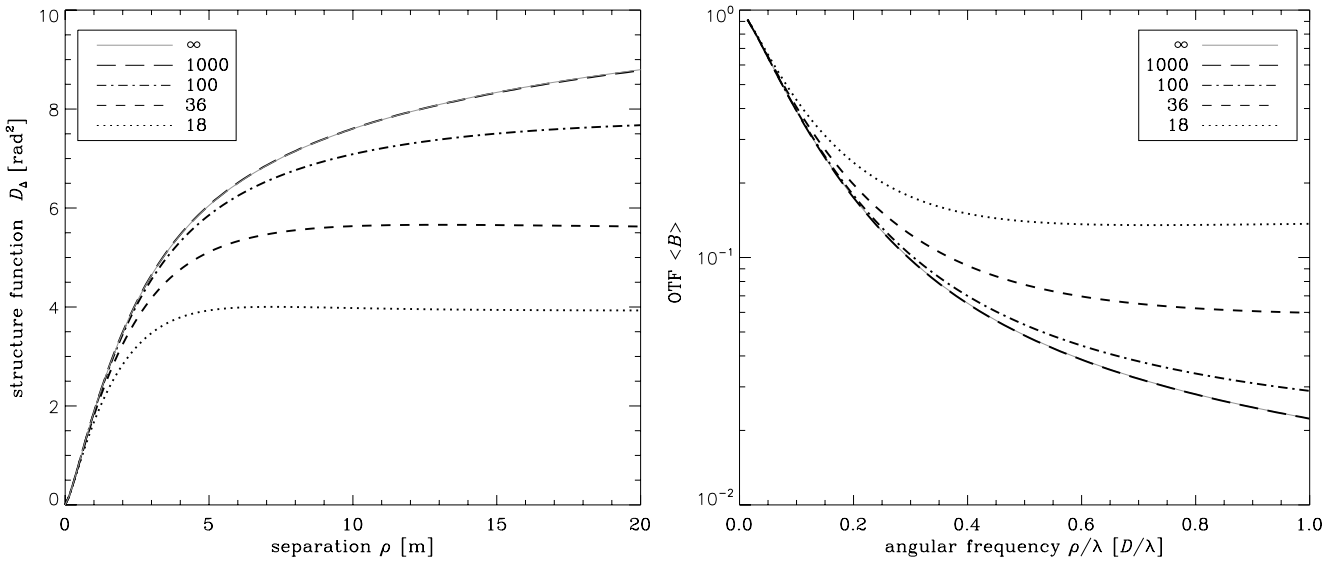

Figure 6: Left: Angular anisoplanatism (NGS) structure functions for different L_0 (cut along the positive x-axis) at $\theta = 42.4''$. Angular anisoplanatism (NGS) OTFs for different L_0 (cut along the positive x-axis) at $\theta = 42.4''$.

$$= \langle|\phi_a(\mathbf{r}_1)|^2\rangle + \langle|\phi_b(\mathbf{r}_1)|^2\rangle + \langle|\phi_a(\mathbf{r}_2)|^2\rangle + \langle|\phi_b(\mathbf{r}_2)|^2\rangle \quad (104)$$

$$- \; 2\langle\phi_a(\mathbf{r}_1)\phi_b(\mathbf{r}_1)\rangle - 2\langle\phi_a(\mathbf{r}_2)\phi_b(\mathbf{r}_2)\rangle - 2\langle\phi_a(\mathbf{r}_1)\phi_a(\mathbf{r}_2)\rangle - 2\langle\phi_b(\mathbf{r}_1)\phi_b(\mathbf{r}_2)\rangle \quad (105)$$

$$+ \; 2\langle\phi_a(\mathbf{r}_1)\phi_b(\mathbf{r}_2)\rangle + 2\langle\phi_b(\mathbf{r}_1)\phi_a(\mathbf{r}_2).\rangle \quad (106)$$

Britton [6], based on the work of Tyler [35, 36], derives the following form for the anisoplanatism structure function under Kolmogorov turbulence statistics

$$D_\Delta(\boldsymbol{\rho},\boldsymbol{\theta}) = 2.91k^2\int_0^\infty dz\, C_n^2(z)\left\{2|z\boldsymbol{\theta}|^{5/3} + 2|\boldsymbol{\rho}|^{5/3} - |\boldsymbol{\rho}+z\boldsymbol{\theta}|^{5/3} - |\boldsymbol{\rho}-z\boldsymbol{\theta}|^{5/3}\right\}, \quad (107)$$

where $C_n^2(z)$ is the refractive index structure constant, $k = 2\pi/\lambda$ and λ is the imaging wavelength. This structure function is stationary, since D_Δ depends spatially only on the separation $\boldsymbol{\rho} = \mathbf{r}_1 - \mathbf{r}_2$ and not on $\mathbf{r}_1$ and $\mathbf{r}_2$ independently. To include a finite outer scale L_0, we must calculate the covariance terms in Eq. (103) using the von Karman power spectrum. Ellerbroek [12] derives a general expression for a covariance element of the type $\langle c_i c_j\rangle$ in von Karman statistics, where

$$c_i(t) = \int d\mathbf{r}\, w_i(\mathbf{r})\,\phi_i(\mathbf{r},t), \quad (108)$$

$$\phi_i(\mathbf{r},t) = k\int_0^\infty dz\, n[\mathbf{p}_i(\mathbf{r},z),z,t], \quad (109)$$

where n is the refractive index along the ray path $\mathbf{p}_i$ of ray i, and w_i is a weighting function. In the form that applies to the current analysis, the covariance element is calculated by Ellerbroek as

$$\langle c_i c_j\rangle = 0.060912k^2L_0^{5/3}\iint d\mathbf{r}\,d\mathbf{r}'\,w_i(\mathbf{r})w_j(\mathbf{r}')\int_0^\infty dz\, C_n^2(z)\, I[\alpha_{ij}(\mathbf{r},\mathbf{r}',z)]. \quad (110)$$

The function $I(\alpha)$ is given by

$$I(\alpha) = \frac{\alpha^{5/6}K_{5/6}(\alpha)}{2^{5/6}\Gamma(11/6)}, \quad (111)$$

where K is a modified Bessel function of the second kind, and the argument α_{ij} is given by $\alpha_{ij} = f_0|\mathbf{p}_i(\mathbf{r},z) - \mathbf{p}_j(\mathbf{r}',z)|$ with $f_0 = 2\pi L_0^{-1}$. Note that L_0 here denotes the propagated outer scale as observed in optical wave-fronts at the

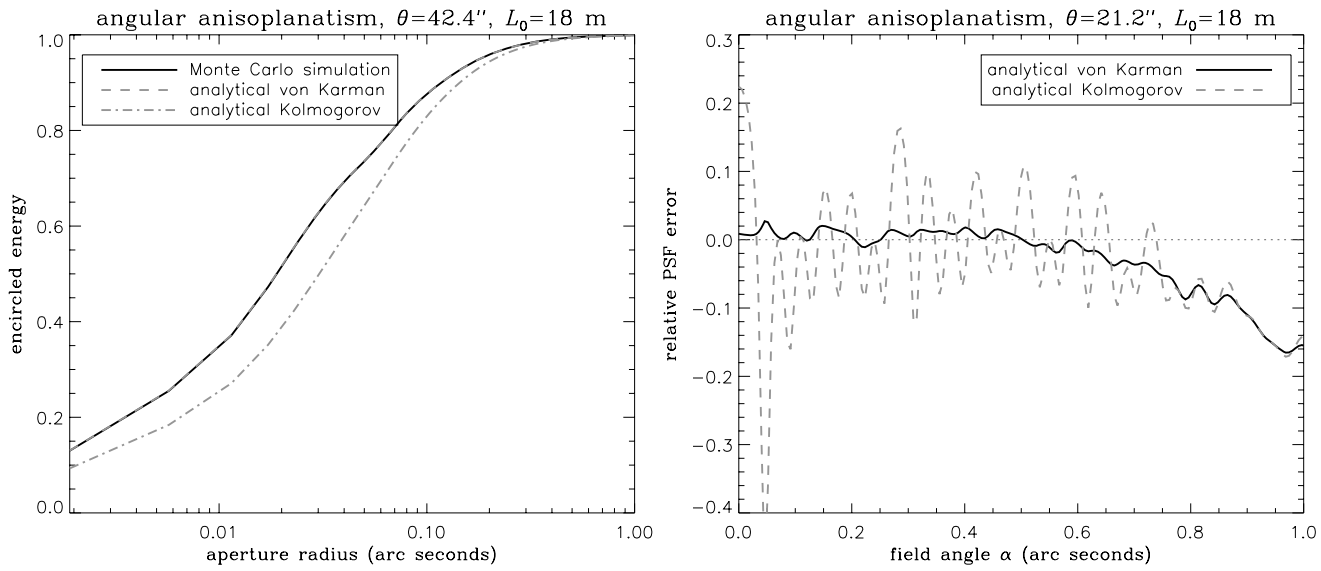

Figure 7: Left: Normalized encircled energy of PSF in the analytical von Karman and Kolmogorov models of NGS anisoplanatism, comparing to the numerical von Karman simulation. Right: Relative PSF error of the analytical von Karman (solid black line) and Kolmogorov (dashed gray line) models measured against the numerical simulation, for NGS anisoplanatism (cut of PSFs along the positive x-axis).

ground, and not a physical scale in the atmosphere itself. By specifying the weighting function w_i, different types of covariances can be computed. Setting $w_i(\mathbf{r}) = \delta(\mathbf{r} - \mathbf{r}_i)$, where δ is Dirac's delta function, turns the covariance element into the point-wise phase covariance function $\langle c_a c_b \rangle = \langle \phi_a(\mathbf{r}_1, t)\phi_b(\mathbf{r}_2, t)\rangle$, which allows us to evaluate the anisoplanatism phase structure function as a sum of variants of the general covariance function

$$\langle \phi_a(\mathbf{r}_1, t)\phi_b(\mathbf{r}_2, t)\rangle = 0.060912 k^2 L_0^{5/3} \int_0^\infty dz\, C_n^2(z)\, I[\alpha_{ab}(\mathbf{r}_1, \mathbf{r}_2, z)]. \tag{112}$$

In ordinary NGS angular anisoplanatism, the geometry of the rays ϕ_a and ϕ_b is such that $\mathbf{p}_a(\mathbf{r}, z) = \mathbf{r}$ and $\mathbf{p}_b(\mathbf{r}, z) = \mathbf{r} - z\boldsymbol{\theta}$. Evaluating the argument α for the ten different covariance terms in Eq. (106) gives:

$$\alpha_{aa}(\mathbf{r}_1, \mathbf{r}_1) = \alpha_{bb}(\mathbf{r}_1, \mathbf{r}_1) = 0, \tag{113}$$
$$\alpha_{aa}(\mathbf{r}_2, \mathbf{r}_2) = \alpha_{bb}(\mathbf{r}_2, \mathbf{r}_2) = 0, \tag{114}$$
$$\alpha_{ab}(\mathbf{r}_1, \mathbf{r}_1) = \alpha_{ab}(\mathbf{r}_2, \mathbf{r}_2) = f_0|z\boldsymbol{\theta}|, \tag{115}$$
$$\alpha_{aa}(\mathbf{r}_1, \mathbf{r}_2) = \alpha_{bb}(\mathbf{r}_1, \mathbf{r}_2) = f_0|\mathbf{r}_1 - \mathbf{r}_2|, \tag{116}$$
$$\alpha_{ab}(\mathbf{r}_1, \mathbf{r}_2) = f_0|\mathbf{r}_1 - \mathbf{r}_2 + z\boldsymbol{\theta}|, \tag{117}$$
$$\alpha_{ba}(\mathbf{r}_1, \mathbf{r}_2) = f_0|\mathbf{r}_1 - \mathbf{r}_2 - z\boldsymbol{\theta}|. \tag{118}$$

We thus retain the property of the Kolmogorov model that the structure function is spatially stationary and only a function of $\boldsymbol{\rho} = \mathbf{r}_1 - \mathbf{r}_2$. The von Karman anisoplanatism structure function can then be expressed as

$$D_\Delta(\boldsymbol{\rho}, \boldsymbol{\theta}) = 0.12184 k^2 L_0^{5/3} \int_0^\infty dz\, C_n^2(z) \left\{2I(0) - 2I(f_0 z\theta) - 2I(f_0\rho) + I(f_0|\boldsymbol{\rho} + z\boldsymbol{\theta}|) + I(f_0|\boldsymbol{\rho} - z\boldsymbol{\theta}|)\right\}, \tag{119}$$

where $\rho = |\boldsymbol{\rho}|$, $\theta = |\boldsymbol{\theta}|$ and $I(0) = 3/5$. Since the structure function is stationary, the OTF computation required for PSF reconstruction is straightforward. In practice we calculate the expression by employing the discrete turbulence model $C_n^2(z) = \mu_0 \sum_l f_l \delta(z - z_l)$, where z_l are the layer altitudes and f_l their relative power ($\sum_l f_l = 1$), and $\mu_0 = 0.06\lambda^2 r_0^{-5/3}$. With this, the integral turns into a summation over a small number of layers, which makes the structure function readily computable.

4.2 Focal anisoplanatism

The structure function of focal anisoplanatism in laser guide star (LGS) AO systems can also be modeled using the methodology developed in Sect. 4.1. In LGS AO, the relative close proximity of the reference source requires us to treat the wave-front as a propagating spherical wave rather than a plane wave. In the geometric approximation, the result at the telescope pupil is a transversal scale change (magnification) of the wave-front, equal to $1 - z/H$, if H is the range of the LGS. The wave-front error resulting from wave-front sensing on a conical beam is called focal (or focus) anisoplanatism, or the cone-effect.

For a LGS AO system, we can derive the focal anisoplanatism structure function in the von Karman model using again the covariance element in Eq. (110). For generality we may include an additional angular offset $\boldsymbol{\theta}$, thereby combining angular and focal anisoplanatism, whereby $\mathbf{p}_a(\mathbf{r}, z) = \mathbf{r}(1 - zH^{-1})$ and $\mathbf{p}_b(\mathbf{r}, z) = \mathbf{r} - z\boldsymbol{\theta}$. This describes the intersection of a conical beam on the optical axis with a cylindrical beam offset by $\boldsymbol{\theta}$. The shorthand notation $\gamma = zH^{-1}$ will be used. The argument α_{ij} for the different covariance terms now evaluates to

$$\alpha_{ab}(\mathbf{r}_1, \mathbf{r}_1) = f_0|\gamma\mathbf{r}_1 - z\boldsymbol{\theta}|, \tag{120}$$
$$\alpha_{ab}(\mathbf{r}_2, \mathbf{r}_2) = f_0|\gamma\mathbf{r}_2 - z\boldsymbol{\theta}|, \tag{121}$$
$$\alpha_{aa}(\mathbf{r}_1, \mathbf{r}_2) = f_0|\mathbf{r}_1 - \mathbf{r}_2|(1 - \gamma), \tag{122}$$
$$\alpha_{bb}(\mathbf{r}_1, \mathbf{r}_2) = f_0|\mathbf{r}_1 - \mathbf{r}_2|, \tag{123}$$
$$\alpha_{ab}(\mathbf{r}_1, \mathbf{r}_2) = f_0|\mathbf{r}_1 - \mathbf{r}_2 - \gamma\mathbf{r}_1 + z\boldsymbol{\theta}|, \tag{124}$$
$$\alpha_{ba}(\mathbf{r}_1, \mathbf{r}_2) = f_0|\mathbf{r}_1 - \mathbf{r}_2 + \gamma\mathbf{r}_2 - z\boldsymbol{\theta}|. \tag{125}$$

We can see that the structure function will be non-stationary in this case. Changing variables according to $\mathbf{x} = \mathbf{r}_1$ and $\boldsymbol{\rho} = \mathbf{r}_1 - \mathbf{r}_2$ gives the final result

$$D_\Delta(\mathbf{x}, \boldsymbol{\rho}, \boldsymbol{\theta}) = 0.12184k^2L_0^{5/3}\int_0^H dz\, C_n^2(z)\left\{2I(0) - I(f_0\rho) - I[f_0\rho(1-\gamma)] + I(f_0|\boldsymbol{\rho} - \gamma\mathbf{x} + z\boldsymbol{\theta}|)\right. \tag{126}$$
$$\left. - I(f_0|\gamma\mathbf{x} - z\boldsymbol{\theta}|) - I(f_0|\gamma(\boldsymbol{\rho} - \mathbf{x}) - z\boldsymbol{\theta}|) + I(f_0|(1-\gamma)\boldsymbol{\rho} + \gamma\mathbf{x} - z\boldsymbol{\theta}|)\right\}. \tag{127}$$

This expression reduces to Eq. (119) when $\gamma = 0$. For PSF reconstruction, the non-stationary structure function does not need to be computed explicitly, only point-wise in order to evaluate the OTF integral

$$\langle B(\boldsymbol{\rho}/\lambda, \boldsymbol{\theta})\rangle = \int d\mathbf{x}\, P(\mathbf{x})P(\mathbf{x} + \boldsymbol{\rho})\exp\left[-\frac{1}{2}D_\Delta(\mathbf{x}, \boldsymbol{\rho}, \boldsymbol{\theta})\right], \tag{128}$$

where P is the aperture transmission function and $\langle B\rangle$ is the long-exposure OTF. The validity of Eq. (128) rests on the assumptions that there is no scintillation and that the residual phase ϕ_Δ follows Gaussian statistics. A common technique for computing the OTF from a non-stationary structure function is to invoke the pupil-averaging approximation, as introduced by Véran [41]. Advances in computing power have partly rendered this approximation unnecessary, and the focal anisoplanatism OTF can be readily computed point-wise using the exact expressions in Eq. (127) and Eq. (128).

4.3 Sample numerical results

Figures 6-10 present some sample numerical results, comparing the analytical von Karman model in Eq. (119) and Eq. (127) to numerical Monte Carlo simulations, and in the case of NGS angular anisoplanatism also comparing to the analytical Kolmogorov model in Eq. (107). For all numerical results, the W.M. Keck Observatory (WMKO) telescope and AO system was used as the model, which gives the characteristic PSF shape shown in Fig. 8. The turbulence model was the 7-layer Mauna Kea Ridge (MKR) model[1] with an overall $r_0 = 0.16$ m, $\theta_0 = 2.57''$ and $d_0 = 4.65$ m (for a definition of these quantities see e.g. [23]). All calculations were done at 2 μm imaging wavelength and at zenith, and the LGS beacon altitude was 90 km. The PSFs were computed at three evaluation points $(\theta_x, \theta_y) = \{(0,0), (15,15), (30,30)\}$, equaling radial off-axis offsets of, respectively, 0, 21.2 and 42.4 arc seconds. The

[1]The MKR model was produced within the framework of the WMKO Next-Generation Adaptive Optics (NGAO) project in collaboration with the Thirty-Meter Telescope (TMT) site monitoring campaign, by use of their MASS/DIMM instrument on Mauna Kea. The statistical data are currently proprietary of TMT and are therefore not reproduced in this paper.

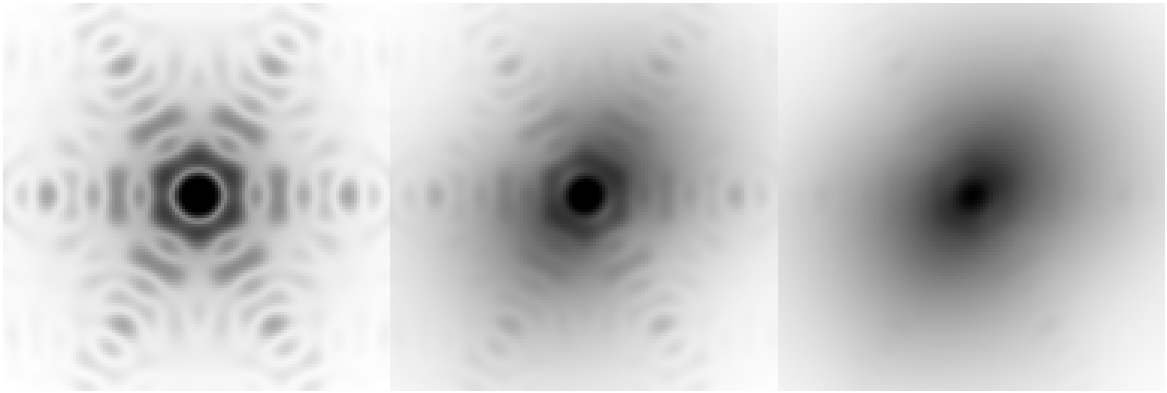

Figure 8: Focal and angular anisoplanatism PSFs (0.73×0.73 arc second field of view) in the analytical von Karman model with $L_0 = 36$ m, at $(0,0), (15,15)$ and $(30,30)$ arc seconds.

outer scale in the analytical von Karman calculations varied between $L_0 = \{1000, 100, 36, 18\}$ meters, while the numerical simulation only produced results at $L_0 = \{36, 18\}$ meters (since the phase screens were FFT-based with a length of 72 meters).

An overview of Strehl ratios obtained in the various cases are given in Table 1, showing exancellent agreement between the analytical von Karman model and numerical simulations. The von Karman model also reproduces the Kolmogorov result at very large outer scales. The effect of the finite outer scale on the structure function and the OTF can be plotted in the case of NGS anisoplanatism (since it is stationary), as shown in Figs. 6 and 6. Figures 7 and 9 plot the relative PSF error, i.e. the normalized PSF subtraction computed as (numerical − analytical)/numerical, for a line segment of the PSFs (the positive x-axis). While in some parts the reported numbers may seem large (0.5 implies a 50% error), the relative error in the PSF halo should be weighted by the fact that the energy levels are two or three orders of magnitude lower than in the central region of the PSF. The encircled energy curves in Fig. 7 and 10 also show that even when the relative error in the wings of the PSF is large, this still amounts to a negligible error in an absolute sense. As long as the overall energy distribution is correct, a small error in the PSF halo has no impact on the encircled energy. Even in the worst case considered (dashed gray curves in Fig. 9 and 9), the analytical von Karman model is still very accurate and the error practically negligible.

NGS ANISOPLANATISM	$0''$	$21.2''$	$42.4''$
analytical Kolmogorov			
$L_0 = \infty$	1.000	0.343	0.101
analytical von Karman			
$L_0 = 1000$	1.000	0.343	0.101
$L_0 = 100$	1.000	0.350	0.106
$L_0 = 36$	1.000	0.380	0.127
$L_0 = 18$	1.000	0.438	0.183
numerical von Karman			
$L_0 = 36$	1.000	0.383	0.127
$L_0 = 18$	1.000	0.442	0.183
LGS ANISOPLANATISM	$0''$	$21.2''$	$42.4''$
analytical von Karman			
$L_0 = 36$	0.782	0.387	0.143
$L_0 = 18$	0.803	0.440	0.192
numerical von Karman			
$L_0 = 36$	0.791	0.385	0.137
$L_0 = 18$	0.812	0.445	0.192

Table 1: NGS and LGS anisoplanatism Strehl ratios, comparing analytical predictions to numerical simulations, for different outer scales and different off-axis angles θ.

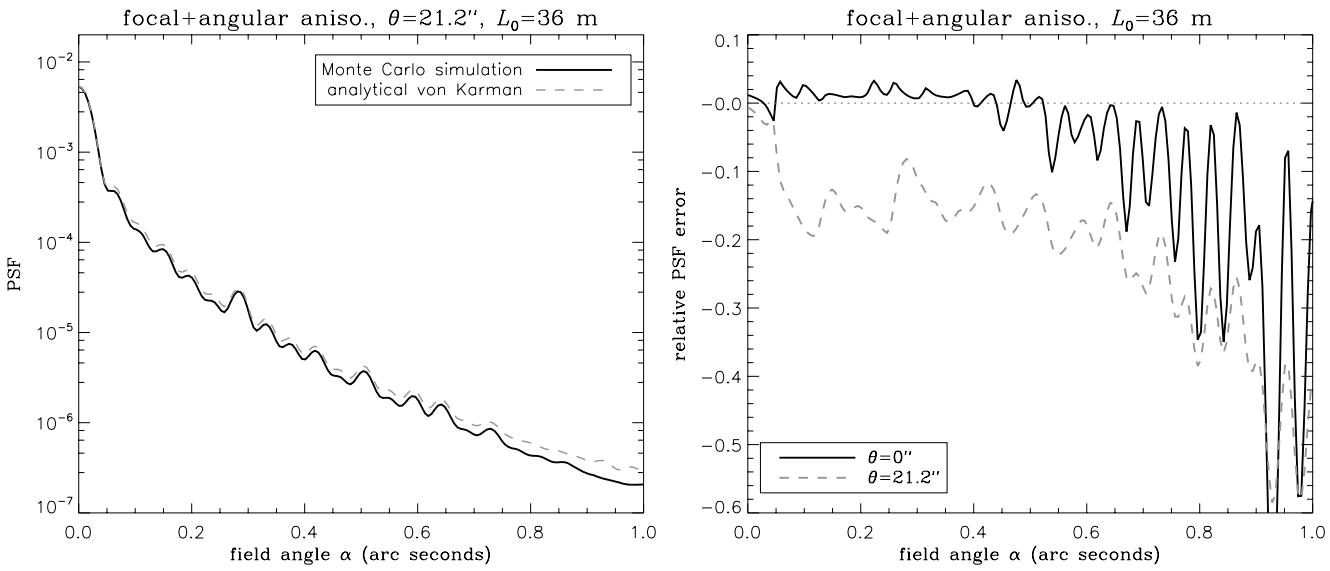

Figure 9: Left: Sample LGS anisoplanatism PSF profile (cut along the positive x-axis), comparing the numerical simulation (solid black line) and the analytical von Karman model. Right: Relative PSF error of the analytical von Karman model for LGS anisoplanatism, measured against the numerical simulation for the $\theta = 0''$ and $\theta = 21.2''$ cases (cut of PSFs along the positive x-axis).

4.4 Conclusions

Structure functions for angular and focal anisoplanatism were derived analytically including a finite outer scale in a von Karman type turbulence model. The analytical result is in excellent agreement with numerical Monte Carlo simulations, and offers an analytical method to produce anisoplanatism kernels for PSF reconstruction problems and PSF modeling in general. The model may replace Kolmogorov-based models where the impact of a finite outer scale becomes non-negligible. In the current investigation it is found that for 10-meter-class telescopes, an outer scale smaller than ∼30 meters may have a non-negligible impact on the anisoplanatism estimation, and under these conditions the von Karman model should be preferred.

Not taken into account in the current analysis is the spatial filtering of the wave-front performed by the AO system. This effect can be accounted for by setting the weighting functions w_i equal to the deformable mirror (DM) influence functions in Eq. (110). This renders the structure function non-stationary, but in the case of NGS anisoplanatism the expression can still be put on a form that allows for a relatively efficient computation of the OTF. For completeness, this result is given in Appendix A, but the method is unlikely to be employed for PSF reconstruction since: 1) in the case of focal anisoplanatism, the expression becomes computationally expensive and impractical for PSF reconstruction, so the approximation in Eq. (127) must be invoked in any case, and 2) the effect is small in high-order AO systems that have $d/r_0 < 1$, where d is the DM actuator spacing. As shown in Fig. 10, the effect of spatial filtering is to reduce the amount of scattered light from anisoplanatism in the PSF halo, which should be modeled by the fitting error instead. If the fitting error is small, however, omitting spatial filtering in the anisoplanatism model has a small effect on the the PSF structure, on the Strehl ratio, and on the resulting photometry estimates produced with this model. For the current WMKO AO system ($d = 0.56$ m), in this model the LGS Strehl ratio at $L_0 = 36$ m at the three evaluations points without spatial filtering is $[0.792, 0.384, 0.134]$, and with spatial filtering they are $[0.829, 0.416, 0.0.147]$. Given that the added complexity of trying to model this effect realistically makes it impractical for LGS PSF reconstruction, one possible compromise might be to use the unfiltered models derived in Sect. 4.1 and Sect. 4.2, and implement a heuristic adjustment to the fitting error in order to account for the fact that some high-spatial-frequency wavefront error is added by the anisoplanatism term. This route is being further investigated within the PSF reconstruction project that motivated the current research.

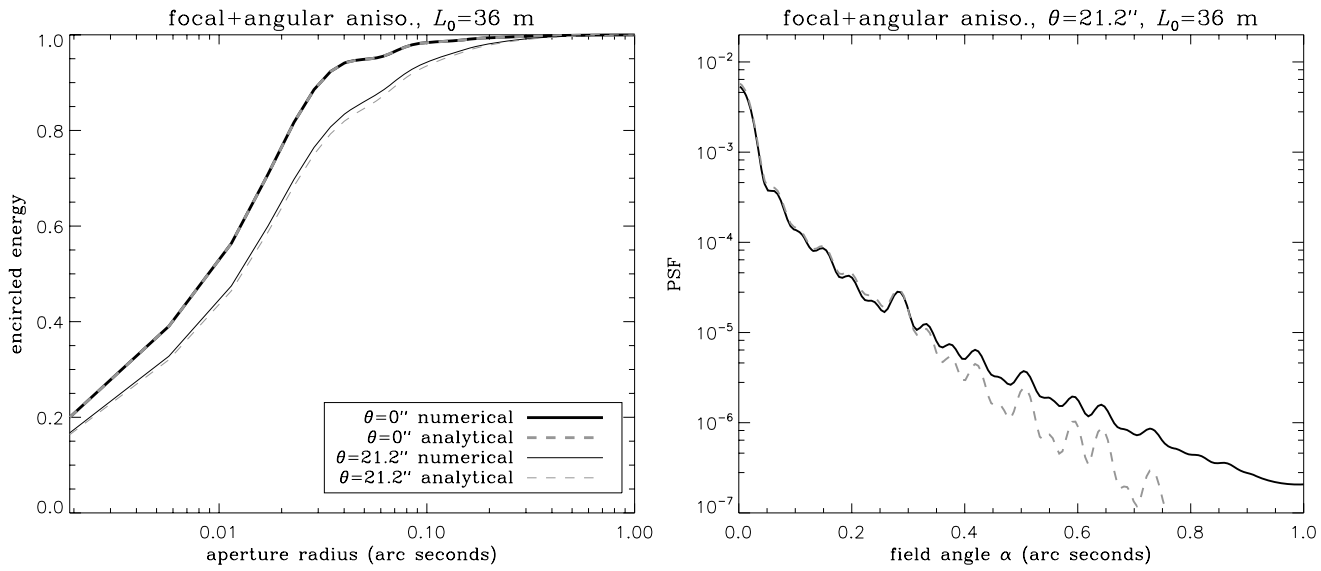

Figure 10: Left: Normalized encircled energy of PSF in the analytical von Karman model of LGS anisoplanatism, comparing to the numerical von Karman simulation. Right: Simulation showing the effect of spatial filtering on LGS anisoplanatism.

4.5 Spatial filtering

In a real AO system, anisoplanatism manifests only on the subspace of controlled modes. Applying the full power spectrum of turbulence will overestimate the anisoplanatism error by counting the fitting error to the anisoplanatism error budget. If the fitting error is small, this approximation might be acceptable. In order to project the anisoplanatism wave-front error onto controlled modes we rewrite Eq. (102) as

$$\phi_\Delta(\mathbf{r},t) = \phi_{\|a}(\mathbf{r},t) - \phi_{\|b}(\mathbf{r},t), \tag{129}$$

where the notation symbolizes that we have retained only the low-frequency (controlled) part $\phi_\|$ of the decomposition $\phi = \phi_\| + \phi_\perp$. This splitting of the phase into two orthogonal components in spatial frequency domain is common in AO PSF modeling and PSF reconstruction methodology, see e.g. [29, 41, 25, 20]. In practice the domain of $\phi_\|$ is defined as the vector space spanned by the set of N_a influence functions $\{h_i(\mathbf{r})\}_{i=1}^{N_a}$ of the DM. Defining w_i as the piston-removed influence function, we have the relations

$$\begin{aligned}
\phi_{\|a}(\mathbf{r},t) &= \sum_{i=i}^{N_a} a_i(t) w_i(\mathbf{r}), && (130)\\
a_i(t) &= \int d\mathbf{r}\, w_i(\mathbf{r}) \phi_a(\mathbf{r},t), && (131)\\
w_i(\mathbf{r}) &= P(\mathbf{r})[h_i(\mathbf{r}) - p_i], && (132)\\
p_i &= \frac{\int d\mathbf{r}\, P(\mathbf{r})\, h_i(\mathbf{r})}{\int d\mathbf{r}\, P(\mathbf{r})}, && (133)
\end{aligned}$$

where p_i is the piston of each mode and $\{a_i\}_{i=1}^{N_a}$ is a set of expansion coefficients (i.e. actuator commands). Analogously, the off-axis beam ϕ_b is projected onto the set $\{b_i\}_{i=1}^{N_a}$. The covariance function now has the general form

$$\langle \phi_{\|a}(\mathbf{r}_1) \phi_{\|b}(\mathbf{r}_2) \rangle = \sum_{i=1}^{N_a} \sum_{j=1}^{N_a} \langle a_i b_j \rangle w_i(\mathbf{r}_1) w_j(\mathbf{r}_2). \tag{134}$$

The covariance matrix $\langle a_i b_j \rangle$ is calculated from Eq. (110). When Eq. (130) is substituted into the expression for the structure function, ten terms of the form above result, containing the two covariance matrices $A_{ij} = \langle a_i a_j \rangle$ and

$B_{ij} = \langle a_i b_j \rangle$. Defining the function $V_{ij}(\boldsymbol{\theta} z_l)$ as

$$V_{ij}(\boldsymbol{\theta} z_l) = 0.144 \left(\frac{L_0}{r_0}\right)^{5/3} [w_i * I * w_j](\boldsymbol{\theta} z_l), \tag{135}$$

where asterisk ($*$) denotes a two-dimensional convolution and I is the function defined in Eq. (111), we have that

$$A_{ij} = V_{ij}(0), \qquad B_{ij} = \sum_{l=1}^{N_l} f_l V_{ij}(\boldsymbol{\theta} z_l). \tag{136}$$

Collecting and factoring terms, the structure function can then be expressed as

$$D_\Delta(\mathbf{r}_1, \mathbf{r}_2, \boldsymbol{\theta}) = \sum_{i=1}^{N_a} \sum_{j=1}^{N_a} (2A_{ij} - B_{ij} - B_{ji}) \left[w_i(\mathbf{r}_1) - w_i(\mathbf{r}_2)\right] \left[w_j(\mathbf{r}_1) - w_j(\mathbf{r}_2)\right]. \tag{137}$$

Introducing the notation Q for the field-dependent symmetric matrix $Q = 2A - B - B^T$ and performing the variable substitution $\{\mathbf{x} = \mathbf{r}_2, \boldsymbol{\rho} = \mathbf{r}_1 - \mathbf{r}_2\}$ gives

$$D_\Delta(\mathbf{x}, \boldsymbol{\rho}, \boldsymbol{\theta}) = \sum_{i=1}^{N_a} \sum_{j=1}^{N_a} Q_{ij} \left[w_i(\mathbf{x}) - w_i(\mathbf{x} + \boldsymbol{\rho})\right] \left[w_j(\mathbf{x}) - w_j(\mathbf{x} + \boldsymbol{\rho})\right]. \tag{138}$$

Readers familiar with PSF reconstruction techniques may recognize this form, as it appears in e.g. [41] before the pupil-averaging approximation is applied. Using the results of Gendron et al. [20] we can compute the OTF without invoking the pupil-averaging approximation. By diagonalizing the covariance matrix $Q = S\Lambda S^T$, with $\{\sigma_k\}_{k=1}^{N_a}$ being the singular values of the diagonal matrix $\Lambda_{ik} = \delta_{ik}\sigma_k$, we obtain the transformed modal basis

$$h'_k(\mathbf{x}) = \sum_{i=1}^{N_a} S_{ik} w_i(\mathbf{x}). \tag{139}$$

In this basis, the structure function can be expressed in the computationally tractable form

$$D_\Delta(\mathbf{x}, \boldsymbol{\rho}, \boldsymbol{\theta}) = \sum_{k=1}^{N_a} \sigma_k \left|h'_k(\mathbf{x}) - h'_k(\mathbf{x} + \boldsymbol{\rho})\right|^2, \tag{140}$$

which enables the OTF to be calculated efficiently. This method is computationally viable to be employed for PSF reconstruction from non-stationary structure functions in general, and not just anisoplanatism, so long as the structure functions can be expressed on the general form in Eq. (138).

4.6 Addendum: alternative anisoplanatism models

In addition to the above demonstrated structure function based anisoplanatism models, there is a simpler PSD based model that can be used with a high degree of realism for the case of NGS. The advantage of the PSD model is that it is vastly easier and faster to compute, but unfortunately no simple LGS model exists. In a geometric model of wavefronts propagating at an angle $\boldsymbol{\theta}$ through the atmosphere, the integrated phase in the telescope pupil plane ($h = 0$) on the controlled subspace is

$$\phi_\parallel(\mathbf{x}, \boldsymbol{\theta}, t) = \sum_{l=1}^{N_l} \phi_\parallel(\mathbf{x} - h_l \boldsymbol{\theta}, t, h_l). \tag{141}$$

The anisoplanatism error is given by

$$\phi_\Delta(\mathbf{x}, \boldsymbol{\theta}, t) = \phi_\parallel(\mathbf{x}, 0, t) - \phi_\parallel(\mathbf{x}, \boldsymbol{\theta}, t), \tag{142}$$

whose spatial Fourier transform is

$$\widetilde{\phi}_\Delta(\mathbf{f},\boldsymbol{\theta},t) = \sum_{l=1}^{N_l} \widetilde{\phi}_\parallel(\mathbf{f},t,h_l)\left[1-\exp(-2\pi i h_l \boldsymbol{\theta}\cdot\mathbf{f})\right], \tag{143}$$

and the anisoplanatism error PSD is

$$\Phi_\Delta(\mathbf{x},\boldsymbol{\theta}) = 2\sum_{l=1}^{N_l} \left\langle \widetilde{\phi}_\parallel(\mathbf{f},t,h_l)\widetilde{\phi}^*_\parallel(\mathbf{f},t,h_l)\right\rangle \left[1-\cos(2\pi h_l \boldsymbol{\theta}\cdot\mathbf{f})\right], \tag{144}$$

assuming the Taylor hypothesis of uncorrelated turbulence layers $\langle\phi(h_l)\phi(h_k)\rangle = \delta_{hk}\langle|\phi(h_l)|^2\rangle$. Invoking the discrete turbulence model (50) gives the simple expression

$$\Phi_\Delta(\mathbf{f},\boldsymbol{\theta}) = 2[1-\mathcal{H}(\mathbf{f})]\Phi(f)\sum_{l=1}^{N_l} f_l\left[1-\cos(2\pi h_l\boldsymbol{\theta}\cdot\mathbf{f})\right], \tag{145}$$

where f_l is the fractional layer turbulence strength ($\sum_l f_l = 1$), $\Phi(f)$ is the von Karman PSD as defined in (47) and $\mathcal{H}(\mathbf{f})$ is the DM spatial filtering function as defined in Sect. 3.2. When a realistic filtering function is used, this simple expression can give a result very close to the much more complicated structure function based analysis with spatial filtering given in Sect. 4.5. Unfortunately this result is not easily extended to focal anisoplanatism. For LGS, the phase is

$$\phi_\parallel(\mathbf{x},\boldsymbol{\theta},t) = \sum_{l=1}^{N_l}\phi_\parallel[\gamma_l(\mathbf{x}-h_l\boldsymbol{\theta}),t,h_l], \tag{146}$$

where $\gamma_l = 1-h_l/H$, and H is the beacon altitude. The Fourier transform is

$$\widetilde{\phi}_\parallel(\mathbf{f},\boldsymbol{\theta},t) = \sum_{l=1}^{N_l}\alpha_l\widetilde{\phi}_\parallel(\alpha_l\mathbf{f},t,h_l)\exp(-2\pi i h_l\alpha_l\boldsymbol{\theta}\cdot\mathbf{f}), \tag{147}$$

where the notation $\alpha_l = \gamma_l^{-1}$ was introduced. The anisoplanatism error in Fourier domain is then

$$\widetilde{\phi}_\Delta(\mathbf{f},\boldsymbol{\theta},t) = \sum_{l=1}^{N_l}\left[\widetilde{\phi}_\parallel(\mathbf{f},t,h_l) - \alpha_l\widetilde{\phi}_\parallel(\alpha_l\mathbf{f},t,h_l)\exp(-2\pi i h_l\alpha_l\boldsymbol{\theta}\cdot\mathbf{f})\right], \tag{148}$$

and the PSD is

$$\Phi_\Delta(\mathbf{x},\boldsymbol{\theta}) = \Phi_\parallel(\mathbf{f}) + \sum_{l=1}^{N_l}\alpha_l^2\Phi_\parallel(\alpha_l\mathbf{f},h_l) - 2\sum_{l=1}^{N_l}\alpha_l\,\mathrm{Re}\Big(\Big\langle\widetilde{\phi}_\parallel(\mathbf{f},t,h_l)\widetilde{\phi}^*_\parallel(\alpha_l\mathbf{f},t,h_l)\Big\rangle\exp(-2\pi i h_l\alpha_l\boldsymbol{\theta}\cdot\mathbf{f})\Big). \tag{149}$$

The first two terms can be computed semi-analytically by applying the DM filter function $\mathcal{H}$ (cf. Sect. 3.2) to $\Phi(\mathbf{f})$ and $\Phi(\alpha\mathbf{f})$ based on the analytical form of the von Karman PSD, but I do not know how to evaluate the cross-PSD in the third term, so we are stuck there.

5 Fourier domain PSD modeling

This section was originally "Analytical evaluations of closed-loop adaptive optics spatial power spectral densities," R. Flicker, 8 February, 2008.

This note rederives and corrects some errors in the analytical expressions for the spatial frequency power spectral densities (PSDs) of servo-lag, noise and spatial aliasing, as previously given in [17, 15]. In addition, the same methodology is also applied to the problem of incoherent segment vibrations, and closed-loop PSDs are dervied for this effect. The work in [17] was based on and a development of the initial studies presented in [29]. The current results may be compared and contrasted to those in [24].

5.1 Fourier domain modeling

The basics

The residual phase φ_c after AO correction is $\varphi_c = \varphi - \widehat{\varphi}$, where φ is the incoming turbulent phase and $\widehat{\varphi}$ is the AO estimated phase. The AO phase estimation involves the temporal and spatial operators $\mathcal{I}$, $\mathcal{M}$ and $\mathcal{R}$ as described below, so that $\widehat{\varphi} = \mathcal{R}\{\mathcal{M}[\mathcal{I}(\varphi)] + \nu\}$, where ν is an additional WFS noise. The phase is split into a low-frequency and a high-frequency part according to $\varphi = \varphi_{\|} + \varphi_{\perp}$, separated by the spatial cut-off frequency $f_c = 1/2d$ of the AO system, where d is the WFS sub-aperture size as well as the DM actuator spacing. The wavefront measurement and reconstruction operators $\mathcal{M}$ and $\mathcal{R}$ are defined so that the low-frequencies within the range of AO attenuation are perfectly measured and reconstructed, i.e. $\mathcal{R}[\mathcal{M}(\varphi_{\|})] = \varphi_{\|}$. With these definitions, the residual phase can be written:

$$\varphi_c = \varphi_{\perp} + \underbrace{\varphi_{\|} - \mathcal{I}(\varphi_{\|})}_{\text{servo-lag}} - \underbrace{\mathcal{R}\{\mathcal{M}[\mathcal{I}(\varphi_{\perp})]\}}_{\text{aliasing}} - \mathcal{R}(\nu). \tag{150}$$

The first term is the fitting error, and the last term is the noise error. Anisoplanatism may also be added as an extra term, but we will not be concerned with anisoplanatism in this text (and its formula is trivial in any case). The spatial PSD of the residual error is calculated as

$$\Phi = \langle |\widetilde{\varphi}_c|^2 \rangle = \left\langle \left| \mathcal{F}\left[\varphi_{\perp} + \varphi_{\|} - \mathcal{I}(\varphi_{\|}) - \mathcal{R}\{\mathcal{M}[\mathcal{I}(\varphi_{\perp})]\} - \mathcal{R}(\nu)\right] \right|^2 \right\rangle \tag{151}$$

$$\approx \left\langle |\widetilde{\varphi}_{\perp}|^2 \right\rangle + \left\langle \left| \widetilde{\varphi}_{\|} - \mathcal{I}(\widetilde{\varphi}_{\|}) \right|^2 \right\rangle + \left\langle \left| \widetilde{\mathcal{R}}\widetilde{\mathcal{M}}[\mathcal{I}(\widetilde{\varphi}_{\perp})] \right|^2 \right\rangle + \left\langle \left| \widetilde{\mathcal{R}}\widetilde{\nu} \right|^2 \right\rangle \tag{152}$$

where Fourier transform is denoted interchangably by tilde $\widetilde{}$ or by $\mathcal{F}$, and the approximation sign signifies that we have discarded all the cross-terms. This is mostly an acceptable approximation, even though we know that there are subtle correlations between some of the terms (e.g. between aliasing and servo-lag).

Taylor hypothesis

For the atmospheric turbulence part of the analysis, the method assumes the Taylor hypothesis of N_l discrete turbulence layers with frozen flow. Ignoring anisoplanatism (i.e. doing all calculations for a fixed θ) and introducing the wind velocity profile $\mathbf{v}_l$, we obtain the phase summed over layers after an arbitrary time delay τ as

$$\varphi(\mathbf{x}, t) = \sum_{l=1}^{N_l} \varphi_l(\mathbf{x} - \mathbf{v}_l\tau, t), \tag{153}$$

which has the Fourier transform

$$\widetilde{\varphi}(\mathbf{f}, t) = \sum_{l=1}^{N_l} \widetilde{\varphi}_l(\mathbf{f}, t) \exp(2\pi i \mathbf{f} \cdot \mathbf{v}_l\tau). \tag{154}$$

It is assumed that each layer φ_l follows von Karman turbulence statistics independently and with separate power, i.e.

$$\langle \widetilde{\varphi}_l{}^{\dagger} \widetilde{\varphi}_l \rangle = \frac{0.023}{r_{0l}^{5/3}} (f^2 + f_0^2)^{-11/6} \tag{155}$$

where $f_0 = 1/L_0$ and L_0 is the turbulence model outer scale, and r_{0l} is the Fried parameter per layer l. The dagger (†) indicates Hermitian conjugate for the case of vectorial variables, and the ordinary complex conjugate for scalar functions.

5.2 Operators

The operator formalism used in the derivations are reviewed here.

Operators: spatial

For a mean-gradient type wavefront sensor, with rectangular sub-apertures in a regular rectangular grid, the measurement operator $\mathcal{M}$ is (see [17]):

$$\mathcal{M} = \text{comb} \times [\Pi * \nabla], \tag{156}$$

which has the Fourier transform

$$\mathcal{F}[\mathcal{M}] = \text{comb} * [\widetilde{\Pi} \times \widetilde{\nabla}], \tag{157}$$

since the comb function is its own Fourier transform (see below). The corresponding functions (and their abbreviated notations) are:

$$\Pi\left(\frac{\mathbf{x}}{d}\right) = \begin{cases} 1, & |x|, |y| \le d/2 \\ 0, & \text{otherwise} \end{cases}, \tag{158}$$

$$\nabla = \frac{\partial}{\partial \mathbf{x}} = \left[\frac{\partial}{\partial x}, \frac{\partial}{\partial y}\right], \tag{159}$$

$$\text{comb}\left(\frac{\mathbf{x}}{d}\right) = \sum_{\mathbf{m}} \delta\left(\frac{\mathbf{x}}{d} - \mathbf{m}\right) = \sum_{m=-\infty}^{+\infty} \sum_{n=-\infty}^{+\infty} \delta\left(\frac{x}{d} - m\right) \delta\left(\frac{y}{d} - n\right), \tag{160}$$

where boldface denotes a (2-element) vector. The spatial plane coordinate is $\mathbf{x} = (x, y)$, with the Fourier conjugate spatial frequency variable $\mathbf{f} = (f_x, f_y)$. The Fourier transforms of (158)-(160) are:

$$\widetilde{\Pi}(\mathbf{f}d) = \text{sinc}(\mathbf{f}d) = \frac{\sin(\pi f_x d)}{\pi f_x d} \times \frac{\sin(\pi f_y d)}{\pi f_y d}, \tag{161}$$

$$\widetilde{\nabla} = 2\pi i \mathbf{f} = 2\pi i [f_x, f_y], \tag{162}$$

$$\mathcal{F}[\text{comb}](\mathbf{f}d) = \sum_{\mathbf{m}} \delta(\mathbf{f}d - \mathbf{m}). \tag{163}$$

A wavefront reconstructor may be defined as the operator $\mathcal{R}$ that fulfills $\mathcal{R}[\mathcal{M}(\varphi_\parallel)] = \varphi_\parallel$). The Fourier domain recostructor that does this is

$$\widetilde{\mathcal{R}} = \frac{\mathbf{f}^{-1}}{4\pi i \,\text{sinc}(\mathbf{f}d)}. \tag{164}$$

Operators: temporal

The measurement operator $\mathcal{M}$ in (156) only represents the spatial wavefront sampling. To account for the finite integration time t_i of the WFS we must evaluate various integrals of the type given below, represented by the WFS temporal integration operator $\mathcal{I}$:

$$\mathcal{I}_n(\widetilde{\varphi}) = \frac{1}{t_i} \int_{-t_i/2}^{+t_i/2} d\tau \, \widetilde{\varphi}(\mathbf{f}, t - t_d - n t_i - \tau), \tag{165}$$

where t_d is an additional temporal delay due to e.g. CCD read-out, centroiding and reconstruction computations. We expressed this directly in the spatial Fourier domain, because that is the most useful form for evaluating the PSDs. The integer index n was included for generality and to show the relation to the closed loop function G_n (see section 5.2), but for the remainder of this section we set $n = 0$ for brevity. Using the result (154) gives

$$\mathcal{I}_o(\widetilde{\varphi}) = \frac{1}{t_i} \sum_{l=1}^{N_l} \widetilde{\varphi}_l(\mathbf{f}, t) \exp(2\pi i \mathbf{f} \cdot \mathbf{v}_l t_d) \underbrace{\int_{-t_i/2}^{+t_i/2} d\tau \, \exp(2\pi i \mathbf{f} \cdot \mathbf{v}_l \tau)}_{I'}. \tag{166}$$

The remaining integral I' can be evaluated to

$$I' = \frac{1}{2\pi i \mathbf{f}\cdot\mathbf{v}_l}\left[\exp(\pi i \mathbf{f}\cdot\mathbf{v}_l t_i) - \exp(-\pi i \mathbf{f}\cdot\mathbf{v}_l t_i)\right] \quad (167)$$

$$= \frac{\sin(\pi \mathbf{f}\cdot\mathbf{v}_l t_i)}{\pi \mathbf{f}\cdot\mathbf{v}_l} = t_i \operatorname{sinc}(\mathbf{f}\cdot\mathbf{v}_l t_i), \quad (168)$$

and the whole expression becomes

$$\mathcal{I}_0(\widetilde{\varphi}) = \sum_{l=1}^{N_l} \widetilde{\varphi}_l(\mathbf{f},t)\operatorname{sinc}(\mathbf{f}\cdot\mathbf{v}_l t_i)\exp(2\pi i \mathbf{f}\cdot\mathbf{v}_l t_d). \quad (169)$$

Closed loop

A simple model of closed loop operation is derived here. For a leaky integrator with a gain g and a leak factor ξ, the mirror shape $s(\mathbf{x},t)$ at any time step nt_i is computed as (omitting an additional time delay t_d and the spatial variable $\mathbf{x}$ for brevity)

$$s(t-nt_i) = \xi s[t-(n+1)t_i] + g\widehat{\varphi}[t-(n+1)t_i], \quad (170)$$

where t_i is the WFS integration time, and $\widehat{\varphi}$ is the AO estimated residual wavefront error. To simplify even more we will use the abbreviated notation

$$s_n = \xi s_{n+1} + g\widehat{\varphi}_{n+1}, \quad (171)$$

which allows us to write compactly $\widehat{\varphi}_n = G_n - s_n$. The function G_n can be thought of as a composite operator, for instance it may be the open-loop reconstruction of the wavefront:

$$G_n = \mathcal{R}\{\mathcal{M}[I_n(\varphi)]\}. \quad (172)$$

But in order to represent the closed-loop effect on different AO errors, G_n will later take on different forms. From the recursive relation (171) it is easy to show that (cf. [17]) the present mirror shape s_0 after N time steps is given by

$$s_0 = (\xi-g)^N s_N + g\sum_{n=1}^{N} G_n(\xi-g)^{n-1}. \quad (173)$$

Obviously $\xi < g$ must be observed for this to converge. If the AO system is operating in a steady state far enough away from the startup phase, so that initial conditions no longer matter, we can for any $0 < g < l$ approximate $N \approx \infty$, which gives

$$s_0 = g\sum_{n=1}^{\infty} G_n(\xi-g)^{n-1}. \quad (174)$$

5.3 PSD evaluations

5.3.1 Servo-lag

In this section $\varphi = \varphi_{\parallel}$ (and we omit the subscript $_{\parallel}$). The closed-loop expression for the servo-lag error PSD Φ_{sl} is

$$\Phi_{sl}(\mathbf{f}) = \left\langle \left|\mathcal{F}\left\{\varphi(\mathbf{x},t) - s_0(\mathbf{x},t)\right\}\right|^2 \right\rangle. \quad (175)$$

In this case we have that the closed loop operator is $G_n = \mathcal{R}[\mathcal{M}(\mathcal{I}_n)]$, cf. equations (174) and (169), which simplifies to $G_n = \mathcal{I}_n$ upon invoking the reconstruction condition $\mathcal{R}[\mathcal{M}(\varphi_{\parallel})] = \varphi_{\parallel}$. This is saying that we just have to give the temporal WFS measurements the closed-loop treatment. Applying the Fourier transform and writing it out gives

$$\Phi_{sl}(\mathbf{f}) = \left\langle \left| \sum_{l=1}^{N_l} \widetilde{\varphi}_l(\mathbf{f},t) - \sum_{l=1}^{N_l} \widetilde{\varphi}_l(\mathbf{f},t)\operatorname{sinc}(\mathbf{f}\cdot\mathbf{v}_l t_i)\, g\sum_{n=1}^{\infty}(1-g)^{n-1}\exp[2\pi i \mathbf{f}\cdot\mathbf{v}_l(t_d+nt_i)] \right|^2 \right\rangle \quad (176)$$

$$= \left\langle \left| \sum_{l=1}^{N_l} \widetilde{\varphi}_l(\mathbf{f},t)\left[1 - \operatorname{sinc}(\mathbf{f}\cdot\mathbf{v}_l t_i)\, g\sum_{n=1}^{\infty}(1-g)^{n-1}\exp[2\pi i \mathbf{f}\cdot\mathbf{v}_l(t_d+nt_i)]\right] \right|^2 \right\rangle \quad (177)$$

$$= \sum_{l=1}^{N_l}\sum_{k=1}^{N_l}\left\langle \widetilde{\varphi}_l^{\dagger}(\mathbf{f},t)\widetilde{\varphi}_k(\mathbf{f},t)\right\rangle \Gamma_l^{\dagger}(\mathbf{f})\Gamma_k(\mathbf{f}), \tag{178}$$

where we defined

$$\Gamma_l(\mathbf{f}) = 1 - \mathrm{sinc}(\mathbf{f}\cdot\mathbf{v}_l t_i)\exp(2\pi i\mathbf{f}\cdot\mathbf{v}_l t_d)\, g\sum_{n=1}^{\infty}(\xi-g)^{n-1}\exp(2\pi i\mathbf{f}\cdot\mathbf{v}_l n t_i). \tag{179}$$

Separate turbulence layers are assumed to be uncorrelated, i.e. $\langle\varphi_l\varphi_k\rangle = \langle|\varphi_l|^2\rangle\delta_{kl}$, so this simplifies to the tubulence PSD (155) and removes one summation. Defining $a = \xi - g$ and $b_l = 2\pi\mathbf{f}\cdot\mathbf{v}_l t_i$, the summation over n in expression (179) can be written

$$S_l = a^{-1}\sum_{n=1}^{\infty} a^n e^{inb_l} \tag{180}$$

$$= a^{-1}\sum_{n=1}^{\infty} a^n(\cos nb_l + i\sin nb_l), \tag{181}$$

This can be evaluated as two Fourier series that have closed analytical forms:

$$\sum_{k=0}^{n} r^k\cos kx = \frac{(1-r\cos x)(1-r^n\cos nx)+r^{n+1}\sin x\sin nx}{1-2r\cos x+r^2}, \tag{182}$$

$$\sum_{k=1}^{n} r^k\sin kx = \frac{r\sin x(1-r^n\cos nx)-(1-r\cos x)r^n\sin nx}{1-2r\cos x+r^2} \tag{183}$$

These sums will convege as $n\to\infty$ for any $|r|<1$. Evaluating the asymptotic forms, substituting back into (181) and combining terms gives eventually

$$S_l = \frac{e^{ib_l}-a}{1-2a\cos b_l + a^2}. \tag{184}$$

We can now jump to the final form of the PSD directly:

$$\Phi_{sl}(\mathbf{f}) = \frac{0.023}{(f^2+f_0^2)}\times\sum_{l=1}^{N_l} r_{0l}^{-5/3}\left|\Gamma_l(\mathbf{f})\right|^2, \tag{185}$$

where

$$\Gamma_l(\mathbf{f}) = 1-\mathrm{sinc}(\mathbf{f}\cdot\mathbf{v}_l t_i)\exp(2\pi i\mathbf{f}\cdot\mathbf{v}_l t_d)\times\frac{g(e^{ib_l}-a)}{1-2a\cos b_l+a^2} \tag{186}$$

with a and b_l defined as above.

5.3.2 Noise

For WFS noise the function $G_n = \mathcal{R}(\nu_n)$, and the closed-loop PSD is given by

$$\Phi_{noise}(\mathbf{f}) = \left\langle\left|\mathcal{F}\left\{s_0(\mathbf{x},t)\right\}\right|^2\right\rangle \tag{187}$$

$$= \left\langle\left|\mathcal{F}\left\{g\sum_{n=1}^{\infty}(1-g)^{n-1}\mathcal{R}[\nu_n(\mathbf{x},t)]\right\}\right|^2\right\rangle \tag{188}$$

$$= g^2\widetilde{\mathcal{R}}^{\dagger}\widetilde{\mathcal{R}}\sum_{m=1}^{\infty}\sum_{n=1}^{\infty}(1-g)^{m+n-2}\left\langle\widetilde{\nu}_m^{\dagger}(\mathbf{f},t)\,\widetilde{\nu}_n(\mathbf{f},t)\right\rangle. \tag{189}$$

Assuming spatially and temporally uncorrelated noise we have that $\left\langle\widetilde{\nu}_m^{\dagger}\widetilde{\nu}_n\right\rangle = \delta_{mn}\Phi_\nu$, the power spectrum of the input noise ν. Defining $a=(1-g)^2$ we have that

$$\Phi_{noise}(\mathbf{f}) = g^2\widetilde{\mathcal{R}}^{\dagger}\widetilde{\mathcal{R}}\,\Phi_\nu(\mathbf{f})\sum_{n=1}^{\infty}a^{(n-1)}. \tag{190}$$

The sum is a geometric series with the closed form $1/(1-a)$, and substituting the form for the reconstructor from (164) gives the final expression

$$\Phi_{noise}(\mathbf{f}) = \frac{g}{2-g} \times \frac{\Phi_\nu(\mathbf{f})}{\mathrm{sinc}^2(\mathbf{f}d)} \left(\frac{1}{f_x^2} + \frac{1}{f_y^2} \right). \tag{191}$$

5.3.3 Aliasing (open loop)

In this section $\varphi = \varphi_\perp$ (and we drop the subscript $_\perp$), and $G_n = \mathcal{R}[\mathcal{M}(\mathcal{I}_n)]$, because perfect reconstruction can no longer be invoked. This, generally speaking, leads to a mess. Doing the calculation first for the open-loop case (the closed loop adjustment will be easier to implement afterward this way), the form of the PSD is

$$\Phi_{alias}(\mathbf{f}) = \left\langle \left| \mathcal{F}\left\{ s_0(\mathbf{x},t) \right\} \right|^2 \right\rangle \;=\; \left\langle \left| \widetilde{\mathcal{R}}\widetilde{\mathcal{M}}[\mathcal{I}_n(\widetilde{\varphi})] \right|^2 \right\rangle. \tag{192}$$

Taking this one step at a time, we have that

$$\widetilde{\mathcal{M}}[\mathcal{I}_0(\widetilde{\varphi})] = \mathrm{comb}(\mathbf{f}d) \;*\; [\mathrm{sinc}(\mathbf{f}d) \times 2\pi i \mathbf{f} \mathcal{I}_0(\widetilde{\varphi})]\,. \tag{193}$$

Introducing the shorthand notation $\mathbf{f}_m = \mathbf{f} - \mathbf{m}d^{-1}$, we can evaluate this as

$$\widetilde{\mathcal{M}}[\mathcal{I}_0(\widetilde{\varphi})] = 2\pi i \sum_{\mathbf{m}} \mathbf{f}_m \,\mathrm{sinc}(d\mathbf{f}_m) \sum_{l=1}^{N_l} \widetilde{\varphi}_l(\mathbf{f}_m, t)\, \mathrm{sinc}(\mathbf{f}_m \cdot \mathbf{v}_l t_i) \exp(2\pi i \mathbf{f}_m \cdot \mathbf{v}_l t_d). \tag{194}$$

Including the reconstructor we can write

$$\widetilde{\mathcal{R}}\widetilde{\mathcal{M}}[\mathcal{I}_0(\widetilde{\varphi})] = \frac{1}{2\,\mathrm{sinc}(\mathbf{f}d)} \times \sum_{\mathbf{m}} A(\mathbf{f}_m, t) \sum_{l=1}^{N_l} \widetilde{\varphi}_l(\mathbf{f}_m, t) E_l(\mathbf{f}_m, t), \tag{195}$$

where we defined the two quantities

$$A(\mathbf{f}_m, t) \;=\; (\mathbf{f}^{-1} \cdot \mathbf{f}_m)\,\mathrm{sinc}(d\mathbf{f}_m), \tag{196}$$

$$E_l(\mathbf{f}_m, t) \;=\; \exp(2\pi i \mathbf{f}_m \cdot \mathbf{v}_l t_d)\,\mathrm{sinc}(\mathbf{f}_m \cdot \mathbf{v}_l t_i). \tag{197}$$

Evaluating the modulus squared and applying ensemble averaging gives

$$\Phi_{alias}(\mathbf{f}) = \frac{1}{4\,\mathrm{sinc}^2(\mathbf{f}d)} \times \sum_{\mathbf{m}} \sum_{\mathbf{m}'} \sum_{l} \sum_{l'} A^\dagger(\mathbf{f}_m, t) A(\mathbf{f}_{m'}, t) E_l^\dagger(\mathbf{f}_m, t) E_{l'}(\mathbf{f}_{m'}, t) \left\langle \widetilde{\varphi}_l^\dagger(\mathbf{f}_m, t) \widetilde{\varphi}_{l'}(\mathbf{f}_{m'}, t) \right\rangle. \tag{198}$$

We are saved from total catastrophe by assuming that separate turbulence layers are uncorrelated, and that turbulence at different spatial frequencies are uncorrelated also. The last term then becomes $\langle \widetilde{\varphi}_{lm}^\dagger \widetilde{\varphi}_{l'm'} \rangle = \delta_{ll'}\delta_{mm'} \langle |\widetilde{\varphi}_{lm}|^2 \rangle$, and the E_l term loses its complex exponential to the modulus, which leaves the almost manageable final expression:

$$\Phi_{alias}(\mathbf{f}) = \frac{0.00575}{\mathrm{sinc}^2(\mathbf{f}d)} \times \sum_{\mathbf{m} \neq (0,0)} (|\mathbf{f}_m|^2 + f_0^2)^{-11/6} (\mathbf{f}^{-1} \cdot \mathbf{f}_m)^2 \,\mathrm{sinc}^2(d\mathbf{f}_m) \sum_{l=1}^{N_l} r_{0l}^{-5/3}\, \mathrm{sinc}^2(\mathbf{f}_m \cdot \mathbf{v}_l t_i). \tag{199}$$

Note that the origin $\{m = 0, n = 0\}$ is exluded from the double sum, but otherwise it runs over infinity. The terms of the sum quickly tend toward zero thanks to the steep power law of Kolmogorov turbulence, so in practise no more than a handful of terms need to be summed in each direction; this makes the expression possible to compute.

5.3.4 Aliasing (closed loop)

Looking to the closed loop modifications, we are now rewarded for having done most of the cumbersome calculations already. The adjustment is simplest to account for by entering it into equation (197) of the E_l term by simply substituting

$$\exp(2\pi i \mathbf{f}_m \cdot \mathbf{v}_l t_d) \;\rightarrow\; g \sum_{n=1}^{\infty} (\xi - g)^{n-1} \exp[2\pi i \mathbf{f}_m \cdot \mathbf{v}_l (t_d + n t_i)] \tag{200}$$

$$\;=\; g\, \exp(2\pi i \mathbf{f}_m \cdot \mathbf{v}_l t_d) \times \frac{e^{i b_l} - a}{1 - 2a\cos b_l + a^2}. \tag{201}$$

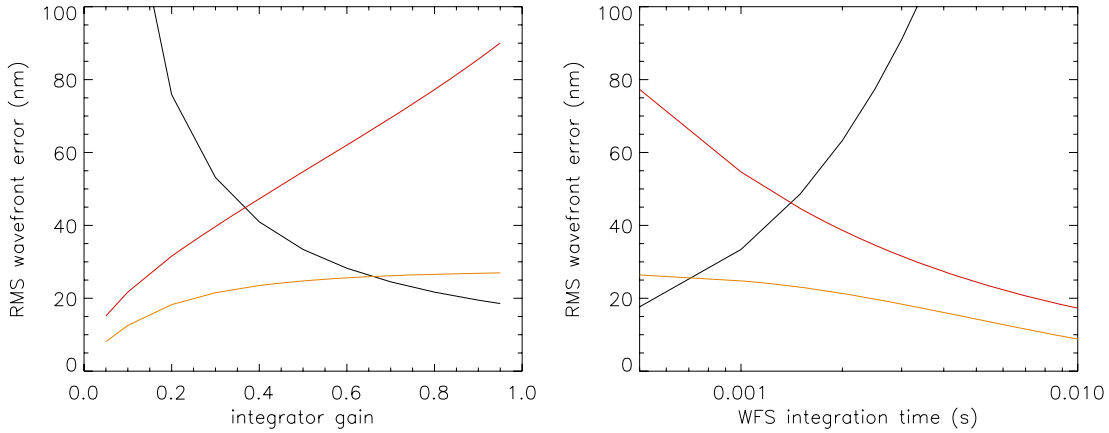

Figure 11: Servo-lag (black line), noise (red) and aliasing (orange) wavefront errors as functions of the integrator gain g (left) and the WFS integration time t_i (right).

We had evaluated the sum already in the expression (186) for Γ_l, and the form (169) is retained with $\mathbf{f}$ replaced by $\mathbf{f}_m$ in the definition of b_l. We now re-evaluate $E_l^\dagger E_l$. Defining $c = 2\pi\mathbf{f}_m \cdot \mathbf{v}_l t_d$ and $z = e^{ic}(e^{ib_l} - a)$ as the complex numerator of (201) we have that

$$\begin{aligned} z^\dagger z &= e^{-ic}(e^{-ib_l} - a) \times e^{ic}(e^{ib_l} - a) && (202)\\ &= 1 + a^2 - a(e^{ib_l} + e^{-ib_l}) && (203)\\ &= 1 + a^2 - 2a\cos b_l, && (204) \end{aligned}$$

which is exactly the denominator of (201). Hence the modified expression for $E_l^\dagger E_l$ in closed loop is simply

$$E_l^\dagger(\mathbf{f}_m, t)E_l(\mathbf{f}_m, t) = \frac{g^2\,\mathrm{sinc}^2(\mathbf{f}_m \cdot \mathbf{v}_l t_i)}{1 - 2a\cos b_l + a^2}, \tag{205}$$

And the closed loop aliasing PSD is finally

$$\Phi_{alias}(\mathbf{f}) = \frac{0.00575}{\mathrm{sinc}^2(\mathbf{f}d)} \times \sum_{\mathbf{m}\neq(0,0)} \frac{(\mathbf{f}^{-1}\cdot\mathbf{f}_m)^2\,\mathrm{sinc}^2(d\mathbf{f}_m)}{(|\mathbf{f}_m|^2 + f_0^2)^{11/6}} \sum_{l=1}^{N_l} r_{0l}^{-5/3}\,\frac{g^2\,\mathrm{sinc}^2(\mathbf{f}_m \cdot \mathbf{v}_l t_i)}{1 - 2a\cos b_l + a^2}, \tag{206}$$

where $a = \xi - g$ and $b_l = 2\pi\mathbf{f}_m \cdot \mathbf{v}_l t_i$.

6 Null-mode tilt anisoplanatism

This section was originally "Analysis of low-order tomography errors in LTAO systems," R. Flicker, 14 September, 2007.

6.1 Introduction

This working note is an addendum to KAON 492, wherein the NGAO wavefront error resulting from tomographic null-modes was discussed and analyzed briefly. This update comments on a number additions to the simulation code, with the aim to improve its realism and make it useful for system design, science simulations and observation planning. The major changes that have taken place are:

- Zernike interaction matrices are now generated by the monomial transformation method used in Clare 2006[8], which makes this part of the code much faster.
- The code now includes correction terms from control loop dynamics as in Flicker & Rigaut 2001[13], which require temporal Zernike PSDs to be generated, which makes the code much slower. The PSDs only need to be computed once for each wind profile, however.
- In addition to the purely geometrical least-squares estimator, it now also offers a Gauss-Markov (noise-weighted LSQ) and a Bayesian (maximum a posteriori, MAP) estimator.
- Appended to the end of the code is now also a tip/tilt PSF reconstruction algorithm that can produce a grid of Gaussian PSF kernels that describe the tilt anisoplanatism over the field of view, also from [13].
- The high-order LGS system is now also included in the noise/servo-lag calculation, since noise on the high-order modes will propagate into the null-modes.

6.2 Modal description

We may describe a two-dimensional phase map in polar coordinates by the Zernike expansion

$$\varphi(\rho,\theta,t) = \sum_{i=1}^{N} a_i(t) Z_i(\rho/R,\theta) = Za(t), \tag{207}$$

where $a_i(t)$ are time-dependent Zernike coefficients, Z is the matrix of Zernike polynomials, N is the number of Zernike polynomials included in the expansion, and R is the pupil radius. We are concerned with calculating the residual pupil plane phase error φ_ε upon attenuating the turbulence-induced aberrations $\varphi = Za$ with an AO system introducing the phase shift $\widehat{\varphi} = Z\alpha$

$$\varphi_\varepsilon = \varphi - \widehat{\varphi} = Z(a-\alpha) = Z\varepsilon, \tag{208}$$

where ε is the vector of residual Zernike coefficients. This generic formulation needs to be furnished somewhat by noting that we compute the phase error ε_i in a given direction i, and that both a and α are represented by sets of Zernike coefficients defined on the meta pupils of a finite number of discrete layers (turbulence model layers, number of DMs) at different conjugate altitudes. Hence we need projection operators P_{ai} and P_{mi} that integrate the atmospheric and DM Zernike coefficients in a given direction according to

$$\varepsilon_i = P_{ai}a - P_{mi}\alpha. \tag{209}$$

The AO system performs two basic operations, measuring the turbulence indirectly and reconstructing the wavefronts, which we describe the matrix operations

$$s = G_a a + Tn, \tag{210}$$

$$\alpha = Es, \tag{211}$$

where G_a and E are, respectively, the (combined LGS and NGS) measurement and reconstruction operators acting on the input turbulence mode a and the resulting measurement vector s. There is also an additive noise component n, originating in the WFS and propagated onto Zernike modes by the noise propagator T. With these basic equations the residual mean-square error $\sigma_i^2 = \langle \varepsilon_i^T \varepsilon_i \rangle$ can be computed at varying levels of sophistication and realism, depending on which properties of a and α are included in the analysis. The simplest analysis is purely geometrical, while more realistic computations include the control loop dynamics of the AO system.

6.2.1 Geometric error

The specific geometry of the LGS, NGS, turbulence and DM layers set a fundamental limit on the performance in each case, based solely on the existence of tomographic null-modes that remain undetected and uncorrected, and the specific estimator E used. Combining equations (209)-(211) we obtain

$$\varepsilon_i = (P_{ai} - P_{mi}EG_a)a - P_{mi}ETn = Q_i a - R_i n, \tag{212}$$

where I defined the operator $Q_i = P_{ai} - P_{mi}EG_a$ and $R_i = P_{mi}ET$. The variance of the residual phase error is then

$$\begin{aligned} \sigma_i^2 &= \langle \varphi_\varepsilon^T \varphi_\varepsilon \rangle = \mathrm{Tr}\left[\langle \varphi_\varepsilon \varphi_\varepsilon^T \rangle\right] = \mathrm{Tr}\left[Z\langle \varepsilon_i \varepsilon_i^T \rangle Z^T\right] && (213)\\ &= \mathrm{Tr}\left[ZQ_i\langle aa^T\rangle Q_i^T Z^T\right] + \mathrm{Tr}\left[ZR_i\langle nn^T\rangle R_i^T Z^T\right] && (214)\\ &= \mathrm{Tr}\left(Q_i C_{aa} Q_i^T\right) + \mathrm{Tr}\left(R_i C_{nn} R_i^T\right), && (215)\end{aligned}$$

where Tr() denotes the matrix trace operation, and we exploited the invariance of the trace under a similarity transform $\mathrm{Tr}(BAB^{-1}) = \mathrm{Tr(A)}$, since $Z^T = Z^{-1}$ by orthogonality of the Zernike modes. $C_{aa} = \langle aa^T \rangle$ and $C_{nn} = \langle nn^T \rangle$ are the covariance matrices of Zernike coefficients and WFS noise respectively. C_{aa} can be computed for Kolmogorov (Noll, 1976; Wang & Markey 1978)[28, 43] or von Karman (Winker, 1991)[44] statistics. For low-order modes and a large aperture, von Karman statistics should be used. The $QC_{aa}Q^T$ term is essentially the same as what is computed by Clare 2006[8]. The noise covariance was modeled here from simple formulas of the standard deviation of the (one-axis) angular position measurement in a Shack-Hartmann type sub-aperture, cf. Eqns. 5.13-5.17 in Hardy 1998[23]:

$$\begin{aligned} \sigma_2 &= \frac{8}{\pi}\frac{\theta}{SNR}, && (216)\\ SNR &= \frac{n_{phot}}{\sqrt{n_{phot} + N_{pix}(n_{bg} + e^2)}}. && (217)\end{aligned}$$

In this geometric calculation it does not make much sense to actually include the noise term, since we can drive it to zero without penalty by turning down the frame rate indefinitely in order to get a high SNR. In a real system, this strategy would be penalized by an increasing servo-lag error, which is why we must include the control loop dynamics next.

6.2.2 Open loop variance

Because the analysis becomes complicated in the general case, I will start with a few special cases where we can easily find exact analytical solutions. First consider the case of an open loop AO system with a single WFS frame rate and control bandwidth $\omega_s = 1/t_s$, where t_s is the integration time of the WFS. Referring to Fig. 12, we find the modified spatial-temporal relationship after applying the temporal Fourier transform to the quantities:

$$\widetilde{\alpha}(\omega) = C(\omega)D(\omega)E[S(\omega)G_a a(\omega) + T\widetilde{n}(\omega)], \tag{218}$$

and

$$\begin{aligned} \widetilde{\varepsilon}_i(\omega) &= P_{ai}\widetilde{a}(\omega) - P_{mi}\widetilde{\alpha}(\omega) && (219)\\ &= \underbrace{[P_{ai} - P_{mi}C(\omega)D(\omega)ES(\omega)G_a]}_{Q_i(\omega)}\widetilde{a}(\omega) - \underbrace{P_{mi}C(\omega)D(\omega)ET}_{R_i(\omega)}\widetilde{n}(\omega) && (220)\\ &= Q_i(\omega)\widetilde{a}(\omega) - R_i(\omega)\widetilde{n}(\omega), && (221)\end{aligned}$$

where the quantities Q and R were redefined to include the current temporal filter definitions. The residual phase variance may be computed as before, with the added operation of integrating over temporal frequencies, that is:

$$\begin{aligned} \sigma_i^2 &= \int d\omega\, \mathrm{Tr}\Big[\langle \varepsilon_i(\omega)\varepsilon_i^\dagger(\omega)\rangle\Big] && (222)\\ &= \mathrm{Tr}\left[\int d\omega\, Q_i(\omega)\langle \widetilde{a}(\omega)\widetilde{a}^\dagger(\omega)\rangle Q_i^\dagger(\omega)\right] + \mathrm{Tr}\left[\int d\omega\, R_i(\omega)\langle \widetilde{n}(\omega)\widetilde{n}^\dagger(\omega)\rangle R_i^\dagger(\omega)\right], && (223)\end{aligned}$$

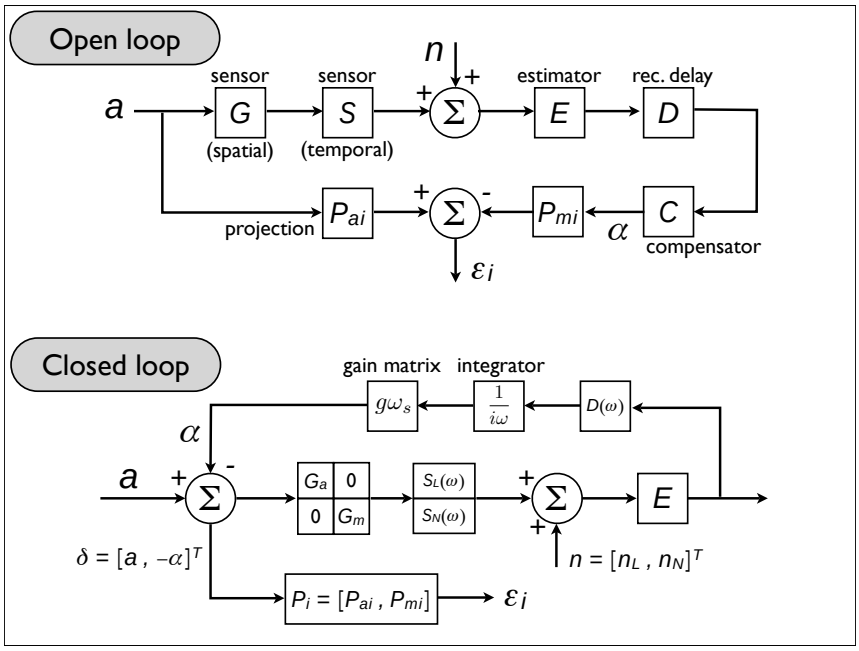

Figure 12: Schematic of the simplified open loop and closed loop cases.

where † denotes the Hermitian conjugate (i.e. transpose and complex conjugate) of a complex matrix. Assuming that the temporal spectrum of $\widetilde{n}$ is white, we have that $\langle \widetilde{n}(\omega)\widetilde{n}^\dagger(\omega)\rangle = C_{nn}$ at all frequencies. The temporal PSDs $\Phi(\omega) = \langle \widetilde{a}(\omega)\widetilde{a}^\dagger(\omega)\rangle$ of Zernike coefficients can be computed in Kolmogorov statistics by the formula derived in Roddier *et al.* 1993[30]:

$$\langle \widetilde{a}(\omega)\widetilde{a}^\dagger(\omega)\rangle \;=\; \Phi(\omega) \;=\; \frac{0.0072}{v\pi^2}\left(\frac{D}{r_0}\right)^{5/3}(-1)^{(n+n'-m-m')/2}\sqrt{n+1}\sqrt{n'+1} \tag{224}$$

$$\times \int d\kappa_y\, \xi^{-17/3} J_{n+1}(2\pi\xi) J_{n'+1}(2\pi\xi) u_m(b) u^*_{m'}(\beta), \tag{225}$$

where

$$\xi(\omega,\kappa_y) = \frac{D}{2}\sqrt{\omega^2/v^2+\kappa_y}\,, \quad \text{and}: \quad u_m(\beta) = \begin{cases} (\sqrt{-1})^m\sqrt{2}\cos m\beta, & m \text{ even} \\ (\sqrt{-1})^m\sqrt{2}\sin m\beta, & m \text{ odd} \\ 1, & m=0 \end{cases}. \tag{226}$$

The details of all this can be found in the paper [30], but just to mention briefly that this model assumes the Taylor hypothesis and a turbulence layer that is translating in the x-direction across a telescope aperture of diameter D, at a wind speed v. The remaining difficulty of calculating the integrals in (223) now rests on the issue whether the various filters components $S(\omega)$, $D(\omega)$ and $C(\omega)$ are matrix-valued or scalars. If they are scalar, the order of multiplication can be switched around to simplify the computation greatly, whereby we obtain

$$\sigma_i^2 \;=\; \mathrm{Tr}(P_{ai}C_{aa}P_{ai}^T) + \mathrm{Tr}\big[P_{mi}ETC_{nn}(P_{mi}ET)^T\big]\int d\omega\,|C(\omega)D(\omega)|^2 \tag{227}$$

$$+ \;\; \mathrm{Tr}\left[P_{mi}EG_a\left(\int d\omega\,\Phi(\omega)|\mathcal{H}(\omega)|^2\right)(P_{mi}EG_a)^T\right] \tag{228}$$

$$- \;\; 2\,\mathrm{Tr}\left[P_{ai}\,\mathrm{Re}\left(\int d\omega\,\Phi(\omega)\mathcal{H}^\dagger(\omega)\right)(P_{mi}EG_a)^T\right]. \tag{229}$$

where $\mathcal{H}(\omega) = C(\omega)D(\omega)S(\omega)$ is the open loop transfer function. The first term resulted from the integral because $\int d\omega\,\Phi(\omega) = C_{aa}$. The integrals are now straightforward and fast to compute, but this formulation does not allow multiple for control bandwidths. The WFSs can still be read out at different frame rates, which will affect the SNR and the noise computation (217), but the loop control rate has to be driven by the fastest camera.

6.2.3 Closed loop variance

In closed loop we have a different input-output relationship: referring to Fig. 12 we find that

$$[I + C(\omega)D(\omega)ES(\omega)G_m]\widetilde{\alpha}(\omega) = C(\omega)D(\omega)ES(\omega)G_a a(\omega) + C(\omega)D(\omega)ET\widetilde{n}(\omega), \tag{230}$$

where I is the identity matrix. Now the problem of solving for $\widetilde{\alpha}$ is compounded by the generally matrix-valued nature of the expression within square brackets on the left. As it stands, this matrix would need to be inverted for every value of ω, which becomes impractical. Note that the problem and the formula is exactly the same as in Sect. 3.4, so for PSF reconstruction of null-modes we have exactly the same formalism, only a different set of modes. To proceed, we must again make some assumptions. First we will assume that the filter functions are all scalar, like in the previous open loop scenario. Second, we will invoke the approximation $EG_m \approx I$. It may be possible to derive an estimator that explicitly fulfills this requirement by invoking the constraint as a Lagrange multiplier, but for now it will be treated as an approximation in conjunction with the SVD or MAP estimators. With these two assumptions the expression becomes manageable, and we obtain

$$[1 + \mathcal{H}(\omega)]\widetilde{\alpha}(\omega) = \mathcal{H}(\omega)EG_a\widetilde{a}(\omega) + C(\omega)D(\omega)ET\widetilde{n}(\omega), \tag{231}$$

or

$$\widetilde{\alpha}(\omega) = \mathcal{H}_{cl}(\omega)EG_a\widetilde{a}(\omega) + \mathcal{H}_n(\omega)ET\widetilde{n}(\omega), \tag{232}$$

where

$$\mathcal{H}_{cl} = \frac{\mathcal{H}}{1+\mathcal{H}}\,, \quad \text{and} \quad \mathcal{H}_n = \frac{CD}{1+\mathcal{H}} \tag{233}$$

are the closed-loop and noise transfer functions respectively. This could be used to evaluate the phase variance already, but it turns out to be instructive and numerically prudent to use the error transfer function $\mathcal{H}_\varepsilon = 1 - \mathcal{H}_{cl}$ instead, so with this substitution we finally have

$$\widetilde{\alpha}(\omega) = EG_a\widetilde{a}(\omega) - \mathcal{H}_\varepsilon(\omega)EG_a\widetilde{a}(\omega) + \mathcal{H}_n(\omega)ET\widetilde{n}(\omega). \tag{234}$$

The residual Zernike error is then

$$\widetilde{\varepsilon}_i = \underbrace{(P_{ai} - P_{mi}EG_a)}_{Q_i}\widetilde{a}(\omega) + P_{mi}EG_a\widetilde{a}(\omega)\mathcal{H}_\varepsilon(\omega) - P_{mi}ET\widetilde{n}(\omega)\mathcal{H}_n(\omega), \tag{235}$$

where we can see that we will obtain again the purely geometric term computed in (215), plus correction terms from control loop dynamics, as well as cross-terms. Skipping to the result, this is what we get:

$$\begin{aligned}
\sigma_i^2 &= \mathrm{Tr}(Q_i C_{aa} Q_i^T) + \mathrm{Tr}\big[P_{mi}ETC_{nn}(P_{mi}ET)^T\big]\int d\omega\,|\mathcal{H}_n(\omega)|^2 && (236)\\
&+ \mathrm{Tr}\left[P_{mi}EG_a\left(\int d\omega\,\Phi(\omega)|\mathcal{H}_\varepsilon(\omega)|^2\right)(P_{mi}EG_a)^T\right] && (237)\\
&+ 2\,\mathrm{Tr}\left[Q_i\,\mathrm{Re}\left(\int d\omega\,\Phi(\omega)\mathcal{H}_\varepsilon^\dagger(\omega)\right)(P_{mi}EG_a)^T\right]. && (238)
\end{aligned}$$

7 Numerical computation

This section contains information that is specific to the "pakalana" computer system at WMKO, which is where the PSF reconstruction package is currently set up (with the caveat that TRS queries can not be done from this machine, and has to be done instead from e.g. k2aoserver, and the saved data then copied over to pakalana). Instructions on how to use the codes and how to relocate the package are given in the following sections.

7.1 General computer information

- The home directory is `/local/home/kpaobld/` and the top-level code directory is `~/IDL/`. Most (but not all) of the top-level codes pertaining to the PSF reconstruction package resides under `~/IDL/projects/psfrec/`.
- The image and TRS data directory is currently an external USB drive `/media/usbdisk/PSFrec/`, with a symbolic link under the home directory `~/PSFdata/`.
- To move the PSF reconstruction package to another computer, it would be easiest to copy the entire IDL directory, since many required routines are located in various sub-directories.
- To move the IDL code package to a different computer, one external library needs to be recompiled, and some shell environment variables specified. This is the sparse matrix package SOI ("Sparse Operations with IDL") and its multi-threaded version "ptsoi" (based on pthreads). The source codes reside under `~/IDL/lib/soi/` and `~/IDL/lib/ptsoi/` and compilation instructions are given in the preamble of the C codes. The location of the shared object libraries `soi.so` and `ptsoi.so` must be specified as shell environment variables `SOI_LIB` and `PTSOI_LIB` (for instance by putting `'export SOI_LIB=$HOME/IDL/lib/soi/soi.so'` in the .bashrc.)

7.2 IDL codes

The main PSF reconstruction algorithm `psfrec.pro` depends on a number of pre-computed components generated in separate pieces of code. The components (and their generating codes) are:

- `kao.pro` – DM influence functions $h_i(\mathbf{x})$, Sect. 3.3
- `dmfit.pro` – DM PSD filtering function $\mathcal{H}(\mathbf{f})$, Sect. 3.2
- `alias.pro` – WFS aliasing covariance matrix $\langle \mathbf{v}\mathbf{v}^T \rangle$, Sect. 3.5
- `gettrs.pro` – TRS data for the $\langle \mathbf{u}\mathbf{u}^T \rangle$ and $\langle \mathbf{m}\mathbf{m}^T \rangle$ covariance matrices, Sect. 3.4

Both `alias.pro` and `dmfit.pro` generate their own DM influence functions, but the DM/WFS geometry setup generated in `kao.pro` creates a sparse DM influence function matrix that exactly follows the real K2AO numbering conventions of actuators and sub-apertures, which is required for the main `psfrec.pro` code.

gettrs.pro

This code does the TRS query for a given input NIRC2 FITS image header, and saves the retrieved data as an IDL save file. The idea is to minimize the amount of number-crunching and bandwidth stolen from k2aoserver so as not to potentially affect simultaneous observing, and do the heavy lifting on another machine. The saved data file then has to be copied over to the data directory of the computer where the rest of the PSF reconstruction is done.

```
SYNTAX
  gettrs [, image=, silent=, buffer=, sdir=]

OPTIONAL ARGUMENTS
  image    string path to input FITS image (with header)
  buffer   string TRS buffer name [default 'ffb_save']
  sdir     string save directory
  silent   [0/1] suppress verbose mode

EXAMPLE CALLING SEQUENCE
  gettrs,image='data/080718/nirc2/n0185.fits',buffer='ffb_save',sdir='data/080718/trs/'
```

dmfit.pro

This code generates the Fourier domain DM filtering function $\mathcal{H}(\mathbf{f})$ that is used for the fitting error modeling in Sect. 3.2. All the relevant parameters of the system is specified in the preamble of the code. The important ones for generating a new filter function are: actuator spacing ("pitch") and resolution ("da"), pupil size ("D") and numerical grid size ("dim"). The configuration used for the narrow-field NIRC2 camera was: `pitch=4, da=0.5625, D=10, dim=320`. The reasons for this combination of grid size and actuator pitch is that it maps almost exactly onto the narrow-field NIRC2 plate scale without any re-scaling (via the Fourier transform into spatial frequency domain), and these are also the exact same numbers used in the main PSF reconstruction code `psfrec.pro`. The principles of this code was described in Sect. 3.2

```
SYNTAX
  dmfit [, /lcov, /load]

OPTIONAL ARGUMENTS
  lcov  load previously stored influence function covariance matrix
  load  load full results from previous run, just for plotting

EXAMPLE CALLING SEQUENCE
  dmfit,/lcov
```

alias.pro

This code generates the propagated aliasing covariance matrix $\langle \mathbf{v}\mathbf{v}^T \rangle$, based on the Fourier domain method described in sections 3.5 and 5.3.4. Only the integrator loop gain and the WFS integration time are input arguments. The remaining key parameters are declared in the preamble of the main routine, including turbulence characteristics such as L_0, r_0 and C_n^2 profile, and WFS parameters like sub-aperture size and sensing wavelength. The first part of the code calculates the spatial aliasing PSD, and the second part calculates (via the Wiener-Khinchin theorem) the inverse DM influence function matrices which propagates the phase correlation onto actuator commands, to give the $\langle \mathbf{v}\mathbf{v}^T \rangle$ matrix.

```
SYNTAX
  alias [, g, ti, /nodisp]

OPTIONAL ARGUMENTS
  g       loop gain (integrator)
  ti      WFS integration time
  nodisp  [0/1] suppress graphical display

EXAMPLE CALLING SEQUENCE
  g,0.5,1.e-3
```

psfrec.pro

This is the main PSF reconstruction routine. It presently relies on a particular data directory structure and some standardized names for the NIRC2 FITS images and also for the data folders, as follows: the NIRC2 FITS image name is assumed to be `nxxxx.fits` where the "x" are numbers; the data directory is given by the observation date `yymmdd/`; under the data directory the NIRC2 and TRS data are located in sub-directories called `nirc2/` and `trs/`. An example calling sequence is given below. Input parameters that must be specified in the preamble of the code are the seeing and turbulence outer scale. If an off-axis angle is specified and different from zero, the NGS anisoplanatism kernel is computed, and if a non-zero LGS altitude is specified, the focal anisoplanatism kernel is used. Tilt anisoplanatism with LGS is currently not implemented (the kernel is simple to compute, but the code has not been calibrated to the STRAP sensor yet). For NGS and/or LGS and tilt anisoplanatism, a layered turbulence profile must also be specified (altitudes h_l and normalized C_n^2, i.e. the f_l from Sect. 3.1)

```
SYNTAX
  psfrec, imn, dir [,dn]
```

```
ARGUMENTS
  imn   string NIRC2 image name (minus ".fits")
  dir   string data directory name

OPTIONAL ARGUMENTS
  dn    string dark frame image name

EXAMPLE CALLING SEQUENCE
  psfrec,'n0075','n0090','080812/'
```

kao.pro

This is a K2AO simulation based on the Monte Carlo principle (it works similar to YAO). It was constructed as a special case of a more generalized AO simulation code (`newao2.pro`), and it has a number of things hardwired into it specifically for K2AO emulation. For instance, the aperture shape and the DM and WFS geometries are fixed, in order to get sub-apertures and actuators that correspond exactly to the numbering conventions of the real K2AO system. This means that the simulated interaction matrices and reconstruction matrices exactly correspond to the real K2AO system, and could potentially even be used with the real system. The simulation code also implements real-time pupil rotation with triggering of new reconstruction matrices and DM/WFS subsets as a function of the illuminated sub-apertures. It implements both NGS and LGS mode, but the tip/tilt sensing in LGS mode has not (yet) been tweaked to represent exactly the characteristics of the STRAP sensor, so the tip/tilt sensor simulation in LGS mode is of a generic kind.

This code also features some wavefront reconstruction options that the real K2AO system does not yet implement, such as a sparse matrix maximum a posteriori (MAP) estimator and a preconditioned conjugate gradient (PCG) iterative solver. This estimator gives exactly the same AO performance as the non-sparse implementation currently in use (as can be demonstrated by simply comparing the two), but it employs a numerical technique that has been proposed for future extremely-high-order AO systems, such as the NGAO. This was implemented in the K2AO simulation just as a proof-of-concept, but in principle, the sparse MAP-PCG estimator could be used already with the existing K2AO system.

The AO system to be simulated is specified in a parameter file, an example of which is given at the end of this section, as prepared specifically for simulation of K2AO with the NIRC2 narrow-field camera. The main code consists of two sections: an initialization step that parses the parameter file and generates architecture dependent objects, and the actual simulation step that loops over random turbulence phase screens and measures the AO performance. So the calling sequence is a little more cumbersome, as exemplified below:

- For every new configuration (parameter file), start by running the parameter file itself at the IDL prompt. This initializes parameters and saves them to file.
- Then run `kao.pro` with the same parameter file as input (see example below)
- If running the same configuration in a new IDL session, set the "/lho" (load HOWFS) keyword to skip the most time-consuming initialization steps by loading the objects saved in the first session.

```
SYNTAX
  kao, name, dir [,/lho]

ARGUMENTS
  name  string simulation name (as given in parameter file)
  dir   string directory of parameter file

OPTIONAL ARGUMENTS
  lho   load high-order WFS/DM structures initialized in a previous session

EXAMPLE CALLING SEQUENCE
  IDL> kao_ngs4
  IDL> kao,'kao_ngs4'
```

Below follows an example parameter file (kao_ngs4.pro) designed to emulate the K2AO system with the NIRC2 narrow-field camera.

```
pro kao_ngs4

; Simulation
sim = {sim}
sim.dir = '/local/home/kpaobld/IDL/projects/kao/parfiles/'
sim.name = 'kao_ngs4'
sim.info = '1-NGS 1-DM AO system'
sim.D = 11.25 ; too large on purpose, to produce the right sub-ap size
sim.cobs = 0.2
sim.hex = 0
sim.ang = 30. ; may specify a fixed pupil rotation angle
sim.dim = 320
sim.niter = 20000L
sim.skip = 100
sim.ndisp = 10
sim.tq = 1.e-3
sim.wim = 2.1685e-6
sim.psfeval = 1
sim.aniso = 0
sim.eval = ptr_new([[0.],[0.]])
sim.seed = sim.dir+'rseed.sav'
sim.nz = 2 ; number of Zernikes to calculate modal performance
restore,sim.seed

; Atmosphere
atm = {atm}
atm.r0v = 0.16
atm.L0 = 30.
atm.zen = 0.
atm.air = 1./cos(!pi*atm.zen/180.)
atm.tmod = 1
atm.frac = ptr_new([0.482,0.133,0.065,0.072,0.109,0.077,0.062])
atm.alt = ptr_new([0.,0.5,1.,2.,4.,8.,16.]*1.e3)
atm.v0 = ptr_new([6.8,6.9,7.0,7.5,10.0,26.8,18.5])
atm.nl = n_elements(*atm.alt)
atm.aseed = ptr_new(rseed)
atm.vdir = ptr_new(randomu((*atm.aseed)[atm.nl*3],atm.nl)*360.)
atm.v = ptr_new([[(*atm.v0)*cos(!pi*(*atm.vdir)/180.)],$
                          [(*atm.v0)*sin(!pi*(*atm.vdir)/180.)]])

; WFS setup
nwfs = 2 ; number of WFS
wfs = replicate({wfs},nwfs)

; HOWFS
n=0
wfs(n).type = 'sh1'
wfs(n).geom = 'sqr'
wfs(n).sys = 1 ; sub-system - for control/reconstruction purposes
wfs(n).cat = 1 ; category - for geometry/architecture initilization purposes
wfs(n).th = 0.4
wfs(n).fsdiam = 0.
wfs(n).nx = 20
wfs(n).pixps = 4
wfs(n).lgs = 0
wfs(n).cl = ptr_new([0,1]) ; indices of DMs that are seen by WFS (-1 = open loop)
```

```
wfs(n).ltype = 'altitude'; 'range' or 'altitude' is fixed
wfs(n).alt = 120.e3
wfs(n).ndx = 4
wfs(n).qcc = 0
wfs(n).dx = 0.235
wfs(n).noise = 0
wfs(n).qe = 0.98
wfs(n).ron = 10.
wfs(n).dc = 0.1
wfs(n).band = ptr_new(['R'])
wfs(n).ot = 0.97
wfs(n).mag = 12.
wfs(n).integ = 1
wfs(n).ker = 0.
wfs(n).initk = 0.
wfs(n).amp = 1.
wfs(n).tt = 1
wfs(n).ext = 0 ; can calibrate on extended source
wfs(n).pos = [0.,0.]


; LOWFS
n=1
wfs(n).type = 'sh1'
wfs(n).geom = 'sqr'
wfs(n).sys = 2
wfs(n).cat = 2
wfs(n).th = 0.5
wfs(n).fsdiam = 0.
wfs(n).nx = 1
wfs(n).pixps = wfs(0).pixps*wfs(0).nx/wfs(n).nx
wfs(n).lgs = 0
wfs(n).cl = ptr_new([0,1])
wfs(n).ndx = 2
wfs(n).dx = 0.45
wfs(n).qcc = wfs(n).ndx/2
wfs(n).noise = 0
wfs(n).qe = 0.98
wfs(n).ron = 10.
wfs(n).dc = 0.1
wfs(n).band = ptr_new(['R'])
wfs(n).ot = 0.97
wfs(n).mag = 12. ; if multi-spectral, this is the magnitude of the FIRST band
wfs(n).integ = 1
wfs(n).ker = 0.
wfs(n).initk = 1.
wfs(n).amp = 1.
wfs(n).tt = 0
wfs(n).pos = [0.,0.]
wfs(n).ext = 0


; DM setup
ndm = 2 ; number of DMS
dm = replicate({dm},ndm)

n=0
dm(n).type = 'pzt'
dm(n).class = 'ho'
```

```
dm(n).sys = 1
dm(n).nc = wfs(0).nx+1
dm(n).pixpa = wfs(0).pixps
dm(n).alt = 0.
dm(n).coupling = 0.2
dm(n).th = 0.25
dm(n).thx = 0.0
dm(n).initc = 1.
dm(n).clev = 4.
dm(n).clim = 0.02
dm(n).xcg = 0.75
dm(n).xact = 1

n=1
dm(n).type = 'zer'
dm(n).class = 'null'
dm(n).sys = 2
dm(n).nc = 2
dm(n).alt = 0.
dm(n).initc = 1.
dm(n).xact = 0

; Wavefront reconstruction
nrec = 2
rec = replicate({rec},nrec)

n=0
rec(n).sys = 1
rec(n).cond = 10.
rec(n).map = 1
rec(n).pcg = 1
rec(n).etol = 1.e-5
rec(n).alpha = 0.01
rec(n).gain = 0.5
rec(n).cl = 1

n=1
rec(n).sys = 2
rec(n).cond = 10.
rec(n).map = 0
rec(n).pcg = 0
rec(n).etol = 1.e-5
rec(n).alpha = 0.1
rec(n).gain = 0.5
rec(n).cl = 1

save,sim,atm,wfs,dm,rec,filename=sim.dir+sim.name+'_pinit.sav'

end
```

A Data sets

Between 2007-12-10 and 2008-08-11 we collected data on the K2 AO system with the narrow-field NIRC2 camera, as summarized in table 2.

Date	Time	Mode	Purpose	Comment
2007-12-10	2h	bench	Noise model validation	Collected data for range of frame rate, SNR and gains
2008-01-16	3h	sky	Bright NGS, r_0 est.	Open/closed loop NIRC2+ACAM; good conditions
2008-04-22	2h	sky	Bright NGS, on-axis	NIRC2+ACAM; bad conditions
2008-04-28	2h	bench	Noise model validation	DLM script
2008-05-06	2h	bench	Noise model validation	same as 4/28 + Jcont and Hcont
2008-07-17	3h	sky	Bright NGS, on-axis	∼2h bad seeing; 30 minutes of data
2008-08-11	3h	sky	NGS	Bright+faint, off-axis; DLM script

Table 2: K2 AO+NIRC2 narrow field camera data collected for PSF reconstruction prototyping and testing.

Observation logs

2008-01-16

```
008             07 19 10.235 -04 58  7.12 2000.0 vmag=12.12 b-v=0.65
009             07 15 14.085 +35 04 53.88 2000.0 vmag=12.05 b-v=0.50
010             07 19 11.884 +15 11 59.51 2000.0 vmag=12.04 b-v=0.36
011             09 18 57.766 +14 49 57.11 2000.0 vmag=12.18 b-v=0.32
012             10 16 20.905 -05 13  2.81 2000.0 vmag=12.29 b-v=0.53
013             10 16 48.640 +34 55 15.22 2000.0 vmag=12.26 b-v=0.47
014             11 22  4.913 +15 07 21.18 2000.0 vmag=12.10 b-v=0.56
015             13 19 39.396 +15 35  3.77 2000.0 vmag=12.18 b-v=0.63
016             13 19 59.257 -04 46 22.08 2000.0 vmag=12.12 b-v=0.32
017             13 19 44.853 +34 53 15.13 2000.0 vmag=12.06 b-v=0.40
018             15 18 27.001 +14 46 20.72 2000.0 vmag=12.01 b-v=0.72
019             16 18 29.111 -05 42 33.79 2000.0 vmag=12.03 b-v=0.39
020             16 16 30.365 +34 50 50.59 2000.0 vmag=12.29 b-v=0.64
021             17 18 39.502 +15 01 16.67 2000.0 vmag=12.10 b-v=0.54

/sdata903/nirc6/2008jan17b/

Star #011 (250 Hz)
ti 0.5 / 10 co / Kp

Acam        NIRC2
#33,34 - 0.9"/0.9"      #6 - 0.505/0.371 TT
#35,36 -  #7 -  TT

-------------------

Changed to 500 Hz  (~275 counts avg.)
DM_gain = 0.5, TT_gain = 0.5

ACAM #40,41,42 (DMTT), 43,44,45 (TT)
                     N2 #10 (TT) (30 s: 10s x 2 coadds)
ACAM #46,47,48 (DMTT), 49,50,51 (TT)
                     N2 #11
ACAM #52,53,54 (DMTT), 55,56,57 (TT)
                     N2 #12
ACAM #58,59,60 (DMTT), 61,62,63 (TT)
                     N2 #13 (TT)
```

```
ACAM #64,65,66 (DMTT), 67,68,69 (TT)
                     N2 #14

-------------------

(faster): N2 coadds: 1 x 10s
ACAM: 5s

ACAM #73-83 (TT), N2 #15-24 (TT)
ACAM #84-88 (DMTT)
ACAM #89-93 (TT), N2 #25,26,27,28 (TT)
ACAM #94-98 (DMTT)
ACAM #99-103 (TT), N2 #29,30,31,32 (TT)
ACAM #104-108 (DMTT)
ACAM #109-113 (TT), N2 #33,34,35,36 (TT)
ACAM #114-118 (DMTT)
ACAM #119-123 (TT), N2 #37,38,39,40 (TT)
ACAM #124-128 (DMTT)
ACAM #129-133 (TT), N2 #41,42,43,44 (TT)
ACAM #134-138 (DMTT)

---------------------

(SAO 98333) HD 77623
(angle = 218.2)

N2 #46 test - 1054 kHz (DMTT)
DM_gain = 0.5, TT_gain = 0.5

N2 -> BrG
#47 test (tint = 0.5) DMTT
#48 test (tint = 2.0) DMTT
#49 test (tint = 1.0s x 20) DMTT

starting

N2: 10s x 2co
ACAM: 5 images

ACAM #141-145 (TT), N2 #51,52 (TT)
ACAM #146-150 (DMTT), N2 #53,54 (DMTT)
ACAM #151-155 (TT), N2 #55,56 (TT)
ACAM #156-160 (DMTT), N2 #57,58 (DMTT)
ACAM #161-165 (TT), N2 #59,60 (TT)
ACAM #166-170 (DMTT), N2 #61,62 (DMTT)
ACAM #171-175 (TT), N2 #63,64 (TT)
ACAM #176-180 (DMTT), N2 #65,66 (DMTT)
ACAM #181-185 (TT), N2 #67,68 (TT)
ACAM #186-190 (DMTT), N2 #69,70 (DMTT)

--------- taking a break ----

N2 #72 - Liz script (dither) DMTT

------------- back

AO -> 438 Hz (avg. intensity ~ 1000 counts)
DM_gain = 0.5, TT_gain = 0.5
1.05 air mass
```

```
N2 -> 5s x 3co
DMTT closed
ACAM -> 1s

N2 #121,122 (DMTT), ACAM #194-198 (DMTT)
ACAM #204-208 (DMTT), N2 #124-126 (DMTT)
ACAM #209-213 (TT), N2 #127,128 (TT)
ACAM #214-219 (DMTT), N2 #129,130,131 (DMTT)
ACAM #220-225 (TT), N2 #132,133 (TT)
ACAM #226-231 (DMTT), N2 #134,135,136 (DMTT)
ACAM #232-237 (TT), N2 #137,138 (TT)
ACAM #238-243 (DMTT), N2 #139,140,141 (DMTT)
ACAM #244-249 (TT), N2 #142,143 (TT)
ACAM #250-255 (DMTT), N2 #144,145,146 (DMTT)
ACAM #256-261 (TT), N2 #147,148 (TT)
N2 #149,150,151 (DMTT)

-----------------------------------

N2 5s x 30co -> #152
taking sky -> #153

-------------------
A0 -> 438 Hz
DM_gain = 0.5, TT_gain = 0.5
air mass = 1.16

Testing coronograph
Kp = clear, largehex
coron600
tint 240
sampmode 3, 16 reads
N2 #154

tint = 300
smallhex
Kp
air mass 1.18-1.20
N2 #155

open
N2 #156

sky -> 157

BrG -> brighter star (?)
AO -> 1054 Hz, gains = 0.5
pupil -> open
coron800
tint 5s, 30 co adds
air mass = 1.32
N2 #158

sky -> N2 #159

pupil -> large hex

N2 #160
```

```
tint 10, coadds 30
air mass = 1.38
N2 #161

sky -> #162

no corona
large hex
tint = 0.01s, 200co
N2 #163,164

sky -> #165
```

2008-04-22

```
Date: 2008-04-23
      start time: 01:30 HST
starlist: /sol/apps1/kroot/starlists/dlm/psf080422.lst
/Users/rflicker/Documents/Work/PSF/psf080422.lst
obsplan: /Users/rflicker/Documents/Work/PSF/eng080423.doc

All tests w/ NIRC2 narrow camera

NIRC3 account

/sdata903/nirc3/2008apr23
Acam: /nightly/tonight/Acam/

1. SETUP AO & Telescope for NIRC2-NGS
a. Switch instrument to NIRC2
b. Bring up NIRC2 tools
c. Restart AO tools & nighttime script
d. Check calibration files

2. Bright star on-axis
a.     Acquire star in NGS mode in vertical angle mode
               (pupil is fixed on NIRC2) on NIRC2 P.O.
b. Optimize NGS using bandwidth widget and Strehl tool
c. Record acam image every 60sec, (record DM-open loop image on NIRC2?)
d. Setup NIRC2 for Kp & record images,
i. write down settings for recording background
ii. write down seeing, exact UT times for RTC ,
e. Re-do for H and J band
f. Record background (mostly for Kp)

UT 11:46 (01:46 HST) - could not connect to TRS, wrong reconstructor, WFC crash, restart TRS:
WFC freeze, failure mode 3.

-> 3 reboots : working 4th time

UT 11:55 - K2AO @ 149 Hz

UT 11:57 - TRS not responding again - BW optimization, seeing tool, not working
   DLM calling Kelly
   DLM calling ErikJ

HST 2:10 - AlC doing Daphne (~1 mag extinction, lots of cirrus)
```

```
HST 2:26 - update from Erik, troubleshooting, partitioning the database created problem
(can not access the data fast enough when the disk is filling up)

HST 2:58 - update from DLM / EJ - TRS fixed - use ffb_3
idl script release

HST 3:07 - on target #0 (075), airmass 1.06, 100 Hz, 100-200 counts
seeing 0.35 (s-tool) 0.5 acam

acam #3

TTgain = 0.3
DMgain = 0.55
cgain = 1.0 (cent-to-arcs 0.49)

N2 - Kp
coadds 10
tint 10   - taking test

HST 3:16 - going to #98 (091) airmass 1.19
seeing (s-tool) 0.6

-> 1000 Hz
TTgain = 0.25
DMgain = 0.8
cent-arcs = 0.59

N2 - setup
n0120
coadds 10
sampmode 2
#reads 4
Kp + clear
open shutter

sdata903/nirc3/2008apr23
#120 (13:26:13.81 UT, 2008-04-23)

starting sequence
100 coadds
#121 seeing = 0.46" (N2 seeing tool)

saturated

subc 512
tint 0.1
200 coadds
N#122, acam#7 (N2-seeing=0.43", acam=0.65)

goi 5 (above settings) N#123-127, acam#8

-> H band
coadd 10 -> test

coadd 200
goi 5
N#128, acam#112-115

-> J band
```

```
coadd 10
test
note : intensity variations
(saturated)
tint 0.07

DMgain = 0.75
TTgain = 0.2

coadd 200
goi 1, N#133
goi 5, 134-138
(seeing lots of distortions in J - also present at Kp)

HST 3:50 - Investigating distortion problem

goi 50 (test)

-> Kp
tint 0.1
coadd 100
test

clouds - 80 counts on WFS

frame rate -> 250

-> 100 Hz
loops faulted blah blah blah

HST 4:08 - WFC freeze failure mode 3

Finally back on star (lost it) @ 100 Hz

HST 4:15 -> Could not write to TRS

HST 4:25 - back up

strong variability in extinction

N2 test, 438 Hz
coadd 200, tint 0.1, Kp, large hex
goi 5, N#145-149 (Strehl = 0.395)
TTgain = 0.35
DMgain = 0.95

-> 1000 Hz
TTgain = 0.2
DMgain = 0.6
cent-arcs = 0.87

(acam#045)

goi 5
N#151-155 (Strehl = 0.22)

-> 500 Hz

TTgain = 0.2
```

```
DMgain = 0.6
cent-arc = 0.67

N#156-159

-> H
tint 0.07
coadds 200

N#161-165

New Star -> #114, air mass = 1.01
subc 1024
250 Hz
Too large separation

-> new star #108 + companion
Kp
438 Hz
TTgain = 0.3
DMgain = 0.6
cent-arcs = 0.44

tint 0.5 coadd 50 goi 3
N#166-168 (Strehl = 0.35)

-> H
goi 5 (strehl ~0.2)
N#169-173

tint 0.2 goi 3
N#174-176

-> J goi 3
N#178-180

(15:28:21.64 UT)

Flats:

Frames 196 to 255 are flats.

The sequence is on/off, hkj, 1024/512, 5 each.

So, for example, 196-200 = dome-lamps-on,  H, 1024
                 201-205 = dome-lamps-off, H, 1024
                 206-210 = dome-lamps-on,  K, 1024
....
                 226-230 = dome-lamps-on,  H,  512
etc
```

2008-04-28

```
NIRC2 AO 2008-04-28

newdir

/sdata903/nirc2eng/2008apr29/
```

```
parameter sets

1. vary DM gain (fixed FR, TTg, Cg)
2. vary TT gain (fixed FR, DMg, Cg)
3. vary Cent gain (fixed FR, DMg, TTg)
4. variable FR (did not do this)

Start: UTC 21:22:39.39, 2008-04-28

(end: 23:01:06.63)

reconstructor matrix: 304b.mr
centroid origins: 24nirc2-N2x2.cog
(calibrated 28 April night)
FR 1054 Hz

BrG
subc 512
tint 0.1
coadd 50
sampmode 2
# reads 4
track true   <-- NOTE!

; Reference
DMg = 0.05
TTg 0.05
Cg = 0.35165 (WSCNGN)
object Bright 1 KHz
tint 0.1
coadd 100
n0003.fits

tint 0.07
n0004

coadd 200
tint 0.07
n0005

object: dark
Dark frame:
n0006,n0007 (200 coadd, tint 0.07)
n0008,n0009 (100 coadd, tint 0.1)

tint 0.07
coadd 200

"tt"
TTg = [0.05,0.2,0.6]
DMg = 0.05
Cg = 0.35

"dm"
DMg = [0.05,0.5,0.9]
TTg = 0.05
Cg = 0.35

"cent"
```

```
Cgain = [0.2,0.4,0.6,0.8]
TTg = 0.2
DMg 0.2

tint 1, coadd 10
#012

tint 2, #13

coadd 30

"tt"
TT=0.05;DM=0.05; C=0.35; n#14
TT=0.2; DM=0.05; C=0.35; n#15
TT=0.6; DM=0.05; C=0.35; n#16

TT=0.05; DM=0.5; C=0.35; n#17 "tt" (forgot to rename)
TT=0.05; DM=0.9; C=0.35; n#18 "dm"

"cent"
TT=0.05; DM=0.05; C=0.2; n#19 "dm" (forgot to rename)
TT=0.05; DM=0.05; C=0.2; n#20 "cent gain"
TT=0.05; DM=0.05; C=0.4; n#21
TT=0.05; DM=0.05; C=0.6; n#22
TT=0.05; DM=0.05; C=0.8; n#23

TT=0.2; DM=0.2; C=0.8; n#24 "cent gain 2"
TT=0.4; DM=0.4; C=0.8; n#25 "cent gain 2"
TT=0.4; DM=0.4; C=0.6; n#26 "cent gain 2"
TT=0.4; DM=0.4; C=0.4; n#27 "cent gain 2"

-> track false

TT=0.4; DM=0.4; C=0.4; n#28 "cent gain 2"

Dark frames 29-31
```

2008-07-18

```
17 July 2008 (UT)
3 h engineering time on K2/AO/NIRC2

nirc2 data directory:sdata903/nirc2eng/2008jul18/
n0001-n0034 ; calibration & flats
n0035-n0046 ; twilight

Bright star
star #1 (list)

~~ new star

seeing 1-1.5"

Kp

running script @ n0169
running script @ n0179-n0181

closing for fog
```

```
Opening up again - seeing 0.5"

starting script @ n0185

H band

starting script @ n0195

darks for H n0205-207
darks for Kp n0208

------- stop

H band
Faint star
Kp band
H band
```

2008-08-12

```
PSF reconstruction
engineering 2008-08-12 (22:00-01:00 HST)

/sdata903/nirc2eng/2008aug12/

Calibration n0001.fits-n0058.fits

/qfix/data/ControlParms/*.dm (DM cal)

22:20 HST (8:20 UT) - start TRS 8:15 UT
tests #59-66

starting DLM script @ n0067-76 BrG

script @ 77-86 H cont

background H cont 87-89
background BrG 90-92

Going to M15 center (R12.4) 250Hz
Kp background 93

exposure BrG 4-coadd #94-103

bxy5 start $ 104 (dither failure after 105)

107 - test on reacquired NGS R11.9

BrG goi 10 109-118

H cont goi 10 start @ #119-128

sky H cont goi 3
Brg sky

-> new NGS R12.9
DLM script on faint star, start #138-147 BrG
BrG sky 148-149
```

References

[1] "Development, implementation and validation of PSF reconstruction techniques," Y9 CfAO proposal (2007) URL: `http://lao.ucolick.org/twiki/pub/CfAO/PsfReconstruction/CfAOY9LeMignant_v3nobudget.pdf`

[2] PSF reconstruction project TWiki web page and document collection, URL: `http://lao.ucolick.org/twiki/bin/view/CfAO/PsfReconstruction`

[3] WMKO Next generation wavefront controller, URL: `http://www2.keck.hawaii.edu/optics/ao/ngwfc`

[4] M. Aubailly, M. C. Roggemann, and T. J. Schulz. Approach for reconstructing anisoplanatic adaptive optics images. *Appl. Opt.*, 46:6055–6063, August 2007.

[5] M. Born and E. Wolf. *Principles of optics*. Pergamon Press, Oxford, 6th edition, 1980.

[6] M. C. Britton. The Anisoplanatic Point-Spread Function in Adaptive Optics. *Publ. Astr. Soc. Pac.*, 118:885–900, June 2006.

[7] D. F. Buscher, J. T. Armstrong, C. A. Hummel, A. Quirrenbach, D. Mozurkewich, K. J. Johnston, C. S. Denison, M. M. Colavita, and M. Shao. Interferometric seeing measurements on Mt. Wilson: power spectra and outer scales. *Appl. Opt.*, 34:1081–1096, February 1995.

[8] R. M. Clare and B. L. Ellerbroek. Sky coverage estimates for adaptive optics systems from computations in Zernike space. *J. Opt. Soc. Am. A*, 23:418–426, February 2006.

[9] A. Consortini and L. Ronchi. Choice of the model of atmospheric turbulence. *Appl. Opt.*, 11:1205–+, May 1972.

[10] G. Cresci, R. I. Davies, A. J. Baker, and M. D. Lehnert. Accounting for the anisoplanatic point spread function in deep wide-field adaptive optics images. *Astron. Astrophys.*, 438:757–767, August 2005.

[11] E. Diolaiti, O. Bendinelli, D. Bonaccini, L. M. Close, D. G. Currie, and G. Parmeggiani. Starfinder: an idl gui based code to analyze crowded fields with isoplanatic correcting psf fitting. In Peter L. Wizinowich, editor, *Adaptive Optical Systems Technology*, volume 4007 of *Proc. SPIE*, pages 879–887, 2000.

[12] B. L. Ellerbroek. Including outer scale effects in zonal adaptive optics calculations. *Appl. Opt.*, 36:9456–9567, 1997.

[13] R. Flicker and F. Rigaut. Tilt anisoplanatism and PSF retrieval for multi-conjugated adaptive optics systems using laser guide stars. In *Beyond Conventional Adaptive Optics*, ESO Conference and Workshop Proceedings No. 58, page 377, 2001.

[14] R. Flicker, F. Rigaut, and B. Ellerbroek. Tilt anisoplanatism in laser-guide-star-based multiconjugate adaptive optics: Reconstruction of the long exposure point spread function from control loop data. *Astron. Astrophys.*, September 2002.

[15] R. C. Flicker. Efficient first-order performance estimation for high-order adaptive optics systems. *Astron. Astrophys.*, 405:1177–1189, July 2003.

[16] R. C. Flicker and F. J. Rigaut. Anisoplanatic deconvolution of adaptive optics images. *J. Opt. Soc. Am. A*, 22:504–513, March 2005.

[17] Ralf C. Flicker. Adaptive Optics: Analytical model for PSF estimation. Master's thesis, Luleå University of Technology, division of physics, Dec. 1998.

[18] D. L. Fried. Anisoplanatism in adaptive optics. *J. Opt. Soc. Am.*, 72(1):52–61, 1982.

[19] D. L. Fried and J. F. Belsher. Analysis of fundamental limits to artificial-guide-star adaptive-optics-system performance for astronomical imaging. *J. Opt. Soc. Am. A*, 11(1):277–287, January 1994.

[20] E. Gendron, Y. Clénet, T. Fusco, and G. Rousset. New algorithms for adaptive optics point-spread function reconstruction. *Astron. Astrophys.*, 457:359–363, October 2006.

[21] E. Gendron and P. Léna. Astronomical adaptive optics I. Modal control optimization. *Astron. Astrophys.*, 291:337–347, 1994.

[22] E. Gendron and P. Léna. Astronomical adaptive optics II. Experimental results of an optimized modal control. *Astron. Astrophys. Suppl. Ser.*, 111:153–167, 1995.

[23] J. W. Hardy. *Adaptive optics for Astronomical Telescope*. Oxford University Press, 1998.

[24] L. Jolissaint, J.-P. Véran, and R. Conan. Analytical modeling of adaptive optics: foundations of the phase spatial power spectrum approach. *Journal of the Optical Society of America A*, 23:382–394, February 2006.

[25] L. Jolissaint, J.-P. Veran, and J. Marino. OPERA, an automatic PSF reconstruction software for Shack-Hartmann AO systems: application to Altair. In D. Bonaccini Calia, B. L. Ellerbroek, and R. Ragazzoni, editors, *Advancements in Adaptive Optics. Edited by Domenico B. Calia, Brent L. Ellerbroek, and Roberto Ragazzoni. Proceedings of the SPIE, Volume 5490, pp. 151-163 (2004).*, volume 5490 of *Presented at the Society of Photo-Optical Instrumentation Engineers (SPIE) Conference*, pages 151–163, October 2004.

[26] Y. Minowa, N. Kobayashi, Y. Yoshii, T. Totani, T. Maihara, F. Iwamuro, H. Takami, N. Takato, Y. Hayano, H. Terada, S. Oya, M. Iye, and A. T. Tokunaga. Subaru Super Deep Field with Adaptive Optics. I. Observations and First Implications. *Astrophys. J.*, 629:29–44, August 2005.

[27] N. S. Nightingale and D. F. Buscher. Interferometric seeing measurements at the La Palma Observatory. *Month. Not. Roy. Astr. Soc.*, 251:155–166, July 1991.

[28] R. J. Noll. Zernike polynomials and atmospheric turbulence. *J. Opt. Soc. Am.*, 66(3):207–211, 1976.

[29] F. J. Rigaut, J. Veran, and O. Lai. Analytical model for Shack-Hartmann-based adaptive optics systems. In Domenico Bonaccini and Robert K. Tyson, editors, *Adaptive Optical System Technologies*, volume 3353 of *Proc. SPIE*, pages 1038–1048, September 1998.

[30] F. Roddier, M.J. Northcott, J.E. Graves, D.L. McKenna, and D. Roddier. One-dimensional spectra of turbulence-induced Zernike aberrations: time-delay and isoplanicity error in partial adaptive compensation. *J. Opt. Soc. Am. A*, 10(5):957–965, 1993.

[31] R. J. Sasiela. Strehl ratios with various types of anisoplanatism. *J. Opt. Soc. Am. A*, 9(8):1398–1406, August 1992.

[32] M. Schöck, D. Le Mignant, G. A. Chanan, P. L. Wizinowich, and M. A. van Dam. Atmospheric turbulence characterization with the Keck adaptive optics systems. I. Open-loop data. *Appl. Opt.*, 42:3705–3720, July 2003.

[33] C. D. Sheehy, N. McCrady, and J. R. Graham. Constraining the Adaptive Optics Point-Spread Function in Crowded Fields: Measuring Photometric Aperture Corrections. *Astrophys. J.*, 647:1517–1530, August 2006.

[34] A. Tokovinin. From Differential Image Motion to Seeing. *Publ. Astr. Soc. Pac.*, 114:1156–1166, October 2002.

[35] G. A. Tyler. Merging: a new method for tomography through random media. *J. Opt. Soc. Am. A*, 11:409–424, January 1994.

[36] G. A. Tyler. Wave-front compensation for imaging with off-axis guide stars. *J. Opt. Soc. Am. A*, 11:339–346, January 1994.

[37] G. A. Tyler. Reconstruction and assessment of the least-squares and slope discrepancy components of the phase. *Journal of the Optical Society of America A*, 17:1828–1839, October 2000.

[38] M. A. van Dam. Measuring the centroid gain of a Shack-Hartmann quad-cell wavefront sensor by using slope discrepancy. *Journal of the Optical Society of America A*, 22:1509–1514, August 2005.

[39] M. A. van Dam, A. H. Bouchez, D. Le Mignant, E. M. Johansson, P. L. Wizinowich, R. D. Campbell, J. C. Y. Chin, S. K. Hartman, R. E. Lafon, P. J. Stomski, Jr., and D. M. Summers. The W. M. Keck Observatory Laser Guide Star Adaptive Optics System: Performance Characterization. *Publ. Astr. Soc. Pac.*, 118:310–318, February 2006.

[40] M. A. van Dam, D. Le Mignant, and B. A. Macintosh. Performance of the Keck Observatory Adaptive-Optics System. *Appl. Opt.*, 43:5458–5467, October 2004.

[41] J.-P. Véran, F. Rigaut, H. Maître, and D. Rouan. Estimation of the adaptive optics long exposure point spread function using control loop data. *J. Opt. Soc. Am. A*, 14(11), 1997.

[42] Jean-Pierre Véran. *Estimation de la réponse impulsionnelle et restauration d'image en optique adaptative. Application au système d'optique adaptative du Télescope Canada-France-Hawaii*. PhD thesis, Ecole Nationale Supérieure des Télécommunication, Paris, Observatiore de Paris-Meudon, 1997.

[43] J. Y. Wang and J. K. Markey. Modal compensation of atmospheric turbulence phase distortion. *J. Opt. Soc. Am.*, 68(1):78–87, 1978.

[44] D. M. Winker. Effect of a finite outer scale on the Zernike decomposition of atmospheric optical turbulence. *J. Opt. Soc. Am. A*, 8(10):1568–1573, 1991.